Roof Deformation in Vehicle Rollover: The Case for Including an Energy Criterion in Vehicle Crashworthiness Evaluation

---

A Thesis Presented to the
Faculty of the School of Engineering and Applied Science
University of Virginia

In Partial Fulfilment
of the Requirements for the Degree of
Master of Science
Mechanical and Aerospace Engineering

by

Jack W. Lockerby

December, 2013

APPROVAL SHEET

The thesis

is submitted in partial fulfillment of the requirements for the degree of

Master of Science

Mechanical and Aerospace Engineering

Jack W. Lockerby

AUTHOR

The thesis has been read and approved by the examining committee:

Jeff Crandall

Advisor

Richard Kent

Mark Sochor

Accepted for the School of Engineering and Applied Science:

James H. Aylor

Dean, School of Engineering and Applied Science

December, 2013

Abstract

Vehicle rollover crashes are a serious public health concern in the United States with far reaching socioeconomic impacts. Rollovers occur in only 3% of crashes, but account for a disproportionately high number of the serious traffic injuries and fatalities, 30% in 2008 (NHTSA, 2010). Currently in the United States, the only federal motor vehicle safety standard (FMVSS 216) governing vehicle crashworthiness for rollover is based on a quasi-static roof crush test that requires each vehicle to have a minimum strength-to-weight ratio (SWR>3.0). FMVSS 216 has been criticized for not accurately representing vehicle structural response to real-world dynamic rollover crashes, as well as for the choice of peak SWR as the evaluation metric. This thesis is a collection of three studies aimed at evaluating the relationships between force, energy, and deformation in rollover crashes. It is hypothesized that for a vehicle in a single roof-to-ground rollover impact that greater total kinetic energy at touchdown will result in larger structural deformation, and that an increase in the peak SWR of the vehicle will not reduce deformation if it is not accompanied by a similar increase in energy absorption.

In Study I, the dynamic force-deformation response of a vehicle subjected to an inverted drop test displayed comparable stiffness, with limited rate dependence, to the quasi-static evaluation on the same vehicle. An on-board optical system was validated against independent deformation measurement from string potentiometers for tracking dynamic high-rate, 3D, multi-point roof deformations across a large area of vehicle structure. In Study II, the effects of variations in touchdown conditions on vehicle kinematic and deformation response were characterized through two full-scale dynamic rollover tests using replicate mid-sized SUV's on the DRoTS. The two tests sustained similar peak roof deformations while the test with less total kinetic energy produced a larger peak reaction force. Contrary to the results of previous finite element (FE) studies (Parent, 2011), the vehicle with the larger drop height did not sustain more deformation. In Study III, the effects of variations in the distribution of initial kinetic energy (vertical, rotational, translation al) on the force and deformation response of the vehicle roof structure in a rollover were characterized through FE simulations. Eight single roof-to-ground impact simulations were performed using a FE model of a mid-sized SUV in LS-DYNA, with the three kinetic energies each varied between a higher and lower value. Only vertical kinetic energy was found to be a significant predictor of peak roof deformation ($p=0.002$), while none of the kinetic energies were a significant predictor of peak reaction force. Further, peak reaction force was not a significant predictor of peak roof deformation.

From the results of the three studies, it was hypothesized that ranking vehicles solely by peak SWR is not an optimal assessment of roof strength, and a more appropriate metric would be based on energy absorption. Two additional simulations were performed on a reinforced version of the FE vehicle which demonstrated that an 11% increase in the normalized energy absorption of the structure reduced deformation in a rollover crash simulation by 5%, whereas a 20% increase to peak SWR had no effect. This lead to the conclusion that an increase in the peak SWR of a vehicle will not reduce deformation if it is not accompanied by a similar increase in energy absorption. Therefore, it is recommended that an energy absorption criterion be added to FMVSS 216.

Table of Contents

Introduction

The Problem

Vehicle rollover crashes are a serious public health concern in the United States with far reaching socioeconomic impacts. Rollovers, occurring in only 3% of crashes, account for a disproportionately high number of the serious traffic injuries and fatalities, 30% in 2008 (NHTSA, 2010). The problem is worse in some types of vehicles, as rollover accounts for 59% of deaths in SUV's as opposed to 25% in passenger cars and minivans (IIHS, 2008). The most effective way to combat rollover injury and death is to prevent vehicles from rolling over at all. Newer technologies like electronic stability control (ESC) have been shown to reduce the number of rollover crashes, particularly single vehicle crashes that result in fatality (Aga, 2003). Also, vehicles are given a static stability factor that compares the height of the CG to the width of the wheelbase to predict how easily a vehicle is to rollover (Boyd, 2005). However, structural crashworthiness remains an important aspect to preventing occupant injury in the event of a rollover.

Rollover Injury Controversy

Epidemiological studies from national crash databases have investigated which factors increase the probability of serious injury and fatality during rollover. Several key factors have been identified as increasing the risk of a severe (AIS 3+) injury including occupant ejection, lack of seat belt use, roof crush, far-side seating position, vehicle type, age and sex of occupant (Parenteau, 2000; Digges and Eigen, 2003; Moore, 2005; Padmanaban, 2005; Conroy, 2006; Gloeckner, 2006; Parker, 2007; Viano , 2007; Mandell, 2010). The National Highway Traffic Safety Administration (NHTSA) has focused on preventing roof crush to reduce occupant injury risk based on a retrospective analysis of rollover crashes. A relationship between roof intrusion (or deformation) and injury severity was found that predicts a fivefold increase in injury risk when negative residual headroom results from a rollover (Austin, 2005; Strashny, 2007). A subsequent study, looking at specific injuries outcomes, concluded that roof crush over the occupant's seating position of more than 15 cm was associated with a 6-7 fold increase in the rates of fatality and cervical spine injury compared to cases with less than 3 cm of roof crush (Funk, 2012).

Correlation, however, does not prove that occupant injury is caused by roof intrusion. There is an on-going debate in the literature about occupant injury mechanisms in a rollover crash, and what role roof crush plays in the outcome. Biomechanical analyses have focused primarily on cervical spine injuries, which are infrequent but catastrophic events for the occupant. Dynamic testing of ATD's in rollover have found that peak neck load is often achieved before significant roof crush occurs, which has led numerous authors to conclude that neck loading cannot be prevented by strengthening the vehicle roof (Orlowski, 1985; Bahling, 1995; Moffat, 2003; Croteau, 2010). Other researchers have concluded that structurally weak roofs are the primary cause of serious head, face, and neck injuries to non-ejected occupants in rollovers (Friedman, 2001; Friedman, 2003). Epidemiological and computational studies have suggested that factors influencing head/face injury risk are different from factors that influence neck injury risk, which indicate the injury mechanisms of head/face and neck injuries are different (Atkinson, 2004; Hu, 2007).

Dynamic Deformation

Previous association of injury to roof deformation through crash database analyses was based on the residual deformation of the vehicle measured by crash investigators after the event, and not on the dynamic intrusion during the rollover impact. Structural restitution of the roof during unloading has been demonstrated in rollover tests, with peak intrusion levels that were up to 50% larger than the residual deformation (Friedman, 2007; Croteau, 2010). The documented methods to record dynamic roof displacement during rollover testing were insufficient in their ability to track 3D, multi-point surfaces (Croteau, 2010; Mattos, 2013). Multi-point tracking allows for identification of peak deformations within an area, and 3D tracking provides the direction of deformation instead of simply the magnitude. Existing photogrammetric processing methods that produce full strain field data have been used in material characterization tests (Heinz, 2010), and could be adapted to fulfill this need in rollover research. Understanding the dynamic time histories of deformation can be an enabler in examining the mechanism of rollover-crash induced injuries, studying the relationship between roof deformations and occupant injury metrics, and validating vehicle finite element model predictions.

Vehicle Crashworthiness Evaluation

Regardless of the debate over the relationship between roof crush and occupant injury, Federal Motor Vehicle Safety Standard (FMVSS) 216 requires a minimum level of roof strength in passenger vehicles. Introduced by NHTSA in 1971, and subsequently updated in 2009, it is currently the only federal safety standard in the United States governing vehicle crashworthiness in rollover. The standard's stated goal is to "reduce deaths and injuries due to the crushing of the roof into the passenger compartment in rollover accidents" (Office of the Federal Register, 1971). The standard established a quasi-static testing procedure where a flat platen is pushed at a constant rate of 0.5 in/s into the roof structure at a 25° roll angle, and a 5° pitch angle. Each vehicle is required to produce a reaction force of 3.0 times its weight (strength-to-weight ratio SWR≥3.0) within the first 5 inches of platen displacement (NHTSA, 2006). NHTSA estimated that the latest (2009) revision to FMVSS 216 will save 135 lives from the recorded 10,000 yearly rollover fatalities (Office of the Federal Register, 2009). The Insurance Institute for Highway Safety (IIHS) performs an almost identical test, where an SWR of 4.0 is required to receive a "good" rating (IIHS 2012). The IIHS tests each vehicle to a full 10 inches of platen displacement, but only count the peak reaction force within the first 5 inches of crush. An IIHS study examining rollover crash injury data determined an association between vehicle roof strength and occupant injury risk, and predicted a 20-25% reduction in the risk of serious injury in rollover for each unit increase in SWR (e.g., from 2.0 to 3.0) (Brumbelow, 2009).

To examine vehicle response to dynamic rollover loading, researchers have performed tests in a variety or manners including vertical drop tests (Batzer, 2005; Mao, 2006), unconstrained dolly tests (Chou, 2005), and full-scale dynamic test systems (Moffat, 2003; Friedman, 2009; Kerrigan, 2011). The arguments against these methods to replace the static procedure have been a lack of repeatability, insufficient dummy biofidelity, the absence of injury criteria and accurate distributions of injuries for occupants (Office of the Federal Register, 2009). The University of Virginia (UVA) Center for Applied Biomechanics (CAB) developed, fabricated, installed, and has been using a new test fixture aimed specifically at generating repeatable test results in controlled rollover crash tests performed inside a laboratory. The CAB's Dynamic Rollover Test System (DRoTS) simulates translational motion with a moving road surface and constrains the vehicle roll axis to remain fixed in a plane during one roof-to-

ground impact (Kerrigan, 2011). It has been used to investigate the structural performance of vehicles, ATD biofidelity, and repeatability in dynamic rollover testing. The DRoTS allows researchers to input a set of touchdown parameters that govern the kinematic condition, and thus the energy, of a vehicle at the initiation of roof-to-ground contact. At the moment of touchdown during a vehicle rollover event, three velocities describe its kinetic energy: vertical velocity, translational velocity, and rotational velocity. When the roof impacts the ground, some kinetic energy is dissipated through structural deformation, some is dissipated through frictional forces between the vehicle and the ground, and some is transferred between the three velocities. The amount of energy dissipated through structural deformation is related to the magnitudes of force and deformation, and their relationship (energy is the integral of the force-deformation curve).

Finite Element Simulation

In addition to experimental testing, finite element simulation has been a successful research tool to investigate vehicle structural integrity in rollover impact loading. Due to the dramatically reduced expense compared to full scale experimental testing, a large number of simulations can be run to study the statistically significant sensitivities of the structure to input parameters and initial touchdown conditions. Previous rollover FE studies have looked at the sensitivity of vehicle deformation and kinematic response to a variety of input parameters and have determined that roll angle, pitch angle, and drop height (vertical kinetic energy) have a significant effect on structural deformation in dynamic simulations (Tahan, 2010; Parent, 2011). Other studies have focused on simulating variations to the FMVSS 216 and IIHS roof strength evaluation tests, to determine vehicle specific conditions that result in the lowest reaction force (Mao, 2005; Tahan, 2010).

FMVSS 216 Criticism

The FMVSS 216 and IIHS roof strength evaluations have been criticized for being quasi-static tests that do not accurately represent vehicle structural response to a real-world dynamic rollover (Mao, 2006; Friedman, 2007; Grzebieta, 2010). The loading vector in the FMVSS 216 test is constant, and does not vary with time as it would for a rolling vehicle interacting with the ground. The tests only specify one combination of roll and pitch angles, which are not necessarily the worst case loading for a given roof structure (Mao, 2005; Mohan 2008). The high strength steel commonly used in vehicle greenhouse design has been found to have rate sensitive properties, with an estimated 8-20% increase in yield strength for different grades of steel for a two order of magnitude increase of strain rate (Shi, 1992; Yan, 2003). The loading rate (0.0127 m/s) is at least two orders of magnitude below what is observed in dynamic roof-to-ground impacts (~1.5 m/s) (Friedman, 2001), which suggests that a quasi-static test may not capture the loading rate sensitivity of modern vehicle structures.

Irrespective of the shortcomings of the quasi-static test procedure, NHTSA has supported the choice of peak SWR as the metric to evaluate roof strength based on a retrospective analysis of rollover crashes, roof deformations, and vehicle SWR's that showed a relationship between increased vehicle SWR and decreased vertical roof intrusion in real-world rollovers (Austin, 2010). The study found SWR to be a statistically significant predictor of vertical deformation, with a 1.0 increase in SWR predicting a 5.6 cm reduction in intrusion. It is assumed that the logic behind the use of the peak SWR metric to evaluate roof strength is that at a given energy level, the force must increase to reduce the amount of deformation. However, the deformation does not only depend on the peak value of force (a single point on the force-deformation curve), but on the entire time history of both variables. FMVSS 216 is not a constant energy

test for each vehicle as the platen inputs a constant deformation and the amount of absorbed energy is a function of the time history of force, and not the peak force. Researchers have argued that solely attaining a level of peak force (or SWR) is not a useful indicator of roof crush resistance performance because the peak forces often drop significantly due to breaking glass and other structural failures, and instead have recommended an energy absorption requirement in order to prevent roof collapse after initial peak forces are attained (Office of the Federal Register Comments, 2009). This assessment is in agreement with findings from the 2009 IIHS study, where a normalized energy absorption criterion (equivalent drop height - EDH) predicted up to an additional 37% reduction in occupant injury risk over peak SWR at 5 inches of platen displacement for passenger cars (Brumbelow, 2009). Despite this recommendations and finding, the FMVSS 216 rule still relies on only a peak force to determine vehicle crashworthiness ratings in rollover.

Thesis Summary

This research thesis represents a collection of three studies performed between 2011 and 2013 at the University of Virginia Center for Applied Biomechanics in Charlottesville, VA. The general focus was to examine the relationships between reaction force, energy, and structural deformation in vehicle rollover crashes. While the debate over whether the relationship between roof crush and injury risk is causal or correlational has not been settled, this thesis did not enter this argument and remained focused on topics surrounding roof crush/intrusion/deformation. It incorporated three full-scale dynamic vehicle experiments performed on the DRoTS, with one dynamic drop test and two full rollover tests. In addition, FE simulation was used to augment findings and evaluate hypotheses developed from the limited number of experimental tests.

Goals

1. Implement and validate an approach to record 3D, multi-point, dynamic roof deformation time histories during rollover tests.
2. Determine whether the difference in loading rate between a quasi-static test (FMVSS 216) and dynamic drop test (DRoTS) changes the force-deformation response of a vehicle's roof structure.
3. Quantify the effects of variations in touchdown conditions on vehicle kinematic and deformation response for two replicate full-scale dynamic rollover tests.
4. Characterize the relationship between the kinetic energy of a vehicle at touchdown, and the force-deformation response through finite element simulation.
5. Demonstrate the application of supplementing FMVSS 216 with an energy-based criterion in reducing vehicle deformation.

Hypotheses

When a vehicle is subjected to a roof-to-ground impact in a rollover crash, the greenhouse structure undergoes deformation as a result of forces transmitted from the ground to the car. The magnitudes of these forces and deformations are related by the amount of energy absorbed by the vehicle structure. For a given vehicle in a single dynamic roof-to-ground interaction, it is hypothesized that:

- The dynamic force-deformation response will be stiffer than the quasi-static response.
- Greater total kinetic energy at touchdown (regardless of distribution) will result in larger structural deformation.

- Peak force will not be a significant predictor of deformation.
- An Increase in the peak SWR of the vehicle will not reduce deformation if it is not accompanied by a similar increase in energy absorption (equivalent drop height).

The following three studies were designed to fulfill the goals and evaluate the hypotheses outlined above. This thesis will show that ranking vehicles based only on peak SWR (FMVSS 216) is not an optimal assessment of roof strength. Including an energy criterion to the existing quasi-static test evaluation would ensure more robust roof designs.

Study I – Optical Measurement of High-Rate Dynamic Vehicle Roof Deformation during Rollover

Abstract

The goals of this study were to examine the dynamic force-deformation and kinematic response of a late model van subjected to an inverted drop test and to evaluate the accuracy of three-dimensional multi-point roof deformation measurements made by an optical system mounted inside the vehicle. The inverted drop test was performed using a dynamic rollover test system (Kerrigan et al., 2011 SAE) with an initial vehicle pitch of -5 degrees, a roll of +155 degrees and a vertical velocity of 2.7 m/s at initial contact. Measurements from the optical system, which was composed of two high speed imagers and a commercial optical processing software were compared to deformation measurements made by two sets of three string potentiometers. The optical and potentiometer measurements reported similar deformations: peak resultant deformations varied by 0.7 mm and 3 ms at the top of the A-pillar, and 1.7 mm and 2 ms at the top of the B-pillar. The top of the vehicle B-pillar sustained peak resultant deformation of 146.2 mm 116 ms after contact, and unloaded to 77.1 mm (47% of peak) at 291 ms. Peak reaction forces at contact were approximately 100 kN, and the force-deflection response between the drop test and the IIHS roof crush test on the same make and model vehicle showed comparable dynamic and quasi-static stiffness. The results presented in this study showed that the optical system can be used to measure dynamic roof deformations, in three dimensions, at high rates, across a large area of the vehicle structure, from inside a vehicle subjected to rollover crash test.

Introduction

Multi-point deformation information can be an enabler in validating vehicle finite element model predictions, examining the mechanism of rollover-crash induced injuries, and studying the type of relationship between the timing, location, and magnitude of roof deformations and occupant injury metrics. Previous research has presented roof deformation measurement techniques using string potentiometers and videogrammetry during multiple rollover events [2]. However, the methods are not described in detail, the results are only presented for single points, and the two techniques are not compared to each other or any other independent deformation measurement technique.

The goal of this study was to evaluate the accuracy of measurements made with a three-dimensional multi-point optical deformation measurement system in a high-rate deformation experiment. The optical approach relies on the principles of stereo videogrammetry to accurately produce three-dimensional displacement time histories for a high resolution multi-point surface. Combined with vehicle kinematics and ground reaction force time histories, the optical output could provide a powerful tool for validating vehicle finite element roof structural models as well as occupant injury metrics. To achieve these goals, an inverted vehicle drop test was performed on a late model passenger van using the University of Virginia Center for Applied Biomechanics' Dynamic Rollover Test System (DRoTS) [5]. For this test, the vehicle roll drives and sled propulsion were disabled. The test parameters were chosen to mimic the loading that occurs in the IIHS roof strength evaluation (similar to the FMVSS 216 test), to allow for a force-deflection comparison between dynamic and quasi-static roof loading conditions on the same make and model vehicle.

Deformation measurement was focused on the passenger side roof rail between the A-pillar and B-pillar, as this was the point of initial roof to ground contact and anticipated location of maximum deformation. Two methods were used to measure the three-dimensional deformation time history of the vehicle roof structure. The optical system utilized two on-board high speed imagers and optical processing software. The second method, based on string potentiometer trilateration, was implemented at two discrete points on the A-pillar and B-pillar to validate the optical system's results. The resultant and component displacements for the A-pillar and B-pillar points were compared against the optical system's output for the same locations.

The optical system incorporated ARAMIS v6 2.0 (GOM Optical Measuring Techniques), a commercially available optical measurement software package. ARAMIS utilized digital images to analyze and report three-dimensional material deformations along with the surface coordinates of points, displacements and velocities, and strain values and rates.

Methods

Test Conditions

The vehicle's as tested mass was 1911.9 kg. The initial conditions for the vehicle were a pitch angle of -5 degrees (front end down), a roll angle of +155 degrees (passenger side impact), and a drop height of 0.398 m (total vertical motion of CG prior to impact), (Figure 1). This produced a 2.706 m/s vertical velocity at contact. Unpublished finite element analysis results suggested that peak reaction force from this drop height would be approximately equal to the peak force achieved in the IIHS roof strength evaluation with the same vehicle.

Figure 1. Initial vehicle orientation for the drop test

The IIHS roof strength evaluation, the quasi-static test on the vehicle used for comparison, consisted of a roof crush test to one side of the vehicle. The test system utilized an upright assembly with attached

loading platen fixed at 25 degrees roll and 5 degrees of pitch [4]. The vehicle roof was crushed to a minimum of 127 mm of platen displacement at a nominal rate of 5 mm/s. Force and displacement data were reported at 100 Hz for the test.

Vehicle Preparation

The vehicle's overall mass and wheel distributions were measured upon delivery at UVA as the test goal weight, and monitored throughout the preparation and installation process. The vehicle fluids were drained and the seats, floor liners, roof liners, and curtain airbags were removed to allow for instrumentation installation. Steel plates were bolted to the vehicle floor to act as mounting locations for instrumentation and data acquisition equipment (Figure 2). A contact strip sensor was taped on the roof in the location of anticipated initial roof-to-ground contact as a trigger. The passenger side interior structural surfaces were painted with a stochastic pattern of black dots, 6 to 12 mm diameter with approximate 40-50% coverage of the patterned area, on a white background to accommodate the optical system.

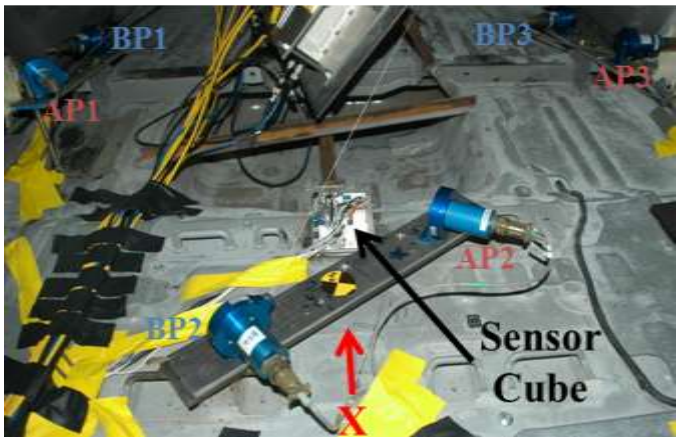

Figure 2. Instrumentation mounting plates and sensor cube installed location on the floor pan of the vehicle

The DRoTS cradle [5], which consisted of two vertically oriented steel tubing towers at the front and rear, connected by a set of telescoping steel tubes 5" in diameter, was installed on the vehicle to fix the location and orientation of the vehicle's roll axis relative to the vehicle (Figure 3). It is about this roll axis that the DRoTS fixture rotates the vehicle in a typical rollover crash test (disabled for this test). Once installed, the telescoping tube ran under the vehicle body from the front to the rear and the towers were oriented perpendicular to the ground. The towers of the cradle were fixed to the vehicle frame rails in the front and rear of the vehicle by removing the fascia and bumper beams and using custom hardware to rigidly connect the towers to the locations where the bumper beams interfaced with the vehicle frame rails. The cradle assembly was centered (left-right) between the bumper beam/frame rail connections at the front and rear of the vehicle. For simplicity, the cradle was installed such that the tube was oriented parallel with the ground when the vehicle was resting on its own suspension/tires, at the curb weight condition. The DRoTS fixture was designed to hold the vehicle cradle in such a way that the vehicle roll axis was parallel to the cradle. Once the vehicle was loaded in the test fixture, the location of the roll axis relative to the vehicle and cradle was adjusted vertically until the roll axis passed through the center of gravity (CG) of the vehicle. If the vehicle CG was not aligned in the center of the frame rails (left-right) then

ballast weight was added to one side to ensure alignment. At the completion of the balancing procedure, the vehicle would not continue to rotate in either direction after being manually rotated and stopped at 45 degree intervals from 0 to 360 degrees. After this adjustment was completed the exact location of the roll axis could be identified from a single marker point at the very front and rear of the cradle.

Figure 3. DRoTS cradle installation on front of vehicle

Force and Kinematics Measurement Sensors

The vehicle was outfitted with an inertial measurement cube containing three accelerometers (Endevco 7290E-30, Meggitt Sensing Systems, San Juan Capistrano, CA) measuring accelerations about the sensor cube's local x, y, and z component directions. Additionally three angular rate sensors were included measuring angular velocities about the same local sensor cube axes (DTS ARS-1500, Diversified Technical Systems, Seal Beach, CA) for the x direction, and two (DTS ARS-300, Diversified Technical Systems, Seal Beach, CA) for the y and z directions. The sensor cube was mounted on the floor of the vehicle, on the lateral center line (Figure 2). The DRoTS roadbed was instrumented with twenty-four uniaxial load cells, spaced evenly across the surface, and oriented to measure in the vertical direction (global Z'). Two accelerometers measuring in the vertical Z' direction were mounted to the underside of the wood surface at the left-front corner and right-rear corner of the center section of the roadbed.

Deformation Measurement Sensors

The passenger side A-pillar and B-pillar were both instrumented with a set of three string potentiometers of 2159 mm maximum travel (Firstmark Model 62, Firstmark Controls, Creedmoor, NC). Two mounting plates (25 x 50 mm) were constructed out of steel stock. To each plate, a single screw and a triax accelerometer were attached (Entran Triax EGAXT3, PandAuto Technology Co., Ltd). One of the two plates was mounted on the passenger-side A-pillar, at a location approximately 150 mm from the intersection of the A-pillar, roof rail, and windshield header. The second plate was mounted on the roof rail, approximately 100 mm forward of the B-Pillar roof rail connection (Figure 4).

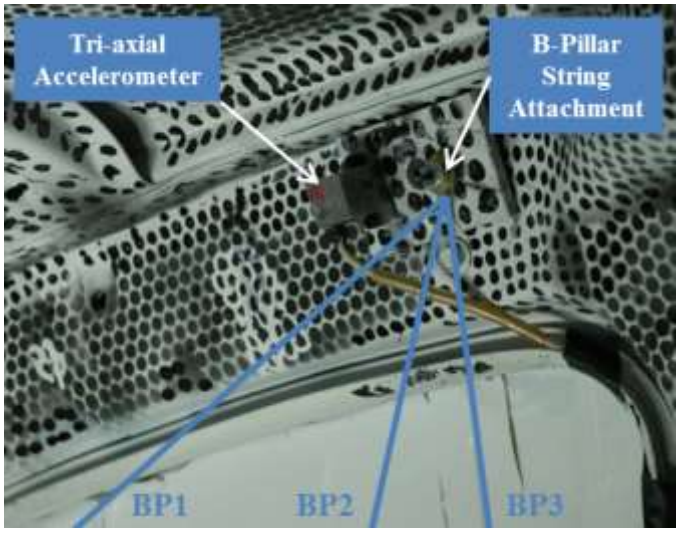

Figure 4. B-pillar string potentiometer attachment plate

The plates were fixed to the vehicle via a single screw inserted into existing threaded holes used for mounting the rollover curtain airbags. Rotation of each plate was prevented with a sharpened screw, inserted in the plate that was tightened against the vehicle interior at the mounting location. The strings from each of three string potentiometers were attached to the screw on each of the two plates (n= 6 string potentiometers). The six string potentiometers were affixed to the floor of the vehicle via rigid steel plates attached to the driver, right front passenger and second row seat mounting locations (Figure 5).

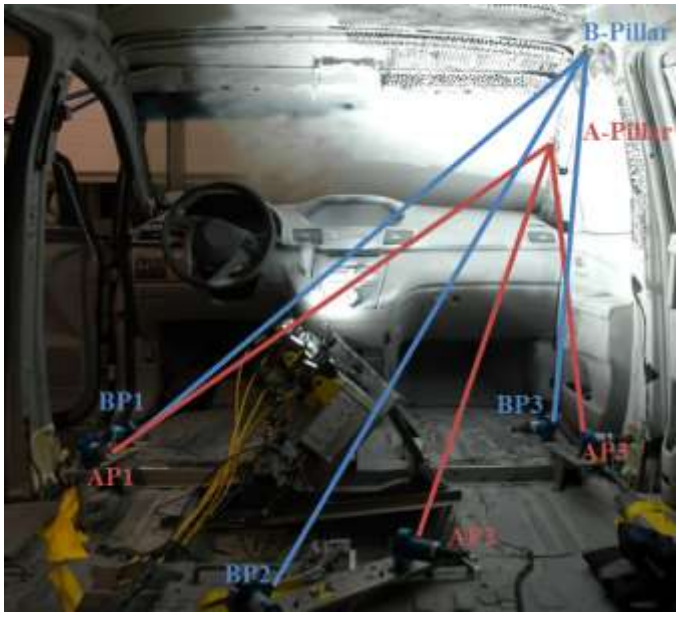

Figure 5. String potentiometer mounting and orientation

Optical System

The optical system was comprised of two high-speed imagers (NAC GX-1, NAC Image Technology, Simi Valley, CA) with 16 mm focal length ruggedized lenses (Schneider Optics, Hauppauge, NY). The

imagers were fixed at a 21 degree horizontal angle with respect to each other, and mounted on a rigid aluminum camera bar along with six high intensity LED, and two laser sights tracing the center pixel of each camera for visual alignment. The camera bar was bolted onto a steel framing structure that was welded into the vehicle floor at the front row seat mounting beam (Figure 6). In the mounted orientation, the cameras shared a focal intersection point 915 mm from the lenses, which was positioned 25 mm in front of the intersection of the vehicle passenger side roof rail with the windshield header (Figure 7). Sections of the roof, roof rail, A-/B-pillars, and windshield header above the passenger seat were included in the shared field of view.

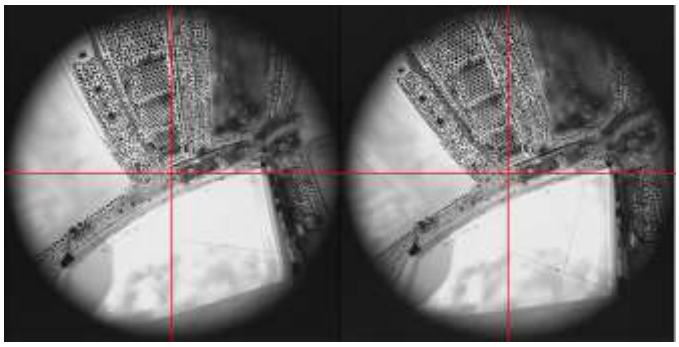

Figure 7. Images from the left and right cameras at t=0 ms, structure undeformed

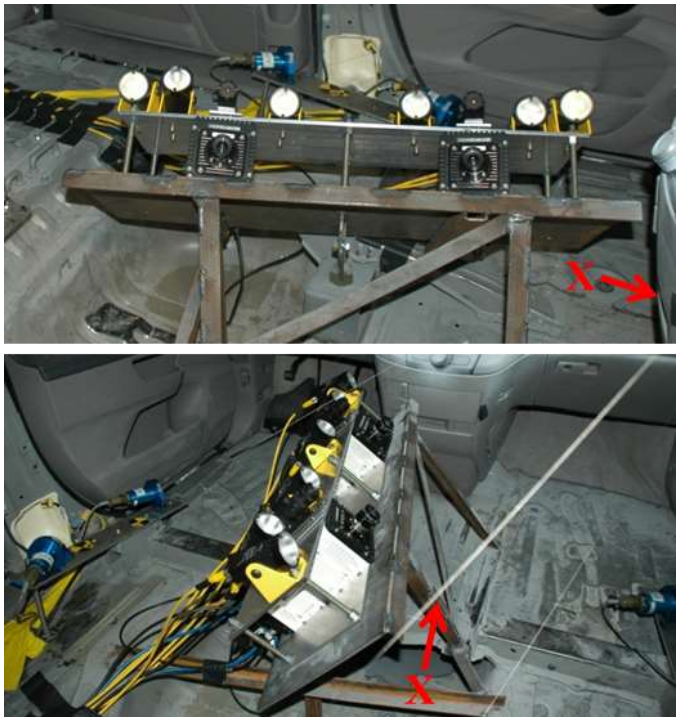

Figure 6. Optical system components and mounting structure on the floor pan of the vehicle

Coordinate Measurements

A coordinate measurement machine (CMM) (Titanium Arm, FARO Technologies, Lake Mary, FL) was used to determine the locations of the front and rear roll axis marker points, side door latch plates, wheel

centers, the inertial measurement cube origin and orientation markers, the locations of the string potentiometer attachment screw locations on the A-/B-pillars, the points where the strings come out of the potentiometer bases, the accelerometers mounted on the string attachment plates, and four points located in the view of the optical system. Since digitizing these points required moving the CMM around the exterior of the car, a series of overlapping points were taken in each measurement location, and each point cloud captured in each measurement location was aligned in a single coordinate system by singular value decomposition [3].

Data Processing

Kinematics Data Processing

All sensor data were filtered and debiased. Road load cells, vehicle accelerometers, and string potentiometers, were filtered to CFC60 and vehicle angular rate sensors were filtered to CFC180 [6]. For the purpose of calculating the angular accelerations necessary for determining vehicle CG kinematics from kinematics measured at the sensor cube, the angular velocity data were filtered with a Butterworth 4-pole zero-phase low-pass digital filter with a 25 Hz cutoff. Road loads were summed to determine total vertical reaction force. The time of initial vehicle to road contact was determined to within 1 ms from high speed video, and all time history data were time shifted so that t=0 corresponded with the time of initial vehicle contact with the road surface.

Once the CMM data point clouds were unified, vehicle local and global (inertial) coordinate systems were defined. A standardized SAE definition for the vehicle coordinate system was used [6]. The vehicle's positive X axis was defined by a vector directed from the rear roll axis point to the front roll axis point; the positive Y axis was defined by an average of vectors connecting similar points from the driver's side to the passenger's side door latch plates; and positive Z was determined by the cross product of X and Y vectors. These vectors were calculated in the CMM coordinate system and were used to define the rotation matrix $\mathbf{R}_{vehcmm}$.

The point cloud was then rotated from the CMM coordinate system to the vehicle local coordinate system by $\mathbf{R}_{vehcmm}$ and its origin was translated to the center of the line connecting the front and rear roll axis marker points. The front/rear right/left weight distribution was used, with the CMM-determined locations of the center of the wheels, to determine the location of the vehicle CG on the XY plane. Then the origin of the vehicle coordinate system was translated to the CG point.

The global (inertial) coordinate system was defined based on the sled system rails used to propel the roadbed. The roadbed motion was defined to travel in the positive X' (global) direction and the Z' axis was defined to be perpendicular to the test facility floor, with positive pointing downward. The global Y' axis was determined by the cross product of Z' with X'.

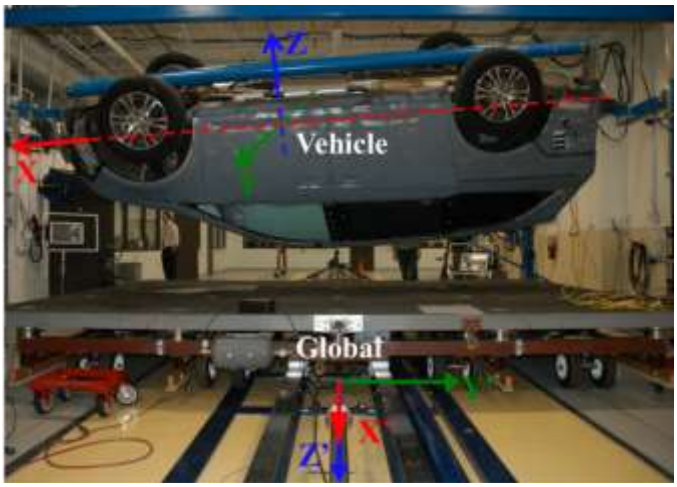

Figure 8. Vehicle local and global (inertial) coordinate systems

To transform the sensor cube kinematics measurements to the vehicle local and global (inertial) coordinate systems rotation matrices defining the relationships between these frames had to be identified. The transformation between the sensor cube and vehicle local coordinate system $\mathbf{R}_{vehcube}$, which remained constant throughout the test, was determined from the set of sensor cube orientation points captured with the CMM. Sensor accelerations and angular rates were transformed to the vehicle local coordinate system by $\mathbf{R}_{vehcube}$.

To calculate vehicle kinematics in the global reference frame, the time history of the transformation $\mathbf{R}_{globalveh}$ relating the vehicle local system to the global system was determined. Beard and Schlick formulated a method to update the matrix $\mathbf{R}_{globalveh}$ at each time step using only local frame angular velocity measurements [1]. The details of this method are presented concurrently with this study (Kerrigan et al. 2013, SAE).

Before transforming the acceleration data from the sensor cube to the local coordinate system using $\mathbf{R}_{vehcube}$, the sensor accelerations were corrected for the effect of gravity. Global acceleration time histories were then calculated by transformation of vehicle frame acceleration (at the vehicle CG) time histories by the $\mathbf{R}_{globalveh}$ time history. Global velocities and displacements were determined by numerical integration of the global acceleration and global velocities, respectively.

String Potentiometer Trilateration

Data were sampled from the potentiometers at 10 kHz during the test. At each time step, 0.1 ms increments, the three-dimensional location of the A-pillar and B-pillar attachment points were solved for using a trilateration technique. For this process it is assumed that the intersection of the three points existed on the surface of three spheres with centers fixed at the locations where the strings come out of the potentiometers. It is also assumed that those string orientation points do not move relative to the vehicle CG and coordinate system during the test. For this analysis, a potentiometer coordinate system is defined to have its origin at the location of one of the points where the string exits the potentiometer sensor. The potentiometer x axis is defined to point in the positive direction such that a second string base is at a location (d, 0,0) and the third potentiometer lies in the +xy plane at a location (i,j,0). From

this the distance from each of the three pots (r1, r2, and r3) to the location of intersection of the three strings can be written as

$$r_1^2 = x^2 + y^2 + z^2$$
$$r_2^2 = (x-d)^2 + y^2 + z^2$$
$$r_3^2 = (x-i)^2 + (y-j)^2 + z^2$$

Rearranging the equations to solve for the unknown coordinates x, y, and z of the intersection point yields

$$x = \frac{r_1^2 - r_2^2 + d^2}{2d}$$
$$y = \frac{r_1^2 - r_3^2 + i^2 + j^2}{2j} - \frac{i}{j}x$$
$$z = \pm\sqrt{r_1^2 - x^2 - y^2}$$

The z coordinate, expressed as the positive or negative square root, can have zero, one, or two possible locations. The positive z location was chosen to locate the point above the vehicle floor. The resulting coordinate location time histories for the A-/B-pillar points were rotated into the standard vehicle coordinate system using the CCM data points.

Optical System Processing

Before installation into the vehicle, the optical system was calibrated in the ARAMIS software using a specialized calibration object from the manufacturer (GOM Optical Measuring Techniques). A measurement volume of 1280 mm by 1280 mm by 1175 mm was produced for the test. Images were captured at 915 by 915 pixel resolution, with an average initial focal length to the structure of 915 mm. Each pixel in the image corresponds to a 1.5 by 1.5 mm square on the vehicle surface. The black dots in the paint pattern corresponded to between 4 to 8 pixels in diameter on average. The imagers recorded synchronized frames at 3000 Hz for 800ms, 100 ms before the event and 700 ms after roof-to-ground contact.

The images were analyzed in ARAMIS at 1000 Hz, using every third frame in the series. ARAMIS recognizes the surface structure of the measured object in an image, and assigns 2D coordinates to the image pixels. For 3D measurements, two cameras are calibrated with the software to record synchronized images. ARAMIS uses photogrammetric methods to combine the 2D coordinates for each pixel, as observed from the left and right camera images, into a common 3D coordinate for the analysis. The software observes the deformation of the object through a series of images by discretizing each image into facets, unique square groupings of pixels, similar to finite elements used in computational analyses. The facets are identified by the gray level structure of the individual pixels within the facet. The software tracks the changing location of each facet throughout the image series to calculate the displacements and strains of the object's surface. The pixel size of each facet and the pixel step, overlapping area of adjacent facets, can be adjusted in the software and manually optimized for the analysis conditions including image resolution, geometric complexity of measured object, and desired resolution of the resulting strain and displacement fields. In order for the software to divide the images into recognizable facets, there must be sufficient variation of pixel gray scale on the object's surface. Surfaces that are

heterogeneous in color require the application of a stochastic paint spray or dot pattern to produce pixel variation.

A facet size of 20 pixels and a facet step of 10 pixels were used in the analysis. This provides an output of individually calculated points in a 10 by 10 pixel grid, equivalent to every 15 mm on the physical surface. Using the physical coordinate locations captured by the CMM and their corresponding locations in the ARAMIS software coordinate system, a transform was applied to the optical output to align it with the SAE vehicle coordinate system.

Results

Force and Kinematics

The peak sum total vertical force recorded by the roadbed was 98,754 N at 40.5 ms after touchdown (Figure 9). After the initial peak, the force time history shows oscillatory behavior of approximately 3 Hz, centered around 19,000 N which corresponds to the weight of the vehicle.

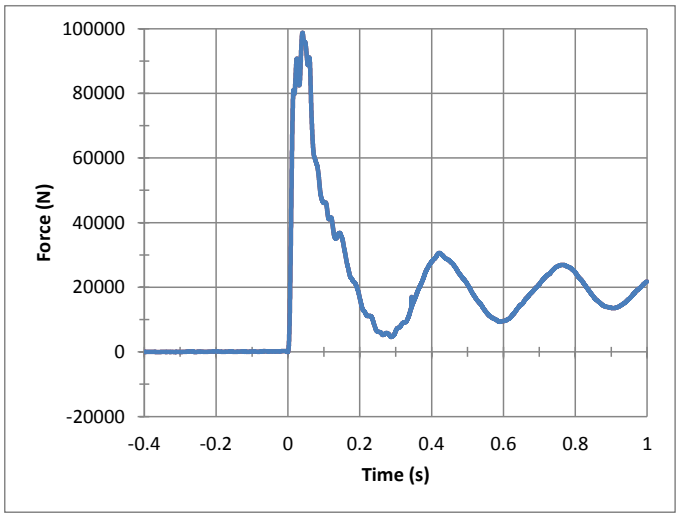

Figure 9. Roadbed sum total vertical force

The peak resultant global vehicle CG acceleration was 7.8 g at 10.9 ms (Figure 10). The peak for global X' acceleration was 7.2 g at 11.0 ms, the global Y' was 4.1 g at 14.9 ms, and the global Z' acceleration was -6.9 g at 24.8 ms. Global velocity resultant reached a maximum of 2.87 m/s at 15.8 ms. The peak global Z' velocity was 2.83 m/s at 9.4 ms (Figure 11). Global resultant displacement had a maximum of 0.566 m at 121.4 ms (Figure 12). The peak global Z' displacement was 0.563 m at 121.7 ms.

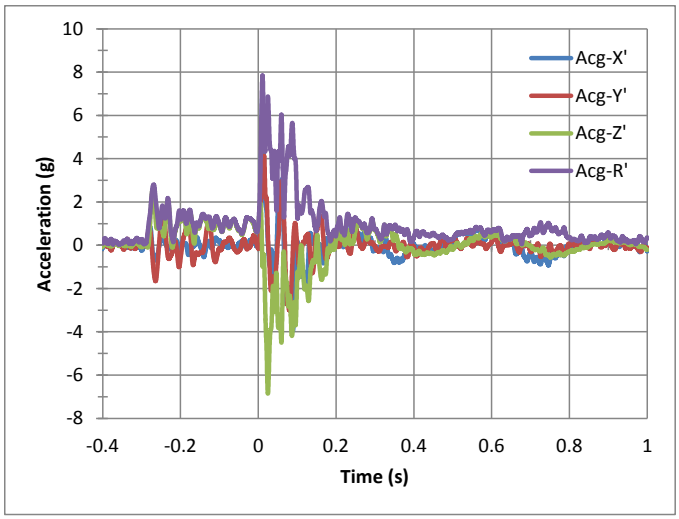

Figure 10. Vehicle CG global accelerations

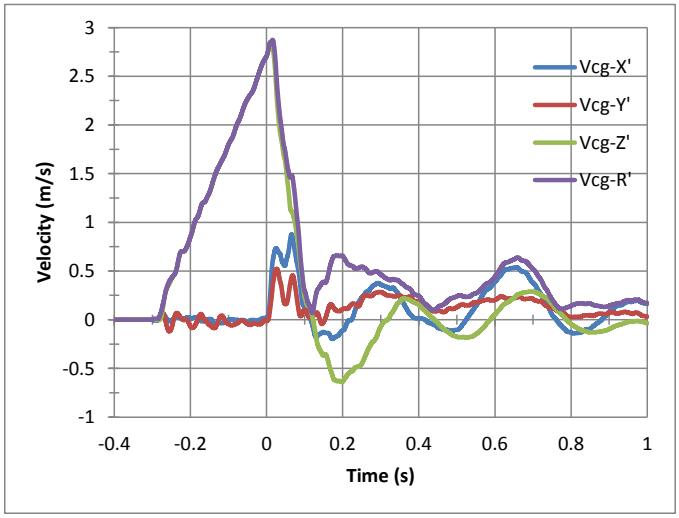

Figure 11. Vehicle CG global velocities

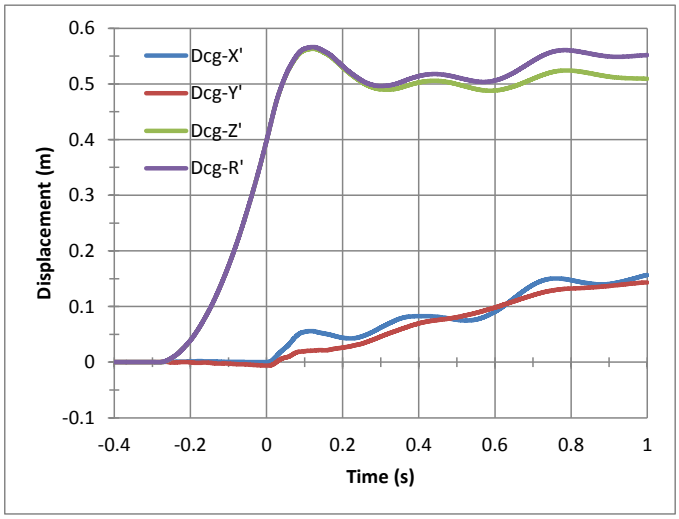

Figure 12. Vehicle CG global displacements

The maximum acceleration measured at the B-pillar was 31.1 g at 5.5 ms after impact, and at the A-pillar was 15.7 g at 7.4 ms (Figure 13). The accelerometers measure approximately 1 g before t=0, as the vehicle is falling under gravity.

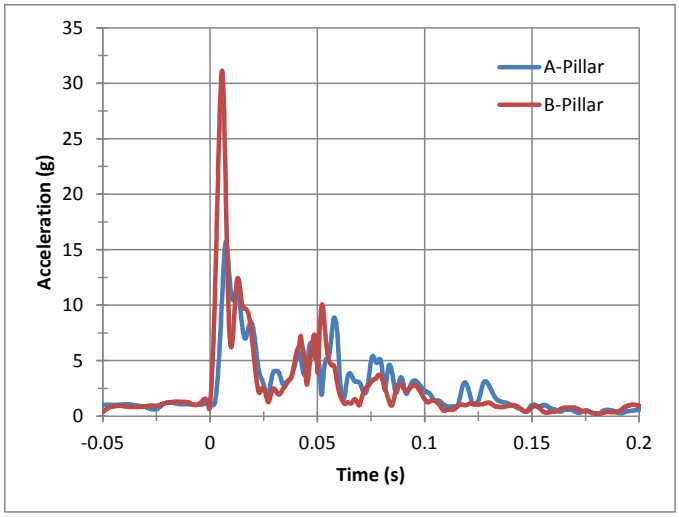

Figure 13. Resultant Acceleration at A-/B-Pillars

Roof Deformation Measurement

The peak resultant deformation reported by the optical system was 146.5 mm at the top of the B-pillar 116 ms after contact (Figure 14). The structure subsequently unloaded to a minimum resultant deformation value of 77.1 mm at 291 ms (Figure 15). This accounted for a 47.3% rebound, normalized by the peak deformation.

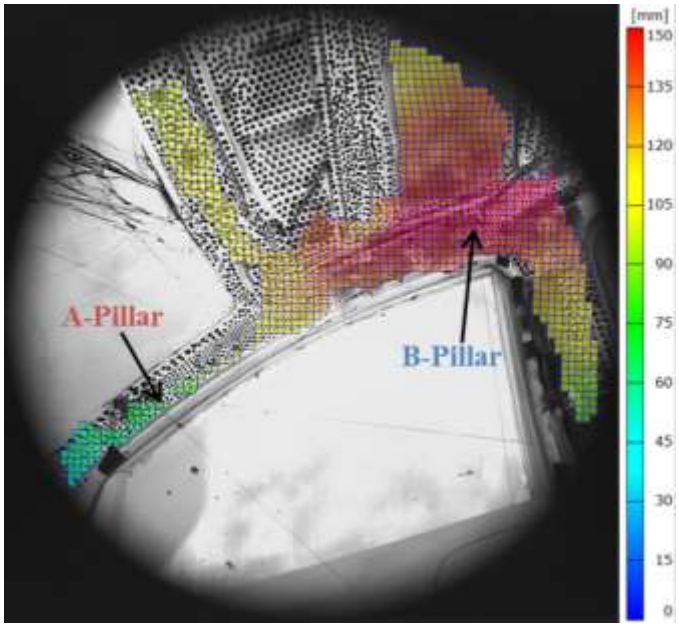

Figure 14. ARAMIS resultant displacement overlaid onto left camera image at t=116ms, maximum 146.2 mm

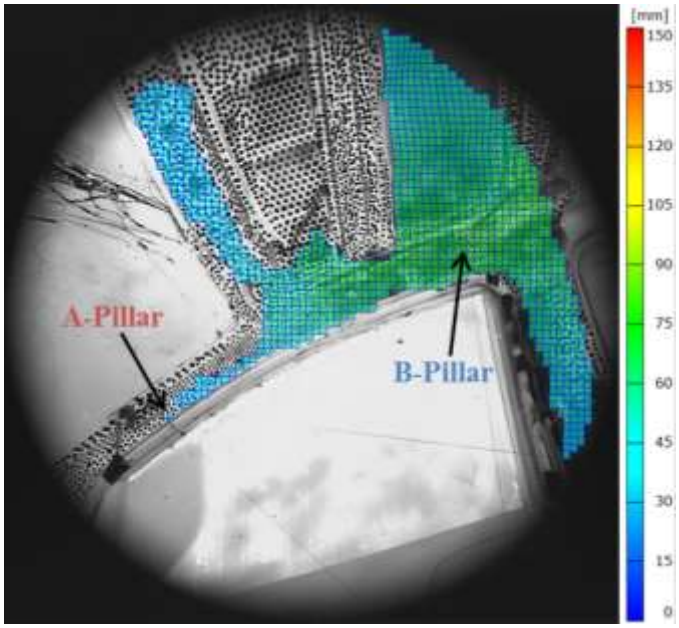

Figure 15. ARAMIS resultant displacement overlaid onto left camera image at t=291ms, maximum 77.1 mm

The maximum resultant deformation at the A-pillar was 87.9 mm at 123 ms reported by the optical system, and 88.6 mm at 121 ms reported by the string potentiometers (Figure 16). At the time of peak resultant, the component deformations reported by the optical system were -20.9 mm in the X, -81.4 mm in the Y, and 25.3 mm in the Z directions. The string potentiometers reported -48.6 mm in the X, -73.5 mm in the Y, and 9.5 mm in the Z directions.

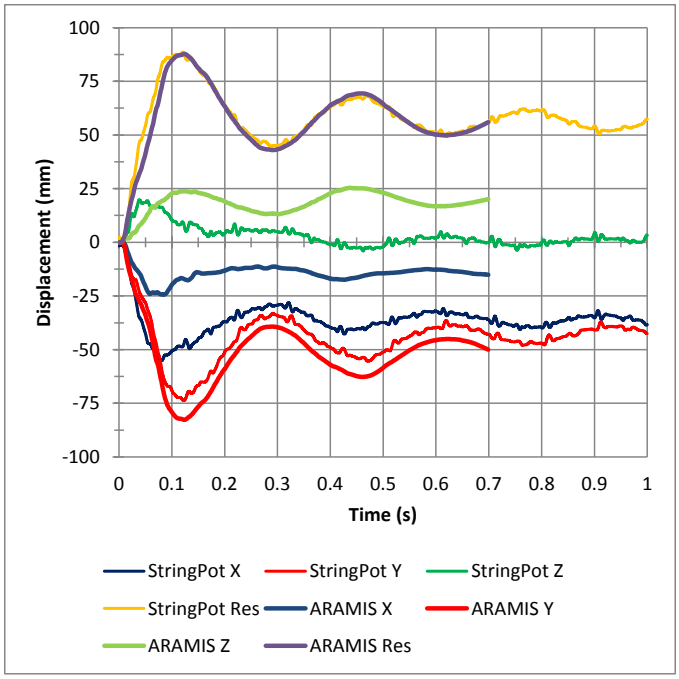

Figure 16. A-Pillar displacement comparison between String Potentiometers and ARAMIS output

The maximum resultant deformation at the B-pillar was 146.2 mm at 112 ms reported by the optical system, and 145.0 mm at 114 ms reported by the string potentiometers (Figure 17). At the time of peak resultant, the component deformations reported by the optical system were -24.1 mm in the X, -134.2 mm in the Y, and 52.8 mm in the Z directions. The string potentiometers reported -27.7 mm in the X, -132.3 mm in the Y, and 52.4 mm in the Z directions. The 3 Hz oscillation is also present in the roof deformation measurements at the A-/B-pillars.

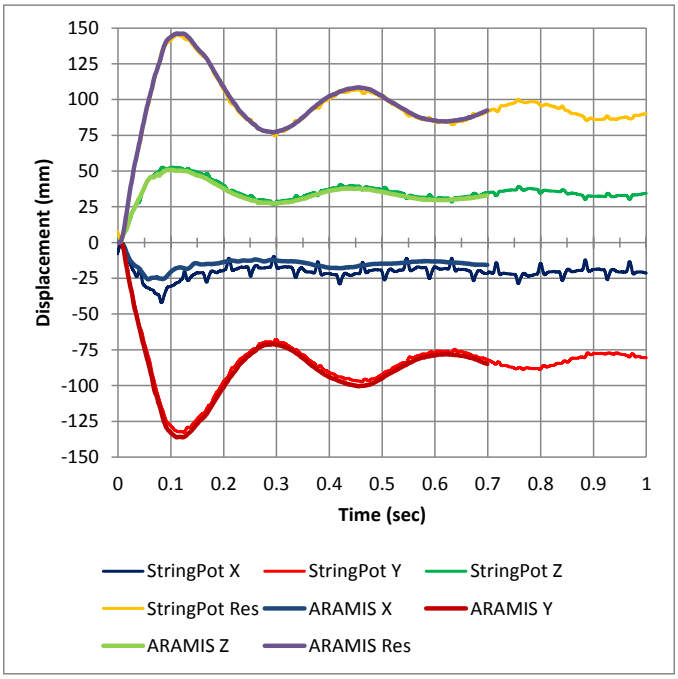

Figure 17. B-Pillar displacement comparison between String Potentiometers and ARAMIS output

The vehicle exhibited elastic rebound effects captured by the optical system (Table 1). The unloaded displacement values are taken from t=291ms when the first deformation minimum occurs after contact. The normalized rebound values are calculated by dividing the amount of deformation rebound (peak minus minimum) by the peak deformation.

Table 1. Optical displacements at the A-/B-pillars for times of maximum deformation and maximum unloading

	Peak Disp. (mm)	Time at Peak (ms)	Unloaded Disp. (mm)	Normalized Rebound
Ax	-20.9	123	-13.2	0.37
Ay	-81.4	123	-38.4	0.53
Az	25.3	123	13.9	0.45
Ar	87.9	123	42.9	0.51
Bx	-24.1	112	-15.4	0.36
By	-134.2	112	-69.9	0.48
Bz	52.8	112	28.6	0.46
Br	146.2	112	77.1	0.47

Force-Deflection

The maximum total sum force measured during the test at the roadbed of 98,754 N was reached at 48 mm of resultant deformation for the A-pillar, 67.5 mm of resultant deformation for the B-pillar, and at 96 mm of global vertical displacement of the vehicle's CG following initial roof-to-ground contact (Figure 18). The maximum force reached in the IIHS roof crush test for this same vehicle was 100,617 N at 85 mm of platen deformation.

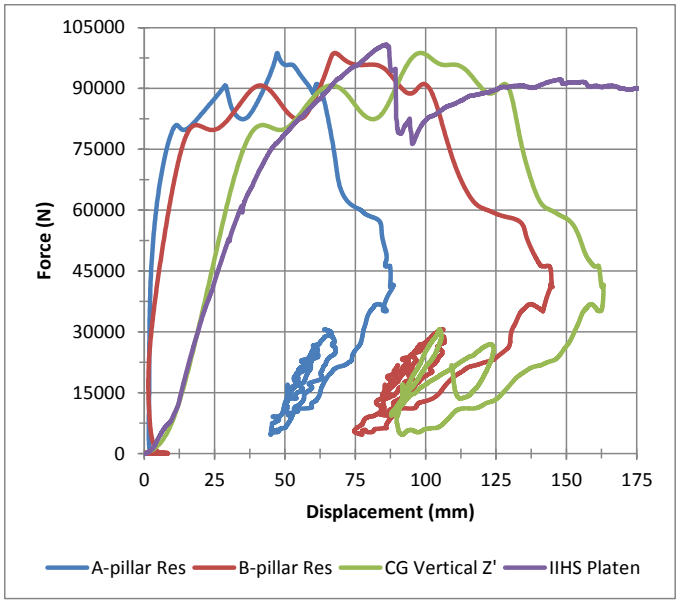

Figure 18. Force vs Deflection curves for the A-/B-Pillar resultants, CG global vertical Z displacement, and IIHS roof crush test

Discussion

Optical System

To successfully implement the optical deformation measurement technique on-board a dynamic test, the calibration and focal intersection of the stereo imagers must be maintained throughout image capture. With peak accelerations of around 8 g, it was imperative that the cameras be rigidly fixed with respect to each other as any divergent motion between the two cameras can cause error or total loss of results. A rigid connection to stiff structural members in the vehicle frame was designed to prevent rigid body motion of the camera beam with respect to the measured surfaces. In this test, the optical system maintained calibration between the two imagers during the vehicle-to-ground impact acceleration spike and subsequent vibrations. The nominal intersection deviation between the two imagers calculated by ARAMIS was 0.8 pixels, and did not change significantly during the impact. Some areas of complex geometry on the hat section roof stiffeners, and areas of significant buckling on the roof sheet were not tracked throughout the entire deformation.

Although the images were recorded at 3000 Hz during the test, they were processed at 1000 Hz in ARAMSIS to reduce computational expense and post processing effort. Due to the limited size of the ruggedized lenses used there was significant vignetteing of the images (Figures 7, 14, 15). The partially blocked view interfered with the software's ability to automatically match facets between the left and right images, requiring manual pairing for each time increment. Future tests should utilize the full image sensor chip to increase resolution and accuracy, while avoiding manual post processing. This was a limitation of the current study; however, it appears that 1000 Hz is sufficient to capture the fast rate deformation of a vehicle roof during an inverted ground contact.

Deformation Measurement Comparison

The string potentiometer attachment locations on the A-/B-pillars were chosen to be the existing curtain airbag tapped holes to minimize the installation's impact on vehicle structure. Due to geometric constraints on the vehicle interior, the string potentiometers were not mounted orthogonally in line with the vehicle coordinate axes, but rather to maximize the angle between the three strings to improve the accuracy of the trilateration technique (Figure 5). Orthogonal alignment is not necessary when utilizing trilateration; however it is imperative that the potentiometer bases are rigidly mounted to the vehicle structure so that they remain fixed in the vehicle coordinate system, and are assumed to not move relative to the vehicle CG. High speed video of the string potentiometers refuted concerns of string oscillations impairing the calculation, as only slight vibrations are apparent in the video and do not translate into the collected data signal. The oscillations in the string potentiometer signal (Figures 16, 17) are present before the drop initiates when the strings are not moving, and are attributed to signal noise.

The deformation time histories of the optical system and string potentiometer trilateration correlated well (Figures 16, 17). The resultant displacements at the A-/B-pillars for the two techniques matched almost exactly, reporting a difference in peak deformation of 0.7 mm and 2 ms at the A-pillar, and a 1.2 mm and 2ms at the B-pillar. The B-pillar component displacements were in good agreement between the two methods with the maximum difference of 13% occurring in the X direction.

Component Disagreement and Ongoing Testing

The lack of A-pillar component agreement was at first hypothesized to be related to a coordinate transformation error in the string potentiometer processing, as the resultant matched closely and the X and Y directions were in phase but differed in magnitude; however, no processing error was found. The same transformation that was applied to the A-pillar was applied to the B-pillar data, which matched between the two measurement methods. A second test on the same vehicle, a full rollover test with vehicle roll and roadbed translational velocity, was performed with the string potentiometers and optical system mounted in the same positions and orientations as the drop test. The output from the two systems produced matching resultants at the A-/B-pillars and components at the B-pillar, but again the component deformations at the A-pillar were in disagreement.

Subsequent full rollover testing on a different vehicle, utilizing the same data collection and processing methods detailed in this paper but with different mounting locations and orientations for the string potentiometers and the optical system, produced matching resultant and component outputs at both of the two compared locations. The discrepancy between the test described in this study and these other tests led to additional review of the drop test. After reviewing the video, it was determined that significant deformation occurs in the rocker rail where the AP3 string pot was mounted (Figure 19). The vertical

load was transmitted through the B-pillar to the rocker rail and vehicle substructure which deformed. The trilateration formulation assumes that the potentiometer bases are fixed relative to each other, so it is hypothesized that the movement of AP3 relative to the other two sting pots created the component errors.

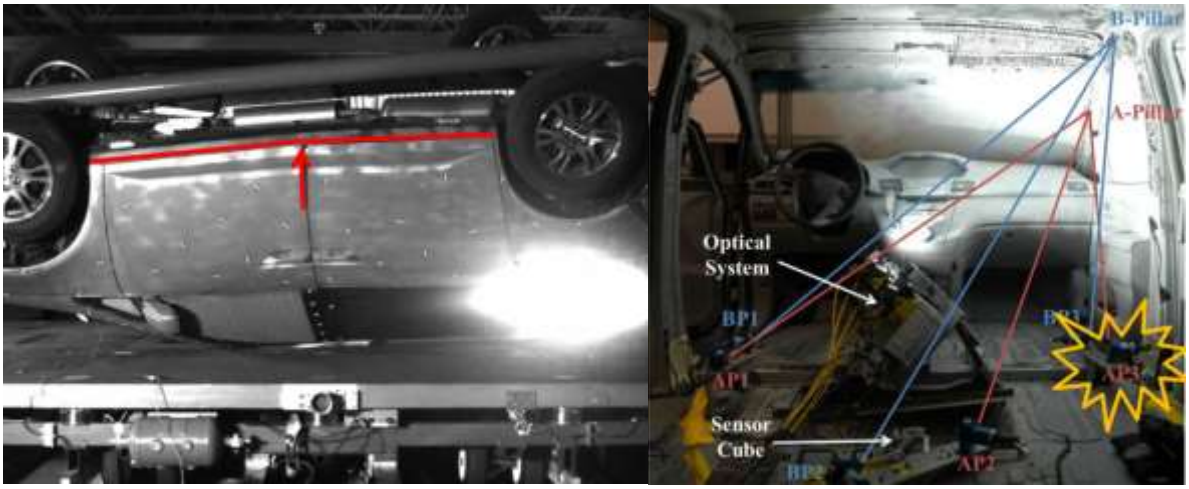

Figure 19: Vehicle frame deformation at the mounting location of string potentiometer base AP3.

In this case of the drop test's A-pillar component disagreement between the two measurement methods, the optical output is hypothesized to be the more accurate of the two methods for several reasons. Firstly, the optical component deformation curves along the roof rail between the A-pillar location (where a discrepancy exists) and the B-pillar (where the two measures agree) exhibited smooth continuity. The string potentiometer component contours did not match the deformation contours at any point on the vehicle structure. Secondly, the string potentiometers predicted over 50 mm of displacement in the X direction at the A-pillar, a value roughly double that of the highest predicted X component anywhere on the structure by the optical system. And thirdly, the string potentiometers predicted complete unloading back to 0 mm in the Z direction within 400 ms of contact in an area that retained measurable plastic deformation post-test.

As observed through the subsequent full rollover tests, the optical system was able to accurately track roof deformation when vehicle roll and sled translational velocities were added to the test conditions. The resulting multi-plane kinematics did not have a noticeable effect on optical recording and processing. It is hypothesized that the optical system would also perform accurately in a multiple roll event, such as the J2114 dolly rollover test, as long as airborne debris did not damage the imagers or obstruct the view of the measured surfaces. The imagers would need to have sufficient on-board memory available for recording the entire multi-roll event at high speed, exceeding the memory requirements for a single roll on the DRoTS.

Validation

Since the two independent techniques were in agreement for the A-/B-pillar resultants and B-pillar component deformations, and they utilized two very different deformation measurement strategies, the optical and string potentiometer systems were validated for the on-board use in high-rate vehicle deformation tests. While the component distribution of measurements was validated at the B-pillar, small differences at the A-pillar suggest that further analysis may provide greater certainty in the component

measurements of the string potentiometers. The optical system produced true multi-point component displacement fields for the vehicle structure, which is ideal for use in validating finite element models.

Component Deformations

Due to the +155 degree initial roll angle and -5 degrees pitch, the Z component of the force vector acting on the vehicle roof was 90.6% of the total force, whereas the Y component was only 42.3% of the total force, roughly half of the Z component. The majority of the loading vector is in the vertical direction; however, the component displacement results show the majority of deformation in the Y direction (Table 1). At the time of peak deformation, the Y component was 92.7% and the Z component was 28.8% of the resultant at the A-pillar. Similar results were recorded at the B-pillar with the Y component 91.8% and the Z component 36.1% of the resultant.

Quasi-Static and Dynamic Loading Comparison

The IIHS roof strength to weight ratio is calculated by dividing the maximum force prior to 127 mm of platen deformation during the quasi-static test by the measured curb weight of the vehicle. This ratio was reported as 5.15 for the tested vehicle. The dynamic strength to weight ratio was calculated from the drop test by using the peak sum total roadbed force (98,754 N) divided by the as tested weight of the vehicle (1911.9 kg * 9.81 m/s^2). The dynamic ratio was 5.27 for the tested vehicle. The force-deflection behaviors between the dynamic and quasi-static roof crush tests were also similar, with the peak force of the quasi-static test 1863 N larger, and the displacement at the time of peak force was 11 mm less (Figure 18). The global CG vertical displacement was used as the deformation measure in the dynamic test, as this was the most accurate analog for total platen deformation from the IIHS test. The vehicle exhibited a stiffness, the slope of the force-deflection curve, under dynamic deformation that is similar to that under quasi-static deformation. No significant rate effects were apparent in the comparison.

Future Research

Unfortunately, neither the optical or string potentiometer deformation measurement approach can be utilized in a vehicle with seated and belted ATD's, roof liners, and curtain airbags due to line of sight and physical string obstructions. This limits direct correlation of roof deformation time histories and occupant injury metrics. Ideally, a method to determine deformation time history that is compatible with simultaneous ATD injury testing could be developed, possibly using strain gauges installed on the vehicle structure behind the roof liner. Another potential approach, measuring roof deformation in one test and occupant injury risk in separate replicate test, is highly dependent on a precisely repeatable rollover test fixture.

Conclusions

This study evaluated the dynamic stiffness (slope of the force-deflection curve) of the tested vehicle as compared to the quasi-static stiffness under similar roof loading. The accuracy of deformation measurements made by an optical system mounted inside a vehicle subjected to dynamic loading was also evaluated against independent deformation measurements by string potentiometers.

The result of this study, validation of the optical system for use in recording multi-point high-rate vehicle deformations in a crash test, provided a methodology for multi-point motion tracking that may be a useful data collection tool in rollover crash testing. The optical system produced deformation data for a wide

area of vehicle structure, which is well suited for vehicle finite element model validation. Use of optical measurements shows promise as a data collection method for researchers studying the complex relationship between roof deformation timing, vehicle to occupant interactions, and injury mechanisms.

The string potentiometer trilateration approach was validated for providing resultant displacement time history of high rate deformation. High speed video of the string potentiometers refuted concerns of string oscillations impairing results.

The roof-to-ground loading vector for +155 degrees roll produced half the component force in the Y direction compared to the Z direction; however the vehicle structure had a majority of deformation in the Y direction.

The dynamic stiffness of the vehicle to roof loading was similar to the quasi-static stiffness, with limited rate dependence shown.

References

1. Beard, D. A., & Schlick, T. (2003). Unbiased Rotational Moves for Rigid-Body Dynamics. Biophysical Journal, 85, 2973-2976.

2. Croteau, J. et al., "Dynamic Response of Vehicle Roof Structure and ATD Neck Loading During Dolly Rollover Tests," SAE Technical Paper 2010-01-0515, 2010, doi: 10.4271/2010-01-0515.

3. Hanson, R. J., & Norris, M. J. (1981). Analysis of Measurements Based on the Singular Value Decomposition. Siam J. Sci. Stat. Comput., 2(3), 363-373.

4. Insurance Institute for Highway Safety, "Crashworthiness Evaluation Roof Strength Test Protocol (Version II)." October 2012.

5. Kerrigan, J., Jordan, A. et al., "Design of a Dynamic Rollover Test System," SAE Technical Paper 2011-01-1116, 2011, doi: 10.4271/2011-01-1116.

6. Society of Automotive Engineers (SAE), Inc., Instrumentation for Impact Tests. SAE J211/1 JUL2007, July 2007.

Study II – Characterizing the Effect of Touchdown Conditions in a Dynamic Rollover Test

Abstract

To quantify the effect of variations in touchdown conditions on vehicle kinematic and deformation response, two full-scale dynamic rollover tests using replicate mid-sized SUV's were performed on the University of Virginia Dynamic Rollover Test System (DRoTS). An on-board optical system was utilized to track the 3D, multi-point dynamic deformation of the interior roof structure for the two tested vehicles. The two tests used different sets of touchdown parameters (roll angles of 181° and 153°, roll rates of 228 and 244 deg/s, road speed of 4.5 and 7.5 m/s, drop heights of 401 and 66 mm) which created variations in vehicle orientation (one near-side, one far-side roof-to-ground contact) as well as in the total and distribution of initial kinetic energy. The maximum reaction forces occurred at similar roll angles (190° and 192°) as did the maximum deformations (200° and 202°). The two tests sustained similar peak roof deformations (149mm and 153mm) while the test with less total kinetic energy produced a larger peak reaction force (135kN vs 120kN). The total kinetic energy dissipated during the roof-to-ground impact of each test was similar (-20.7 kJ and -21.1 kJ) with the two vehicles absorbing similar amounts of energy to structural crush (10.7 kJ). Contrary to the results of previous FE simulation studies, the vehicle with the larger drop height did not sustain more deformation. The effect of the variations in rotational and translational energy on the vehicle deformation was inconclusive from these two tests. Therefore, it is recommended that a subsequent study utilize FE simulation to characterize the relationships between kinetic energy and vehicle force-deformation response in rollover.

Introduction

Currently in the United States, only Federal Motor Vehicle Safety Standard (FMVSS) 216 is used for evaluating vehicle crashworthiness in rollover crashes. This standard requires a minimum level of roof strength in passenger vehicles. Vehicle are evaluated through a quasi-static testing procedure where a flat platen is pushed at a constant rate of 0.5 in/s into the roof structure at a 25° roll angle, and a 5° pitch angle. Each vehicle is required to produce a reaction force of 3.0 times its weight (strength-to-weight ratio SWR≥3.0) within the first 5 inches of platen displacement (NHTSA, 2006). The FMVSS 216 roof strength evaluation has been criticized for being a quasi-static test that does not accurately represent vehicle structural response to a real-world dynamic rollover (Mao, 2006; Friedman, 2007; Grzebieta, 2010).

To examine vehicle response to dynamic rollover loading, researchers have performed tests in a variety or manners including vertical drop tests (Batzer, 2005; Mao, 2006), unconstrained dolly tests (Chou, 2005), and full-scale dynamic test systems (Moffat, 2003; Friedman, 2009; Kerrigan, 2011). The arguments against these methods to replace the static procedure have been a lack of repeatability, insufficient

dummy biofidelity, the absence of injury criteria and accurate distributions of injuries for occupants (Office of the Federal Register, 2009). The University of Virginia (UVA) Center for Applied Biomechanics (CAB) developed, fabricated, installed, and has been using a new test fixture aimed specifically at generating repeatable test results in controlled rollover crash tests performed inside a laboratory. The CAB's Dynamic Rollover Test System (DRoTS) simulates translational motion with a moving road surface and constrains the vehicle roll axis to remain fixed in a plane during one roof-to-ground impact (Kerrigan, 2011). It has been used to investigate the structural performance of vehicles, ATD biofidelity, and repeatability in dynamic rollover testing. The DRoTS allows researchers to input a set of touchdown parameters that govern the kinematic condition, and thus the energy, of a vehicle at the initiation of roof-to-ground contact.

At the moment of touchdown during a vehicle rollover event, three velocities describe its kinetic energy: vertical velocity, translational velocity, and rotational velocity. When the roof impacts the ground, some kinetic energy is dissipated through structural deformation, some is dissipated through frictional forces between the vehicle and the ground, and some is transferred between the three velocities. The amount of energy dissipated through structural deformation is related to the magnitudes of force and deformation, and their relationship (energy is the integral of the force-deformation curve).

This study was aimed at the performance of two full-scale vehicle rollover crash tests on the DRoTS. Instrumentation and data acquisition were focused on capturing detailed structural deformation and vehicle kinematic response data during the tests. The parameters from the first test were chosen to match the touchdown parameters from an unconstrained dolly rollover test performed previously, and the parameters in the second test were chosen to match the results of a reconstruction simulation utilizing a vehicle dynamics model that was matched to parameters from a real crash obtained from the United States National Automotive Sampling System – Crashworthiness Data System (NASS-CDS) database. An optical system, previously validated for a dynamic drop test (Lockerby 2013), was utilized to track the dynamic deformation of the interior roof structure for the two tests. The optical system provided multi-point displacement output to compare the roof deformation between two tests.

The goal of this study was to quantify the effect of variations in touchdown conditions on vehicle kinematic and deformation response for two replicate full-scale dynamic rollover tests. When a vehicle is subjected to a roof-to-ground impact in a rollover crash, the greenhouse structure undergoes deformation as a result of forces transmitted from the ground to the car. The magnitudes of these forces and deformations are related by the amount of energy absorbed by the vehicle structure. For a given vehicle in a single dynamic roof-to-ground interaction, it is hypothesized that greater total kinetic energy at the point of initial roof-to-ground contact (regardless of distribution) will result in larger structural deformation.

Methods

Test Conditions

Two vehicle rollover impact tests were performed on the University of Virginia Dynamic Rollover Test System (DRoTS) with replicate mid-sized SUV's. The first test performed in this study was designed to match a flat-dolly test, with the DRoTS programmed to give the test vehicle a -228 deg/s roll rate (driver's side leading) and a -181° roll angle. The DRoTS fixture does not correct for yaw angle, so the effective yaw angle was -90 degrees in this test. The vehicle was oriented with a pitch angle of 1.3° (front end up). The vehicle was allowed to fall a total of 401 mm to achieve the 2.74 m/s vertical velocity. The roadbed translational velocity was 4.5 m/s at contact. The second DRoTS test performed in this study was designed to match a dynamic rollover simulation with a driver's side leading roll, a roll rate of -245 deg/s and a leading side touchdown at a -153° roll angle. To provide for comparison with the first test, the second test was performed with a pitch rate of -1.3 deg. Since the DRoTS cannot impart a pitch rate, yaw rate, or yaw angle, the pitch and yaw rates of 0 deg/s were used and a -90 deg yaw angle was used. To achieve the drop speed of 1.1 m/s, the vehicle was released from a height of 66 mm. The roadbed translational velocity was 7.5 m/s at contact.

The total mass and mass distribution for the two tests were matched to the dolly test set up (1977.5 kg total, 468 on the driver's side rear, 533 kg on the driver's side front, 528 on the passenger side front, and 448.5 kg on the passenger rear). The vehicles were mounted and balanced in the DRoTS fixture following the procedure outlined in detail in (Kerrigan/Lockerby 2013). The passenger side interior structural surfaces were painted with a stochastic pattern of black dots, 12 to 16 mm diameter with approximate 40% coverage of the patterned area, on a white background to accommodate the optical system.

Test Fixture

The dynamic rollover test system has been previously described in detail (Kerrigan et al. 2011). The system simulated a single roll, with the vehicle roof interacting with the ground only once per test. Vehicle over the ground translation is simulated with a moving road surface (roadbed) that interacts with a vehicle rolling about an axis that is restricted to a plane, which is oriented perpendicular to the direction of roadbed motion. While the roll axis is constrained to remain within this plane, the vehicle is permitted to translate longitudinally and vertically. The test fixture consists of a gantry that holds the vehicle in a pre-test orientation, a roll drive system that rotated the vehicle about the roll axis to the test roll angle and angular velocity, and a suspension/release system that dropped the rotating vehicle onto a moving road surface propelled by a deceleration sled system.

Vehicle Instrumentation and Data Acquisition

Force and Kinematics Measurement Sensors

The road bed was instrumented with 20 uniaxial load cells (SWP-20K, Transducer Techniques, Temecula, CA) that measured forces in the global Z direction. The load cells were evenly spaced in a grid of 5 x 4, 106.7 cm apart, across the 487.7 cm x 365.8 cm road bed surface, and sampled at 10 kHz with a 16 bit data acquisition system (SLICE Micro, Diversified Technical Systems, Seal Beach, CA).

Each vehicle was outfitted with a pyramid-shaped custom inertial measurement unit consisting of accelerometers and angular rate sensors bolted securely to the vehicle floor (**Figure 20** bottom right). Accelerations were measured with two different types of accelerometers: gas-damped 20 g silicon MEMS sensors (MSI 4000A, Measurement Specialties Inc., Hampton, VA), and gas-damped 30 g variable capacitance sensors (Endevco 7290E-30, Meggitt Sensing Systems, San Juan Capistrano, CA). Three accelerometers of each type were aligned so that they measured accelerations about the three perpendicular axes of the unit. Angular rates were measured using three angular rate sensors: a 1500 deg/s sensor on the roll axis, and two 300 deg/s sensors on the other axes (DTS ARS, Diversified Technical Systems, Seal Beach, CA). Lastly, the inertial measurement unit held nine additional 500 g piezoresistive accelerometers (Endevco 7264B-2000, Meggitt Sensing Systems, San Juan Capistrano, CA), which were installed to facilitate calculation of the vehicle angular acceleration by standard nine-accelerometer-package processing techniques (DiMasi, 1995).

Figure 20: Interior view of the instrumentation for the first test (top). Optical system (bottom left), Inertial measurement unit with nine accelerometer package (bottom right).

Deformation Measurement Sensors

Six string potentiometers (model 62-60, Firstmark Controls, Creedmoor, NC) were installed on the vehicle floor in both vehicles (Figure top). The cables from three of the potentiometers were joined together and attached to a plate, that held a triaxial accelerometer (Endevco 7267A, Meggitt Sensing Systems, San Juan Capistrano, CA). Two of these plates were made from the six total string potentiometers. For the first test, the plates were mounted to the passenger side B-pillar at the intersection with the roof rail and the passenger side C-pillar at the intersection with the roof rail. For the second test, one plate was mounted to the passenger side A-pillar about 20 cm below the intersection with the windshield header, and one plate was mounted to the driver side B-pillar intersection with the roof rail. These sensors were installed to measure accelerations and three-dimensional deformations of the roof structure during the tests.

Optical Deformation Measurement System

An optical photogrammetric system capable of dynamic, three-dimensional multi-point in-vehicle deformation measurement tracking was used on both tests (Lockerby, 2013). Deformation measurement was focused on the passenger (trailing or far) side roof rail between the B-pillar and C-pillar in both tests, as this was the anticipated location of maximum deformation. The optical system utilized two on-board high speed imagers (NAC GX-5 S-cams, NAC Image Technology, Simi Valley, CA) with 6 mm lenses (Schneider Optics, Hauppauge, NY) and a commercially available optical processing software, ARAMIS (GOM mbH, Braunschweig, Germany). ARAMIS utilizes digital images to analyze and report 3D material deformations along with the surface coordinates of points. The imagers were fixed at a 21 degree horizontal angle with respect to each other, and installed into the vehicle floor at the 2nd row seat mounting holes on the driver's side (**Figure 20** bottom left). The imagers sampled frames at 1000 Hz at 640 x 480 pixel resolution.

Coordinate Measurements

A coordinate measurement machine (CMM) (Titanium Arm, FARO Technologies, Lake Mary, FL) was used to determine the locations of the front and rear roll axis marker points, the inertial measurement unit origin and orientation markers, the locations of the string potentiometer attachment screw locations on the B-/C-pillars, the points where the strings come out of the potentiometer bases, and four points located in the view of the optical system.

Data Processing

Kinematics Data Processing

All sensor data were filtered, debiased, and processed following the procedure outline in Lockerby, 2013. The time of initial vehicle to road contact was determined to within 1 ms from high speed video, and all time history data were time shifted so that t=0 corresponded with the time of initial vehicle contact with the road surface. Two coordinate systems were defined. The vehicle local coordinate system followed a standardized SAE definition. The global (inertial) coordinate system was defined based on the sled system rails used to propel the roadbed. The roadbed motion was defined to travel in the positive X' (global) direction and the Z' axis was defined to be perpendicular to the test facility floor, with positive pointing downward. The global Y' axis was determined by the cross product of Z' with X'.

Energy Calculations

The kinetic energy of each rollover test was a combination of three components: the translational kinetic energy of the roadbed, and the vertical and rotational kinetic energies of the vehicle. Roadbed translational kinetic energy was calculated by multiplying half of the road weight (1788 kg) by the square of the roadbed velocity time history. Similarly, the vehicle's translational kinetic energy was calculated by taking half the weight of each vehicle and multiplying it by the square of the global vertical velocity time history. Lastly the vehicle's rotational kinetic energy was calculated by multiplying half of the moment of inertia about the roll axis for each vehicle by the square of the local X-axis angular velocity (in radians). The sled propulsion system continued to drive the roadbed through the end of the test, including the duration of vehicle to road contact. To account for the additional energy supplied to the roadbed during vehicle impact, the acceleration of the tow cable was estimated from the sled velocity time history. This acceleration, multiplied by the mass of the roadbed, was integrated over the distance travelled by the road during vehicle contact to produce an energy value which was incorporated into the energy balance of each test.

$$KE_{total} = \frac{1}{2} m_{road} v_{road}^2 + \frac{1}{2} I_{veh} \omega_{veh}^2 + \frac{1}{2} m_{veh} v_{veh}^2 + \int m_{road} a_{road} \, dS$$

Results

Touchdown conditions

The actual touchdown conditions varied slightly from the goal parameters (**Table 2**).

Table 2: Touchdown conditions, goal vs actual.

Vehicle	**1 Goal**	**1 Actual**	**2 Goal**	**2 Actual**
Test Numbers	**1759**	**1759**	**1807**	**1807**
Pitch Angle (deg)*	1.25	0.9	1.25	1.4
Roll Angle (deg)*	181.0	183.8	153.0	155.3
Roll Rate (deg/s)*	228	229.4	244	248.2
Road Speed (m/s)	4.5	4.5	7.5	7.4
Vertical Velocity (m/s)	2.8	2.6	1.1	1.1
Drop Height (mm)	401	381	66	58
Vehicle Radius R (m)	1.07	1.07	1.22	1.22
Tangential Velocity (m/s)	4.27	4.3	5.19	5.3

Kinematics and Kinetics

In the first test, 1759, the angular velocity immediately decreased rapidly as a result of the impact forces (**Figure 21** top). The angular velocity reduced from 228 deg/s to approximately 100 deg/s after only the first 40 ms of loading. In the second test, 1807, the angular velocity increased just after touchdown and throughout the loading event going from about 244 deg/s to well over 300 deg/s after 200 ms of loading. While the roll angle in the second test was much lower at touchdown, the increased roll velocity allowed both vehicles to reach the same roll angle about 240 ms after touchdown (**Figure 21** bottom).

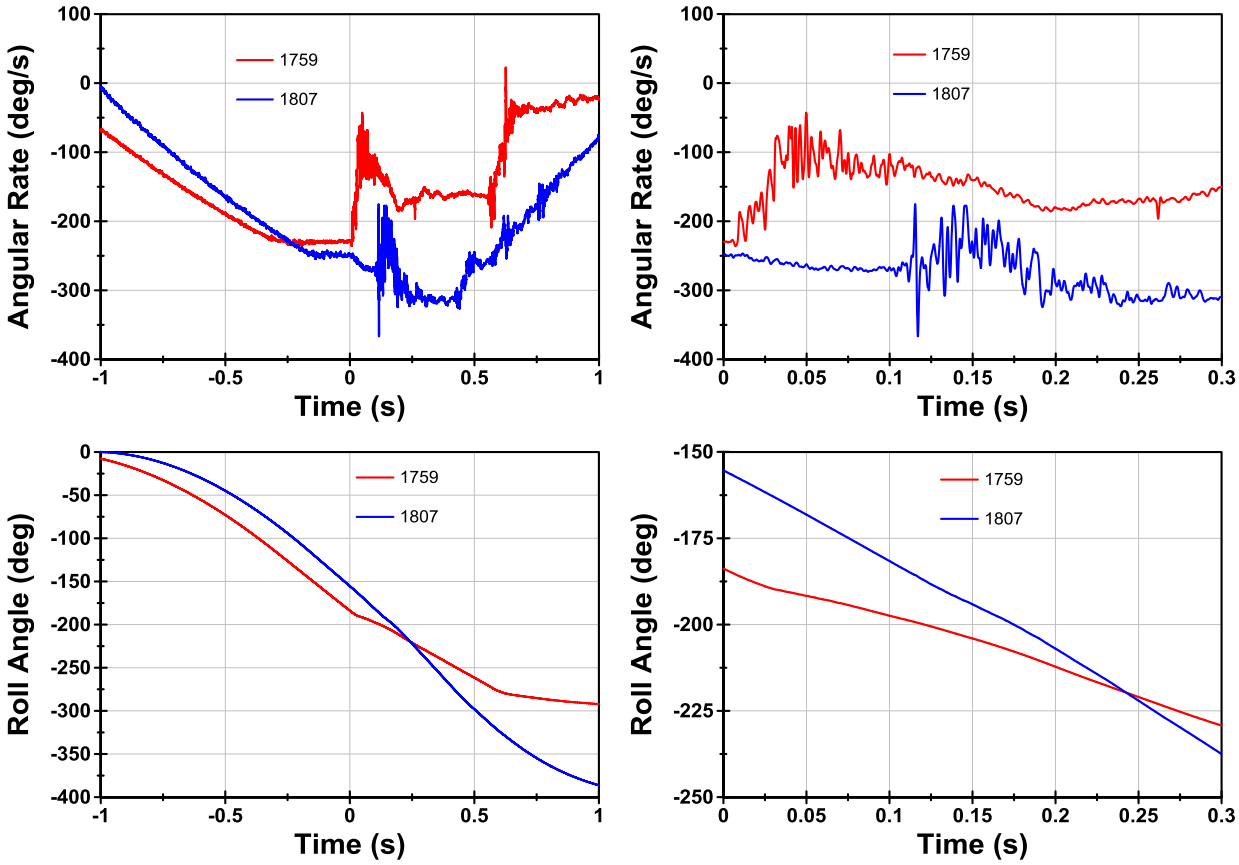

Figure 21: Vehicle local X-axis angular rate (top) and roll angle (bottom).

Both vehicles initiated positive rotational velocities about their local Y-axes after touchdown (**Figure 22** top). In 1759, this positive rotation rate initiated relatively early, whereas, the vehicle in 1807 did not initiate this positive y-axis velocity until after the first 100 ms when the far-side impact occurred. This positive y-axis angular velocity resulted in the vehicle's pitch angle going from a positive (rear end down) pitch angle to a negative pitch angle (**Figure 22** bottom).

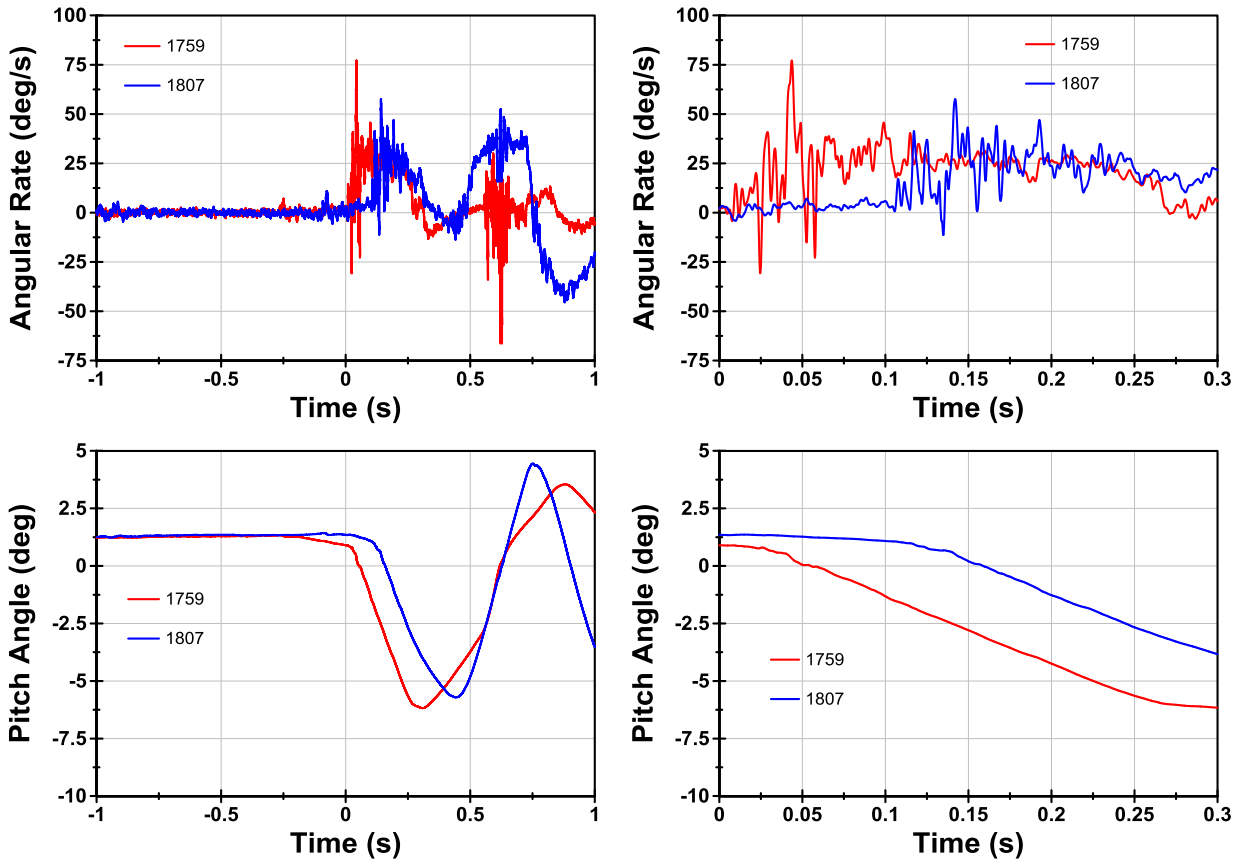

Figure 22: Angular Rate (top) and Pitch Angle (bottom) about the vehicle local Y-axis.

Both vehicles sustained a positive 1 g acceleration after release, and a subsequent negative acceleration as the vertical velocity of the CG was arrested (**Figure 23** top). Global vertical accelerations eclipsed 15 g in test 1759, but remained less than 10 g in 1807. The global velocity data show that the vehicle velocity increased well beyond initial contact with the road, even in test 1759 where the trailing side was targeted in the first impact. Eventually, however, after some loading occurred, the vehicle CG began to slow down and came very close to a stop after about 200 ms. In 1807, the vehicle actually bounced off the road and began to travel upward again after about 200 ms.

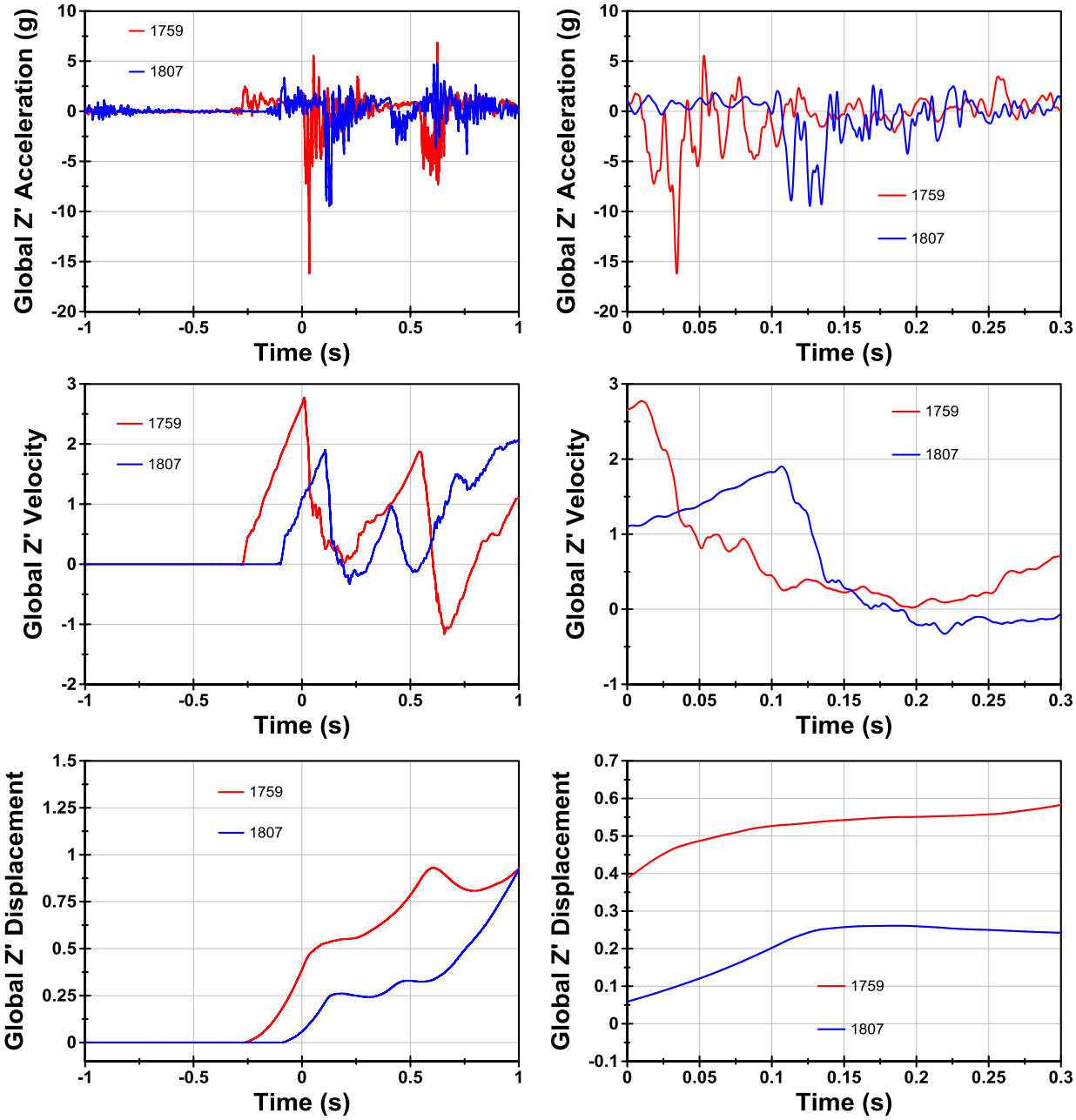

Figure 23: Global Z direction acceleration (top), velocity (middle), and displacement (bottom).

Immediately after initial contact in 1759, the road began to slow down (**Figure 24**). In the case of 1807, the roadbed did not slow down from the near side impact, and increased its speed as the sled system continued to add energy throughout the impact. When the vehicle begin to load the trailing side (after 100 ms), the road speed reduced significantly.

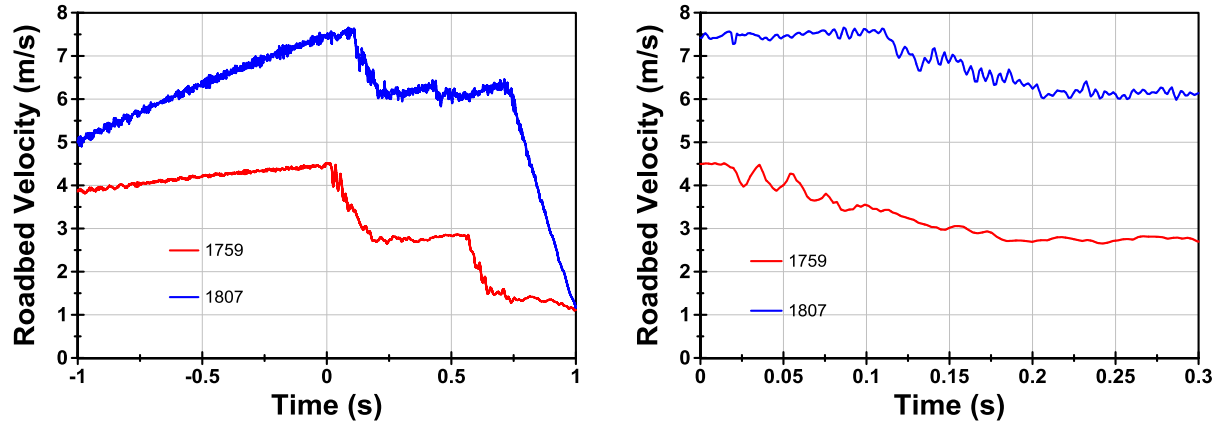

Figure 24: Roadbed velocity.

The peak force recorded in test 1759 (135 kN) exceeded the peak force recorded in 1807 (120 kN) (**Figure 25** top). The peak force normalized by the vehicle weight exceeded 7 g in 1759, and was approximately 6.4 g in 1807. Both vehicles sustained peak forces at similar roll angles (190 deg vs. 192 deg) and similar pitch angles (both 0.6 deg) (**Figure 25** bottom).

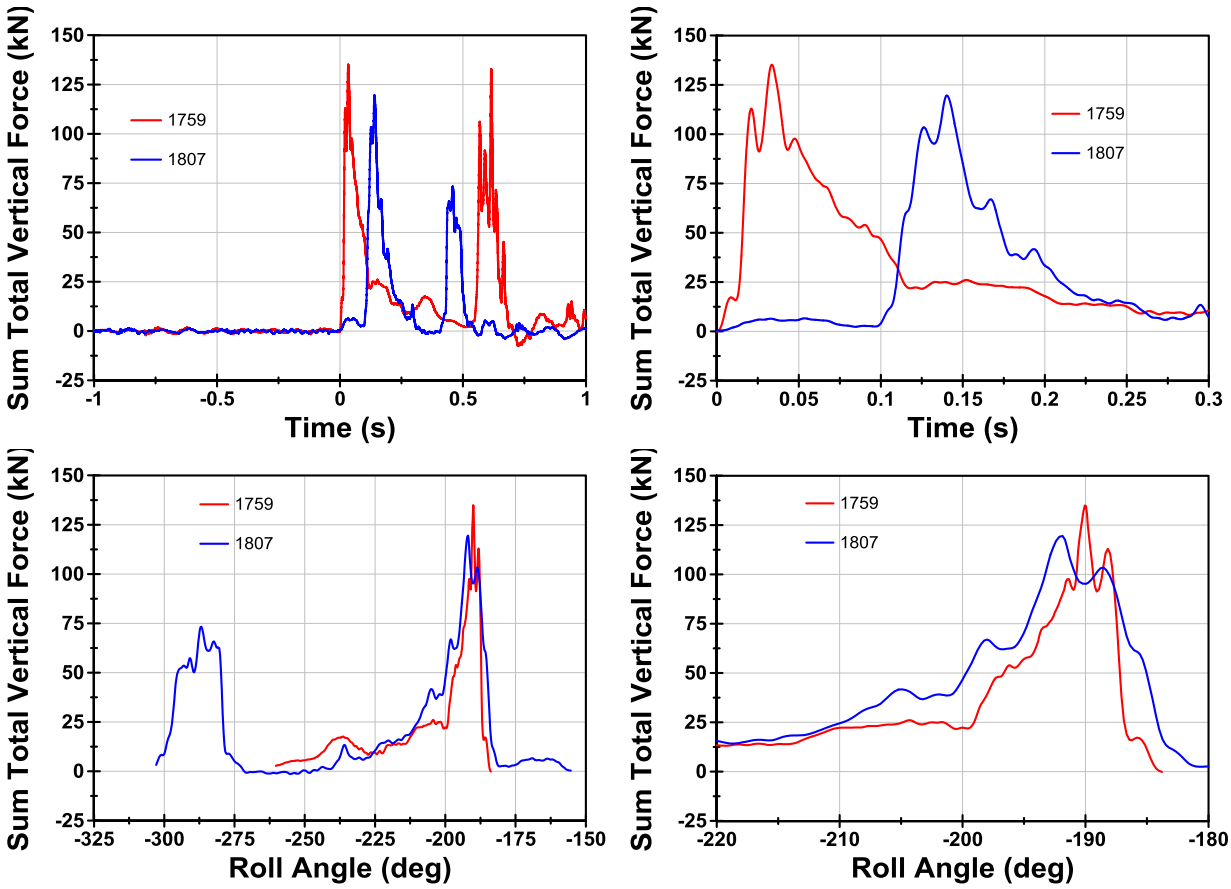

Figure 25: Sum total vertical roadbed reaction force vs time (top) and vehicle local roll angle (bottom).

Energy

The total energy calculation is dominated by the roadbed translational component for both tests, but this resulted in a much higher value of total kinetic energy for the seconds test (**Figure 26** top). The first test had higher vertical kinetic energy from a larger drop height, but lesser rotational kinetic energy due to the slower roll rate (**Figure 26** bottom). The two tests both showed a dramatic reduction in total kinetic energy at far side contact around 183°, with similar reductions in the combined vehicle vertical and rotational kinetic energy (**Figure 27**). The first test had a larger decrease in vertical and rotational kinetic energies (**Table 3**). The second test gained rotational kinetic energy during the event, and lost more roadbed translational energy than the first test. With increased road velocity, the second test had a larger amount of energy by the sled propulsion system.

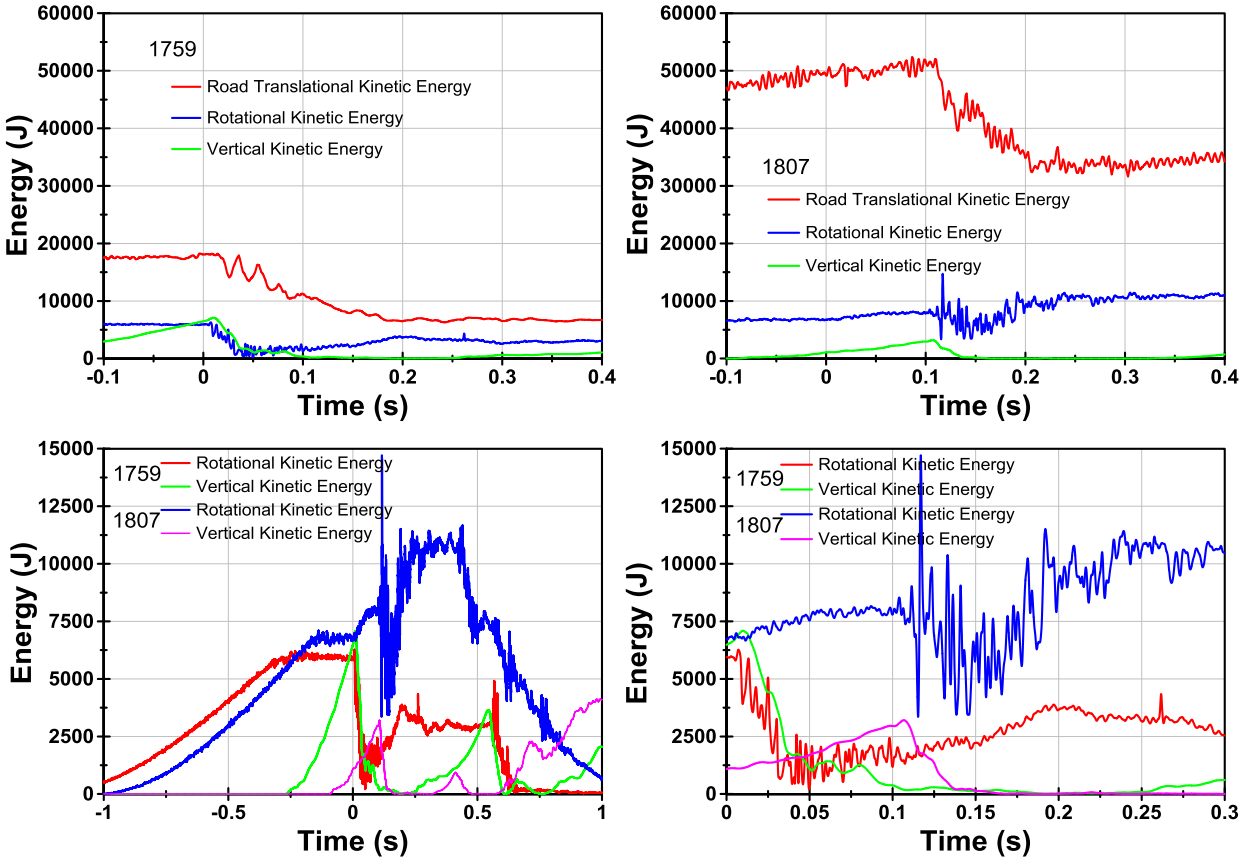

Figure 26: Kinetic Energy. Vehicle vertical, vehicle rotational, and roadbed translational kinetic energies for Test 1 (top left) and Test 2 (top right). Vehicle vertical and rotational compared for both tests (bottom left and right).

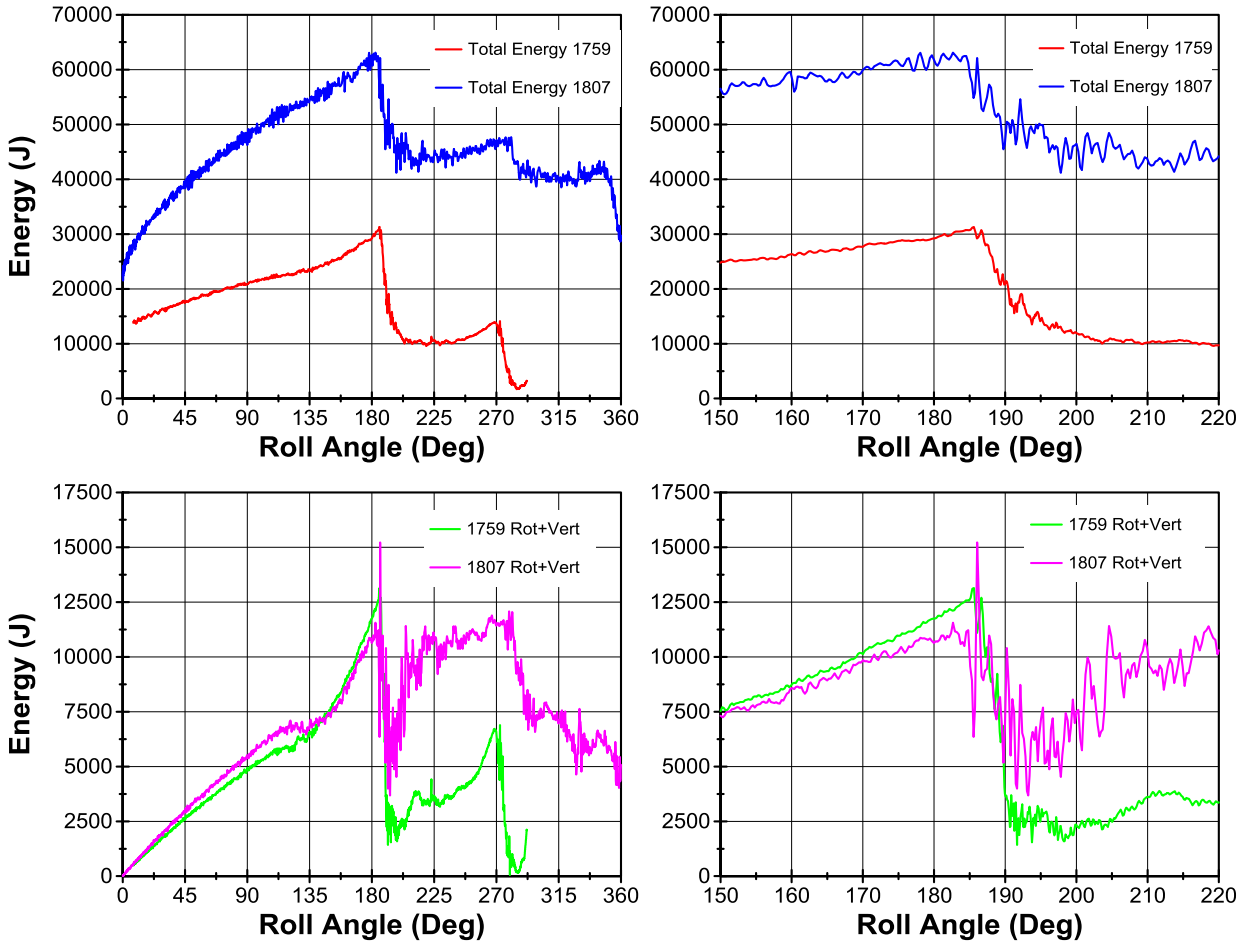

Figure 27: Kinetic energy vs roll angle. Total KE (top), rotational + vertical (bottom).

Table 3: Kinetic energy at far-side contact (t=0 for first test, t=98ms for second test) through a roll angle of 210° (t=188ms, t=210ms). Sled propulsion is the amount of energy added to the system by the sled during far-side impact.

Test	**1st - 1759**			**2nd - 1807**		
Time	**t=0**	**t=188ms**	**Change**	**t=98ms**	**t=210ms**	**Change**
Roll Angle	184°	210°	184°-210°	182°	210°	182°-210°
Vertical KE	6480	0	-6480	2960	0	-2960
Rotational KE	5940	3535	-2405	8030	9500	1470
Road Trans KE	18080	6665	-11415	51210	33600	-17610
Sled Propulsion		-436			-1960	
Sum Total KE	30500	9764	**-20736**	62200	41140	**-21060**

Vehicle Deformation

The peak resultant deformation reported by the optical system (217.7 mm at 120 ms for the first test, 242.0 mm at 179 ms for the second test) occurred in the roof sheet just forward of the C-pillar intersection with the passenger roof rail (**Figure 28**). The structure subsequently unloaded, with the value of residual deformation (151.2 mm for the first test, 165.0 mm for the second test) accounting for substantial restitution (30.5% for the first test, 31.8% for the second test) when normalized by the peak deformation value.

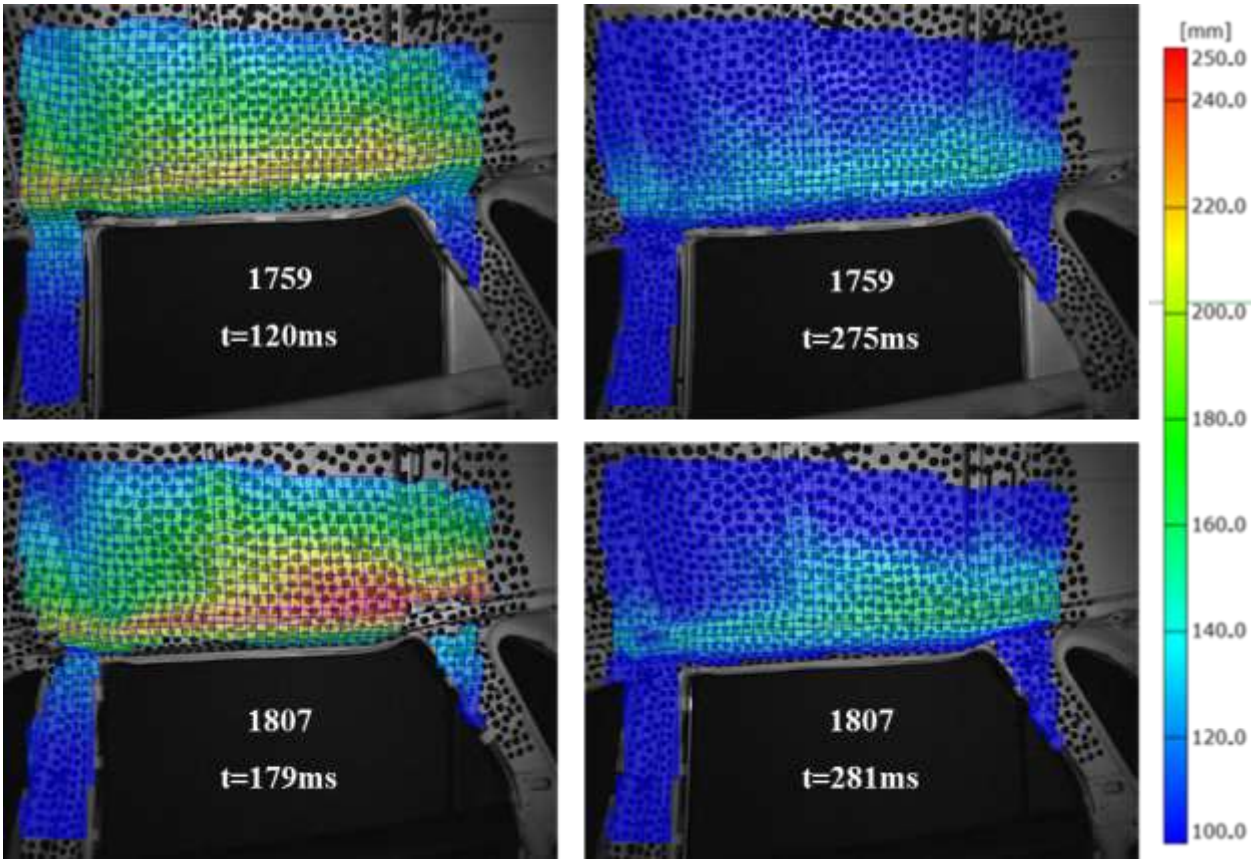

Figure 28: Optical resultant displacement overlaid onto left camera image. 1759 maximum at t=120ms (top left), 1759 residual at t=275ms (top right). 1807 maximum at t=179ms (bottom left), 1807 residual at t=281ms (bottom right).

Component-wise deformation time histories, in the vehicle's local coordinate system, were computed at the same eight locations in both tests (**Figure 29**). The local vehicle X, Y, and Z components of displacement were average for the eight points to create a more general deformation time history of the greenhouse structure for the two tests (**Figure 30**). 1759 had a maximum average resultant deformation of 148.8 mm (X= -30.5 mm, Y= -127.9 mm, Z= 148.8 mm) at a roll angle of 199.6°, while 1807 was slightly higher with 152.5 mm (X= -28.4 mm, Y= -129.2 mm, Z= 82.9 mm) at a roll angle of 202.4°.

Five of the eight points sampled (A, D, E, G, H) had a larger deformation in the second test, 1807. The three points of greater deformation for the first test (B, C, F) were located in the forward portion of the field of view, near the B-pillar. The duration of both the deformation (120ms from initial contact to peak

deformation vs 85ms) and unloading (150ms from peak deformation to full restitution vs 90ms) is longer in the first test.

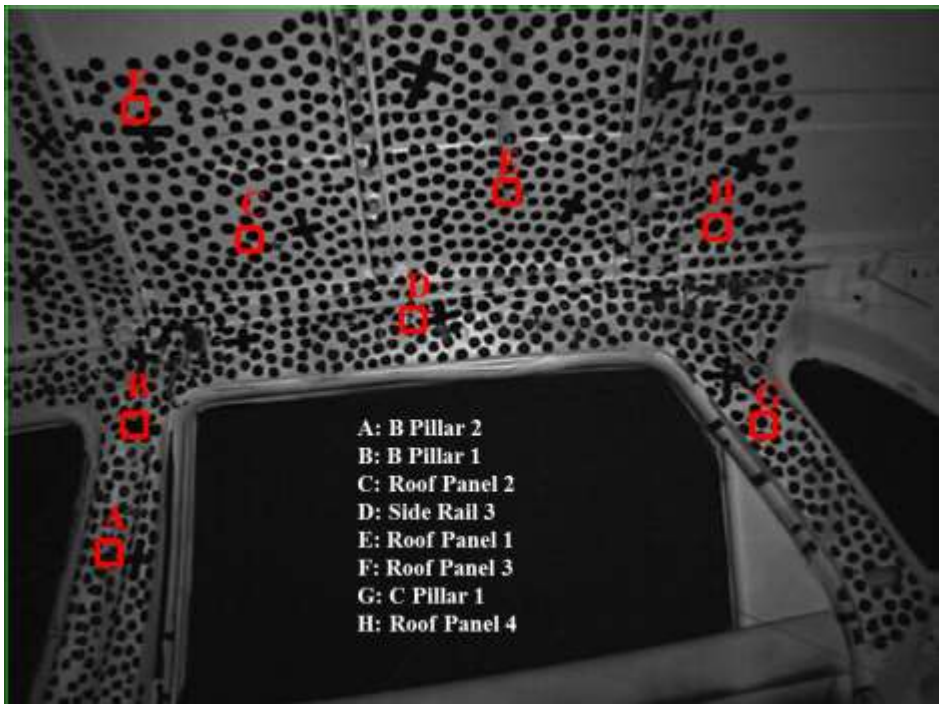

Figure 29: Location of optical output points from 1759 and 1807 for deformation comparison.

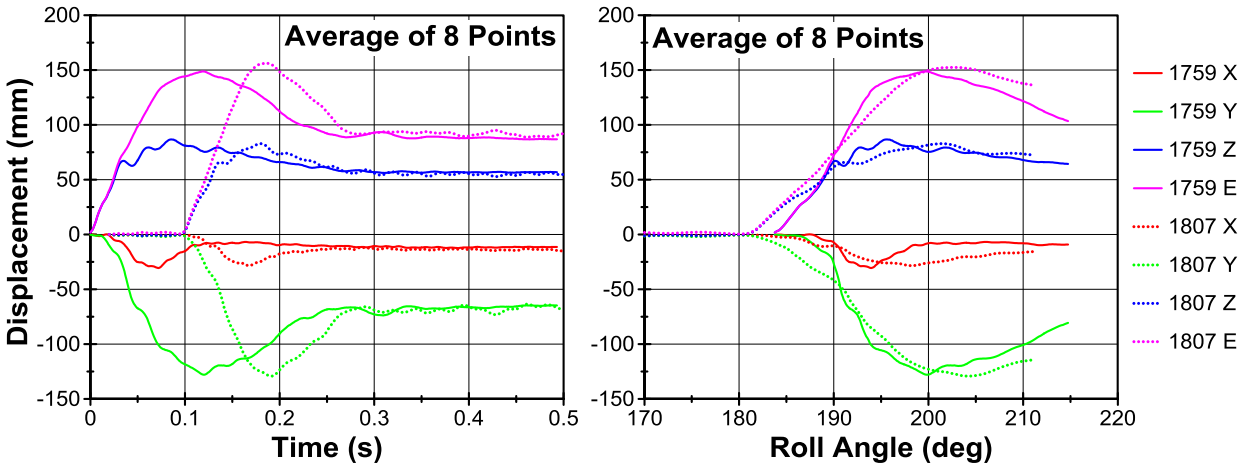

Figure 30: Optical displacement output, average of the eight points A-H.

For the second test, the string potentiometers were mounted outside the view of the optical system and provide additional deformation data. The maximum resultant deformation at the passenger side A-pillar was 71.7 mm (-18.9 mm in the X, -67.7 mm in the Y, and 14.0 mm in the Z directions) at 186 ms (**Figure 31** left). The maximum resultant deformation at the driver side B-pillar was 64.9 mm (5.8 mm in the X, -62.8 mm in the Y, and -15.4 mm in the Z directions) at 165 ms (**Figure 31** right).

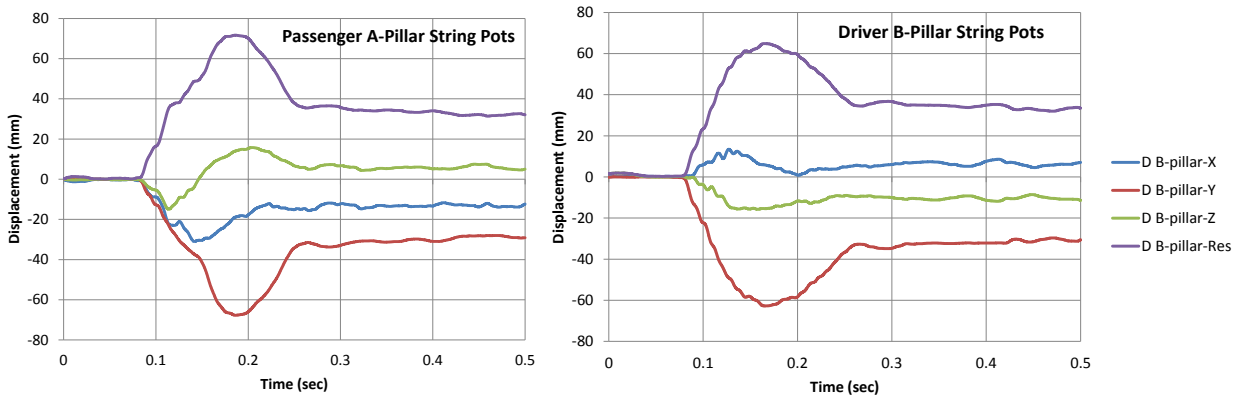

Figure 31: 1807 passenger side A-pillar (Left) and driver side B-pillar (Right) string potentiometer displacement.

Force vs Deformation

When the sum total vertical reaction force of the roadbed was plotted against the resultant of the eight point average displacements from the optical system, both of the dynamic tests displayed significantly stiffer response than the quasi-static IIHS test (**Figure 32** left). The integral of the force-deformation curve was used to estimate the amount of energy absorbed by the greenhouse structure in the form of crush (**Figure 32** right). The crush energy for the two tests is very similar, with the 1st test peaking at 10,755 J and the 2nd at 10,708 J.

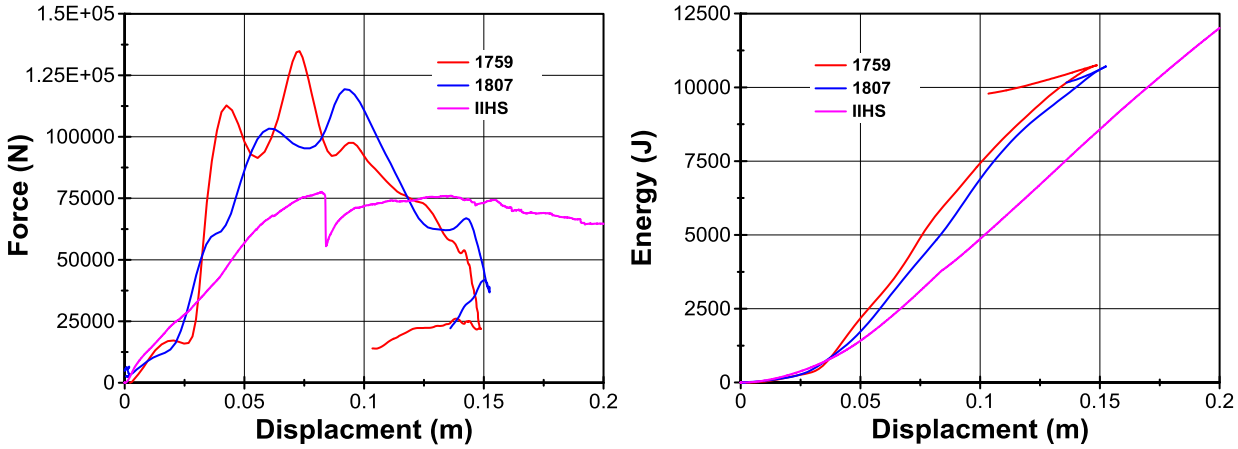

Figure 32: Force-deflection (Left) and integrated crush energy (Right) for the two tests and the IIHS platen test.

Translational vs Tangential Velocity

The dynamic changes in the roadbed translational (V) and vehicle tangential (ωR) velocities were tracked throughout the two tests (**Figure 33**). The vehicle radius used in this calculation changed dynamically to account for both the vehicle geometry and structural deformation. In the first test the translational velocity (4.50 m/s) and tangential velocity (4.25 m/s) were close at touchdown, and both reduced after contact, though the reduction in rotational velocity was much greater. For the second test, the

translational velocity (7.42 m/s) was significantly higher than the tangential velocity (4.99 m/s) at touchdown, with the tangential velocity remaining fairly constant during the near side impact as the reduction in radius was proportional to the increased roll velocity.

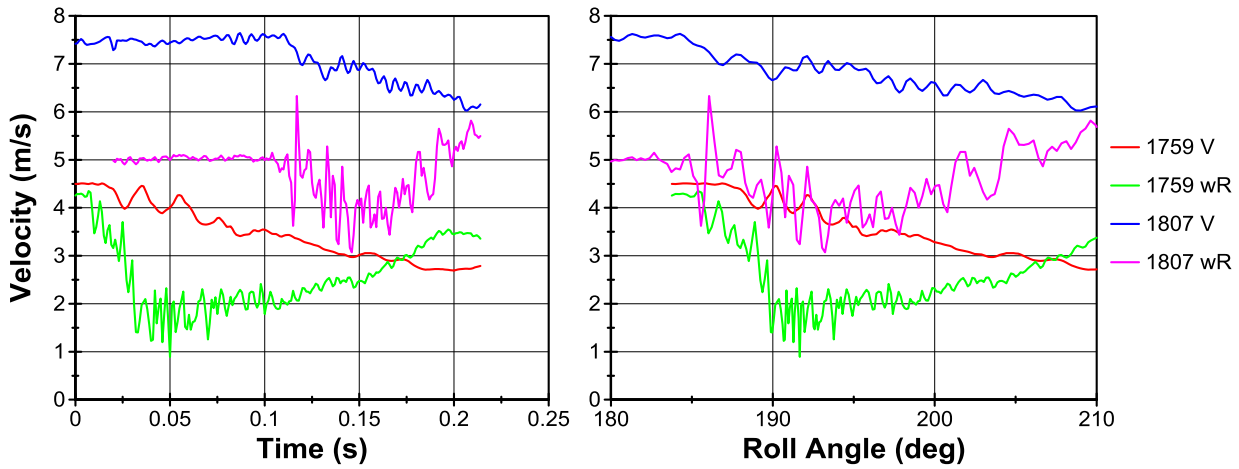

Figure 33: Translational roadbed velocity (V) and vehicle tangential velocity (ωR) vs time (left) and roll angle (right).

Discussion

The conditions at the initiation of far-side impact were similar for the two vehicles, as both were loaded between the passenger B- and C-pillars with comparable pitch, roll, and yaw angles. The maximum reaction forces occurred at similar roll angles (190° and 192°) as did the maximum deformations (200° and 202°). The near-side contact had almost no effect on structural deformation as seen in the near-side B-pillar string potentiometer results, or reaction force recorded by the roadbed. However, it produced a significant increase in the roll rate as translational was converted into rotational velocity through frictional forces at the contact interface between the vehicle roof and the roadbed. During the near-side contact the vertical (FZ) and lateral (FY) reaction forces were both applied with a moment arm around the CG that increased the rotation of the vehicle (**Figure 34** left). On the contrary, for the far-side impact the vertical (FZ) force acted to slow the rotation of the vehicle while the lateral (FY) acted to increase the roll rate (**Figure 34** right). As the vehicle's vertical velocity was arrested by the roadbed, the vertical reaction force was much larger than the lateral friction force which slowed the vehicle's angular velocity. In both tests the minimum values for tangential velocity corresponded with the maximum reaction force.

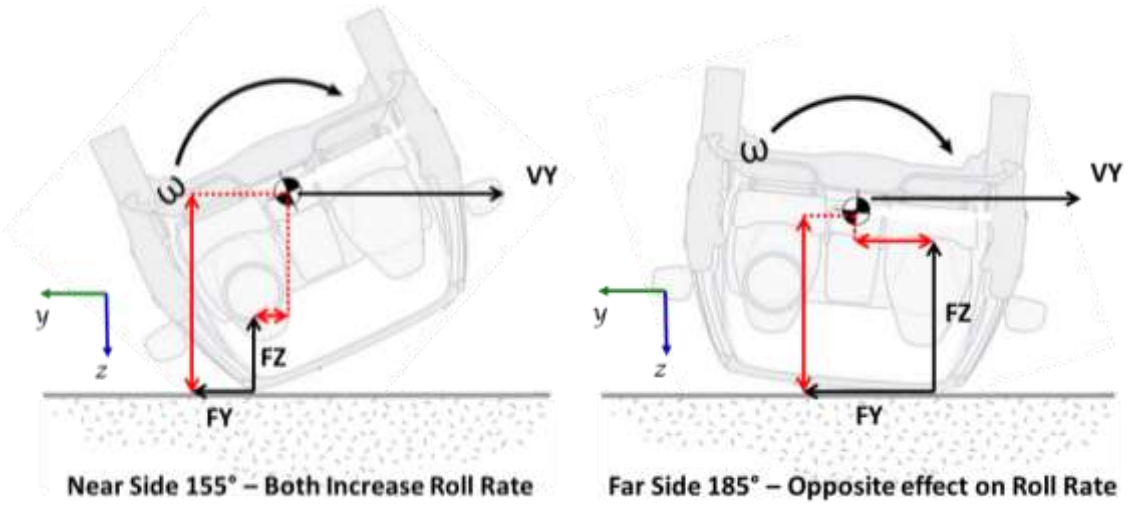

Figure 34: Diagram of forces and moments acting on the vehicle in a near-side (left) and far-side (right) touchdown.

The peak reaction force of the first test was 16.3% larger than that of the second test, with both vehicles reaching peak force at similar roll and pitch angles. It is hypothesized that reaction force is dictated by the structure, and that the increased reaction force of the first test was the result of the loading vector being more axially aligned with the B-pillar. Although the first test had a larger reaction force, the averaged deformations across the optical system's field of view were very similar for the two tests. The peak reaction force (or SWR) was not a strong predictor of peak roof deformation for these two dynamic rollover tests.

The second test had an 11.2% larger localized peak deformation with increased buckling and rotation of the roof rail at the connection to the C-pillar. The average deformation calculated from the eight points showed a closer spread, with the second test being only 2.5% larger. Three of the eight points closest to the front of the vehicle had greater deformation in the first test, thought to be the result of a more forward pitch at the time of maximum deformation (-1.86° compared to -0.71° for the second test). The averaged value was chosen to rank the two vehicles for deformation as this provided a more general metric of structural response, as opposed to a single peak value that was more sensitive to localized buckling and geometric complexities.

The component deformations from both tests show the maximum displacement in the lateral direction (approximately 50% larger than vertical) at the time of peak deformation. For the second test, string potentiometers data from the near-side B-pillar showed outward lateral deformation (65 mm). The lateral stiffness of the roof played a pivotal role in preventing/allowing deformation into the occupant compartment, which can be important as previous studies have shown that occupants move outboard due to centripetal acceleration during rollovers, increasing the chance of contact with the structure. The structural restitution was around 31% for the two tests (peak deformation to final geometry), exhibiting how calculations based only on the residual deformation of a rollover crash would underestimate the amount of dynamic intrusion.

Both dynamic tests exhibited a stiffer response than the quasi-static IIHS test (**Figure 32** left). It is hypothesized that loading different structure (namely the B-pillar and C-pillar instead of the A- pillar in the IIHS test) which are more in line with the mainly vertical loading vector, accounted for this difference. The shape of the force-deformation curve for the two vehicles is similar with two distinct peaks. While the causes of the phase lag of the second test peaks were unknown, they were thought to be influenced by the different kinetic energy distribution between the two tests.

Energy

It was hypothesized that a vehicle with more kinetic energy at touchdown would sustain more structural deformation. At far-side contact, the second test had over twice the total kinetic energy of the first test (62.2 kJ vs 30.5 kJ), dominated by the roadbed translational velocity which accounted for 82.3% of the kinetic energy of the second test. The increased deformation of the second vehicle (11.6%) was not proportional to the difference in total kinetic energy. Removing the roadbed velocity from the kinetic energy calculations, the first test had an 11.5% higher combined total of vertical and rotational kinetic energy. With only two replicate vehicle tests and three kinetic energy variables, the relationship between the distribution of kinetic energy and the reaction force and deformation outputs could not be determined.

Previous finite element studies have concluded that vertical velocity (drop height) is the strongest predictor of roof deformation in a single roof-to-ground rollover impact (Parent, 2011). Contrary to that finding, the vehicle with the higher drop height sustained less deformation between the two dynamic tests. This suggested that rotational and/or translational kinetic energy must have an effect on deformation. It was hypothesized that as higher rotational velocity increased the total velocity of the point in contact with the roadbed (CG vertical plus the component of the rotational velocity that is normal to the reaction surface), it could have increased deformation. On the contrary, a higher rotational velocity could have caused the CG of the vehicle to pass over the loaded structure faster, reducing the amount of time the structure is loaded and thus also deformation. Additionally, It was hypothesized that a higher translational velocity would have no effect on the deformation for a single far-side roof-to-ground impact, as no component of the translational velocity was normal to the ground (assuming a flat surface). However, the remaining translational energy after the first impact could have dictated whether the vehicle completed additional roof inversions in an unconstrained rollover. It was unclear which of these factors (or possibly another confounding factor) contributed to the larger deformation in the second test.

Despite the variation in peak force locations on the force-deformation plot, the integrated crush energies were very similar with peak values within 0.44% of each other (**Figure 32** right). The first test had a larger reaction force, but lower deformation, with those factors balancing out to result in the same amount of energy absorbed by the structure. It was inconclusive whether the similar crush energies were a coincidence or a more fundamental result of the underlying structure. The total change in kinetic energy was almost equal (-20.7 kJ for 1759 and -21.1 kJ for 1807) for the two vehicles during far-side impact. Kinetic energy was lost to vehicle crush and frictional forces between the vehicle and the roadbed, with similar values estimated for crush, the frictional energy dissipation must also have been similar. Although the two vehicles had much different translational and rotational velocities, the frictional forces generated were not dependent on the velocities but on the normal force and friction coefficient. This suggested that additional translational velocity would not have had a significant effect on the energy dissipated to deformation or friction for a single roof-to-ground impact.

Conclusions

Two replicate vehicle full-scale dynamic rollover tests were performed on the dynamic rollover test system with two different sets of touchdown parameters. The goal of this study was to quantify the effect of variations in touchdown conditions (specifically the amount and distribution of initial kinetic energy) on vehicle kinematic and deformation response. The roll, pitch, and yaw angles were equivalent at far-side loading, allowing for a direct comparison of force and deformation between the two vehicles.

The near-side contact in the second test did not have a significant effect on deformation, but it did provide a change in vehicle kinematics by converting translational into rotational velocity. It is unclear whether the two vehicles dissipating similar amounts of energy to roof crush and frictional was a function of the structure, or a coincidence. Both vehicles sustained the majority of their deformation in the lateral direction, highlighting the importance of lateral stiffness in vehicle roof design to prevent loss of occupied volume and roof-to-occupant contact.

The test with greater total kinetic energy sustained larger peak deformation. Contrary to the results of previous FE simulation studies, the vehicle with the larger vertical energy (drop height) did not sustain more deformation. This suggested that rotational and/or translational kinetic energy also contribute substantially to structural deformation. The two vehicles sustained similar amounts of deformation even though the first test produced a higher reaction force, suggesting that peak force (or SWR) might not be the strongest predictor of roof deformation in rollover. As the conclusions from this study are based on only two experiments, it is recommended that a subsequent study utilize FE simulation to characterize the relationships between the kinetic energy distribution and the vehicle force-deformation response in rollover.

References

Batzer, S. A., & Hooker, R. M. (2005). Dynamic roof crush intrusion in inverted drop testing. In 19th international technical conference on the enhanced safety of vehicles (No. 05-0146).

Chou, C. C., McCoy, R. W., & Le, J. (2005). A literature review of rollover test methodologies. International Journal of Vehicle Safety, 1(1), 200-237.

DiMasi, F. (1995). TRANSFORMATION OF NINE-ACCELEROMETER-PACKAGE (NAP) DATA FOR REPLICATING HEADPART KINEMATICS AND DYNAMIC LOADING (No. DOT HS 808 282).

Friedman, D., Nash, C. E., & Caplinger, J. (2007). Results from two sided quasi-static (M216) and repeatable dynamic rollover tests (JRS) relative to FMVSS 216 tests. In 20th International Technical Conference on the Enhanced Safety of Vehicles (ESV), Paper (No. 07-0361).

Friedman, K., & Hutchinson, J. (2009). Review of existing repeatable vehicle rollover dynamic physical testing methods. In ASME International Mechanical Engineering Congress and Exposition (Vol. 16, pp. 51-59).

Grzebieta, R. H., McIntosh, A. S., Bambach, M., & Young, D. P. (2010, August). Dynamic test protocol to assess rollover crashworthiness. In Proceedings of Australasian Road Safety Research, Policing and Education Conference, Canberra,, Australia.

Kerrigan, J. R., Jordan, A., Parent, D., Zhang, Q., Funk, J., Dennis, N. J., ... & Crandall, J. (2011). Design of a dynamic rollover test system. SAE International Journal of Passenger Cars-Mechanical Systems, 4(1), 870-903.

Lockerby, J., Kerrigan, J., Seppi, J., & Crandall, J. Optical Measurement of High-Rate Dynamic Vehicle Roof Deformation during Rollover. Society of Automotive Engineers, 2013-01-0470.

Mao, M., Chirwa, E. C., & Wang, W. (2006). Assessment of vehicle roof crush test protocols using FE models: inverted drop tests versus updated FMVSS No. 216. International Journal of Crashworthiness, 11(1), 49-63.

Moffatt, E. A., Cooper, E. R., Croteau, J. J., Orlowski, K. F., Marth, D. R., & Carter, J. W. (2003). Matched-pair rollover impacts of rollcaged and production roof cars using the controlled rollover impact system (CRIS). SAE transactions, 112(6), 145-152.

National Highway Traffic safety Administration. 2006. Laboratory test procedure for FMVSS 216 roof crush resistance. Report no. TP-216-05. Washington, DC: US Department of Transportation.

Office of the Federal Register, 2009. Federal Register, vol. 74, no. 90, pp. 22348-22393. National Highway Traffic Safety Administration – Final Rule. Docket no. NHTSA-2009-0093; 49 CFR Part 571 – Federal Motor Vehicle Safety Standards, Roof Crush Resistance. Washington, DC.

Study III – Characterizing the Effect of Kinetic Energy Distribution at Touchdown on Vehicle Deformation in Rollover

Abstract

At the moment of roof-to-ground touchdown during a vehicle rollover event, three velocities describe its kinetic energy: vertical, translational, and rotational. Previous FE studies suggest that vertical kinetic energy (drop height) is the strongest predictor of vehicle greenhouse deformation. However, previous full-scale dynamic rollover experiments on replicate SUV's did not confirm this conclusion. The goal of this study was to characterize the relationship between the initial kinetic energy distribution and the force-deformation response of the vehicle roof structure through FE simulation. Eight single roof-to-ground impact simulations were run on a FE vehicle model of a mid-sized SUV in LS-DYNA. The three kinetic energies were varied (with a high and low value for each) in a full factorial design of experiment with the remaining touchdown parameters fixed. Linear regression was performed to determine if there were statistically significant relationships between the input energies and the output force and deformation metrics. Only vertical kinetic energy was found to be a significant predictor of peak roof deformation ($p=0.002$), while none of the kinetic energies were a significant predictor of peak reaction force. Peak reaction force was not a significant predictor of peak roof deformation, but the calculated internal energy (absorbed through crush) was ($p=0.001$). The dynamic force-deformation response (slope and peak) for the eight simulations was dependent on the input parameters. From the outcomes of this study, it is hypothesized that ranking vehicles only on peak SWR (FMVSS 216) is not an optimized assessment of roof strength. Adding an energy criterion to the existing quasi-static test evaluation would ensure more robust roof designs.

Introduction

Federal Motor Vehicle Safety Standard (FMVSS) 216, the only federal safety standard governing vehicle crashworthiness in rollover, requires a minimum level of roof strength in passenger vehicles. The evaluation procedure involves a quasi-static test where a flat metal platen is pushed at a constant rate of 0.5 in/s into the roof structure at a 25° roll angle, and a 5° pitch angle. Each vehicle is required to produce a reaction force of 3.0 times its weight (strength-to-weight ratio SWR≥3.0) within the first 5 inches of platen displacement (NHTSA, 2009). NHTSA has supported the choice of peak SWR as the metric to evaluate roof strength based on a retrospective analysis of rollover crashes, roof deformations, and vehicle SWR's that showed a relationship between increased vehicle SWR and decreased vertical roof intrusion in real-world rollovers (Austin, 2010). The study found SWR to be a statistically significant predictor of vertical deformation, with a 1.0 increase in SWR predicting a 5.6 cm reduction in roof intrusion. Researchers have argued that solely attaining a level of peak force (or SWR) is not a

useful indicator of roof crush resistance performance because the peak forces often drop significantly due to breaking glass and other structural failures, and instead have recommended an energy absorption requirement in order to prevent roof collapse after initial peak forces are attained (Office of the Federal Register Comments, 2009).

While the FMVSS 216 test is quasi-static, researchers have studied rollover crashworthiness with a variety of full scale dynamic test systems (Moffat, 2003; Friedman, 2009; Kerrigan, 2011). In a previous experimental study, two full-scale dynamic vehicle rollover impact tests were performed with replicate mid-sized SUV's on the dynamic rollover test system (DRoTS) at the University of Virginia Center for Applied Biomechanics (Lockerby, 2014 concurrent). The DRoTS simulated translational motion with a moving road surface and constrained the vehicle roll axis to remain fixed in a plane during one roof-to-ground impact (Kerrigan, 2011). The system performed a single roll, with the vehicle roof interacting with the ground only once per test. The test fixture consisted of a gantry that holds the vehicle in a pre-test orientation, a roll drive system that rotated the vehicle about the roll axis to the test roll angle and angular velocity, and a suspension/release system that dropped the rotating vehicle onto a moving road surface propelled by a deceleration sled system. Dynamic roof deformation was captured for the two tests using an optical system mounted in the vehicle (Lockerby, 2013).

The DRoTS allows researchers to input a set of touchdown parameters that govern the kinematic condition, and thus the energy, of a vehicle at the initiation of roof-to-ground contact. At the moment of touchdown during a vehicle rollover event, three velocities describe its kinetic energy: vertical velocity, translational velocity, and rotational velocity. When the roof impacts the ground, some kinetic energy is dissipated through structural deformation, some is dissipated through frictional forces between the vehicle and the ground, and some is transferred between the three velocities. The amount of energy dissipated through structural deformation is related to the magnitudes of force and deformation, and their relationship (energy is the integral of the forc e-deformation curve).

The replicate SUV study quantified the effect of variations in touchdown conditions on vehicle kinematic and deformation response. Of specific interest was the effect of the distribution of initial kinetic energy on the resulting deformation of the vehicle structure. Both vehicles sustained very similar levels of deformation while the vehicle with larger vertical kinetic energy had a larger reaction force, and the vehicle with greater rotational and translational kinetic energies had a lower reaction force. This result suggested that rotational and/or translational kinetic energy had an unexpected influence on the force-deformation response. To investigate this result further, the current study performed rollover simulations on a finite element model of the same mid-sized SUV in LS-DYNA.

Finite element simulation has been a successful research tool to investigate vehicle structural integrity in rollover impact loading. Due to the dramatically reduced expense compared to full scale experimental testing, a large number of simulations can be run to study the sensitivities of the structure to input parameters and initial touchdown conditions. Previous rollover FE studies have looked at the sensitivity of vehicle deformation and kinematic response to a variety of input parameters and have determined that roll angle, pitch angle, and drop height (vertical kinetic energy) have a significant effect on structural deformation in dynamic simulations (Tahan, 2010; Parent, 2011). Other studies have focused on simulating variations to the FMVSS 216 and IIHS roof strength evaluation tests, to determine vehicle specific conditions that result in the lowest reaction force (Mao, 2005; Tahan, 2010).

The goal of this study was to characterize the relationship between the kinetic energy of a vehicle at touchdown, and the force-deformation response through finite element simulation. The same orientation of the vehicle at touchdown (constant roll angle, pitch angle, yaw angle) was imposed on all the simulations. The three parameters that dictate the kinetic energies (vertical velocity, roll rate, and translational velocity) were varied, one at a time, with a high and low value for each. A full factorial design of experiments array was implemented, with two levels of three parameters totaling eight simulations.

When a vehicle is subjected to a roof-to-ground impact in a rollover crash, the greenhouse structure undergoes deformation as a result of forces transmitted from the ground to the car. The magnitudes of these forces and deformations are related by the amount of energy absorbed by the vehicle structure. For a given vehicle in a single dynamic roof-to-ground interaction, it is hypothesized that:

- Greater total kinetic energy at touchdown (regardless of distribution) will result in larger structural deformation.
- Peak force will not be a significant predictor of deformation.

The following study was designed to test these hypotheses through finite element simulation of a single roof-to-ground rollover impact.

Methods

Overview

Rollover simulations on a finite element vehicle model of a mid-sized SUV were performed in LS-DYNA. The FE model had a mass of 1,994.6 kg, and was comprised of 1.93 million nodes and 1.81 million elements, the majority of which were shells. The input to the simulations defined the initial orientation and energy state of the vehicle at the instant of first roof-to-ground contact, and the first 500 ms of interaction were simulated. The output of each simulation tracked the kinematics, kinetics, and structural deformation of the vehicle that resulted from the impact with the ground.

Model Validation

The FE vehicle model's force-deformation response to roof loading was shown to have good agreement with the actual vehicle's response in the IIHS quasi-static roof crush test (**Figure 35**). In the validation simulation, the chassis was constrained, and the loading platen was oriented 5° pitch and 25° roll. The friction coefficient between the vehicle and the platen was set to 0.8. During the IIHS test, the platen loaded the vehicle at a rate of 0.2 in/s and a total displacement of 10 inches. A loading rate of 88.0 in/s was selected to run in the FE simulation, and vehicle part material model were modified to remove the effects of loading rate sensitivity.

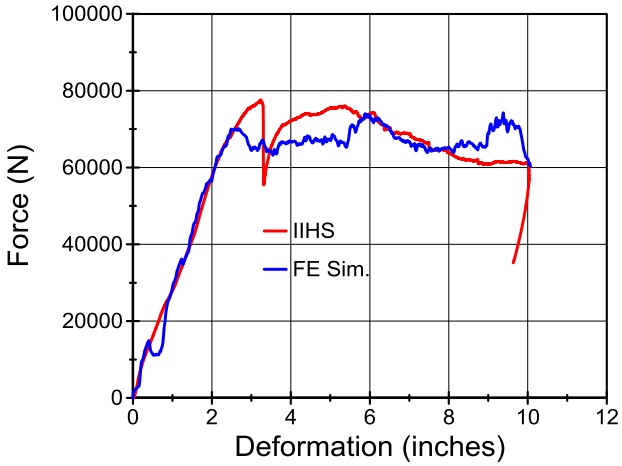

Figure 35: FMVSS 216 simulation results with the LS-DYNA model compared to the IIHS test.

Input Parameters

Nine input parameters (roll rate, pitch rate, yaw rate, roll angle, pitch angle, yaw angle, x velocity, y velocity, z velocity) were required to fully define the initial state of the vehicle upon roof to ground contact at the start of each simulation. Two values were chosen for each of the three parameters (roll rate, x velocity, z velocity) that defined the distribution of vehicle kinetic energy, with the high and low values for vertical and rotational kinetic energy equal so that their sum could be conserved across matched pair simulations (**Table 4**). A full factorial design of experiments array was implemented, with two levels of three parameters totaling eight simulations. In six of the eight cases the vehicle translational velocity was greater than the tangential velocity ($V>\omega r$).

Table 4: Initial conditions and state of kinetic energy for the eight simulations. The cases named based on high (H) and low (L) translational, rotational, and vertical energy in that order.

Case		KE Trans	KE Rot.	KE Vert.	KE Total	V>ω r	Roll Rate	Pitch Rate	Yaw Rate	Roll	Pitch	Yaw	Vx	Vy	Vz
#	T/R/V	kJ	kJ	kJ	kJ		deg/s	deg/s	deg/s	deg	deg	deg	m/s	m/s	m/s
1	LLL	20.00	5.00	5.00	30.00	Yes	200	0	0	190	-5	-90	4.48	0	2.24
2	LLH	20.00	5.00	12.03	37.03	Yes	200	0	0	190	-5	-90	4.48	0	3.48
3	LHL	20.00	12.03	5.00	37.03	No	311	0	0	190	-5	-90	4.48	0	2.24
4	LHH	20.00	12.03	12.03	44.06	No	311	0	0	190	-5	-90	4.48	0	3.48
5	HLL	40.00	5.00	5.00	50.00	Yes	200	0	0	190	-5	-90	6.34	0	2.24
6	HLH	40.00	5.00	12.03	57.03	Yes	200	0	0	190	-5	-90	6.34	0	3.48
7	HHL	40.00	12.03	5.00	57.03	Yes	311	0	0	190	-5	-90	6.34	0	2.24
8	HHH	40.00	12.03	12.03	64.06	Yes	311	0	0	190	-5	-90	6.34	0	3.48

The other six input parameters (pitch rate, yaw rate, roll angle, pitch angle, yaw angle, y velocity) remained the same for all eight simulations with the pitch and yaw rates set to zero. The rotations were applied in the order of yaw (all -90°), pitch (all -5°), and roll (all 190°). The vehicle was aligned

vertically to make the lowest point barely contact the ground, then the two linear velocities (Vx= 4.48 or 6.34 m/s, Vz= 2.24 or 3.48 m/s) and the angular velocity (roll rate= 200 or 311 deg/s) were applied (**Figure 36**).

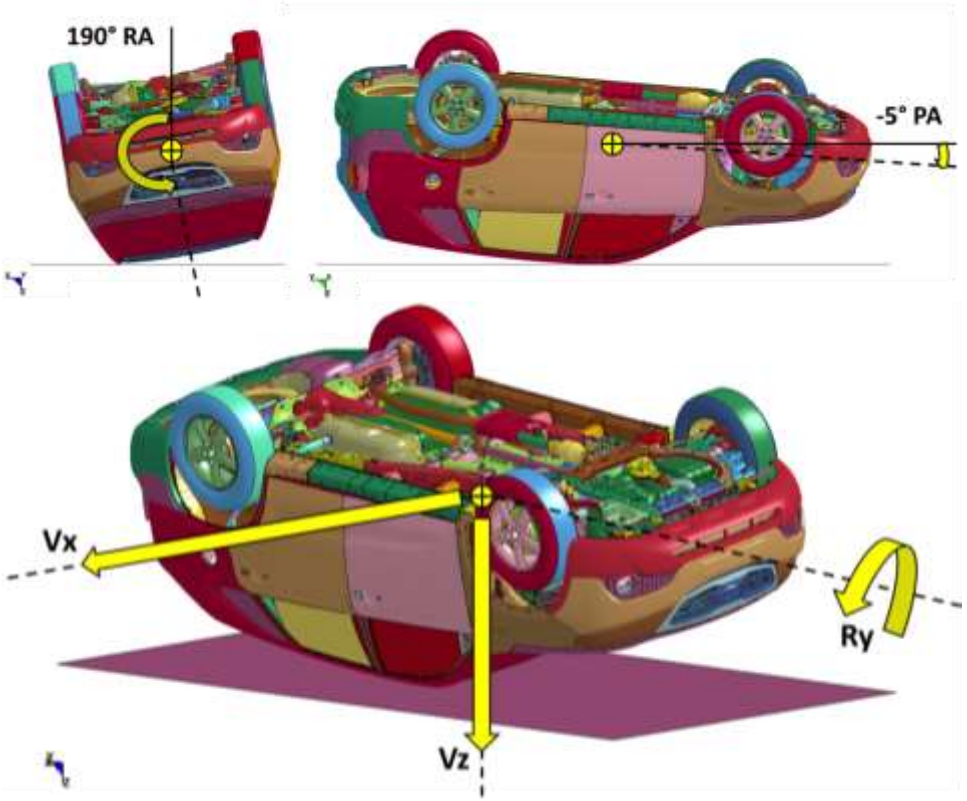

Figure 36: Vehicle model in touchdown orientation.

The global coordinate system was aligned with the vehicle before the yaw, pitch, roll rotations were applied and was contestant. The vehicle coordinate system was defined using standard SAE practice, and rotated/translated relative to the global system during the simulations.

Deformation

The deformation response of the vehicle was quantified by measuring changes in the shape of four distinct rooflines surrounding the driver's seating position. The selected rooflines consisted of all of the model's nodes along simulated lines, two of which were oriented along the length of the vehicle (Driver, Center), and two perpendicular lines across the length of the vehicle (A-pillar, B-pillar) (**Figure 37**). These rooflines were projected onto orthogonal planes (vehicle X-Z for the Driver and Center, and vehicle Y-Z for the A- and B-pillar) and the deformed roofline was compared to the undeformed reference roofline at each time step.

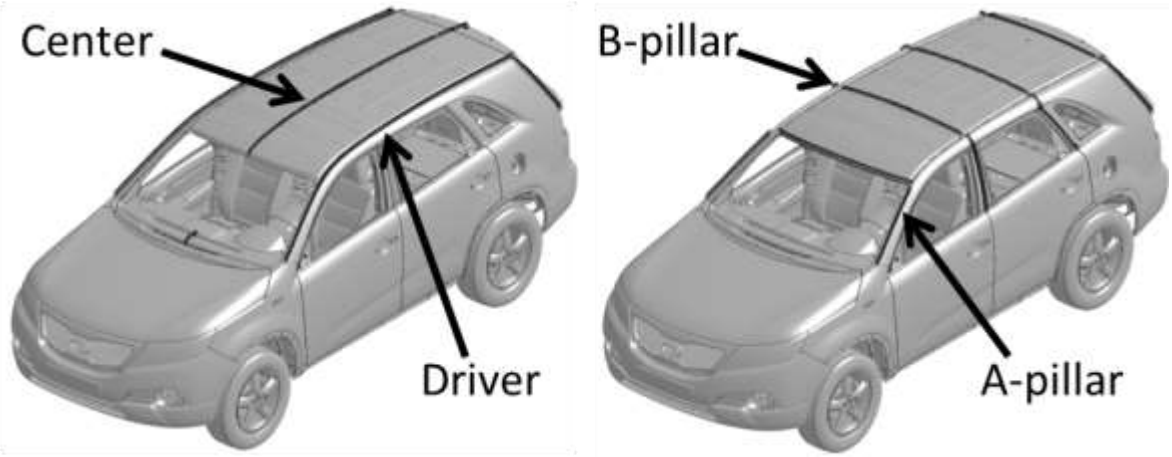

Figure 37: Diagram of roofline geometries in FE model.

The node of maximum displacement at peak deformation on each roofline was determined by tracking the largest distance of any point on the roofline between the current and initial configurations. A time history of displacement was then captured for this node on each roofline for each of the eight cases. The time history of the node of maximum resultant displacement for the Driver, A-pillar, and B-pillar were averaged together for each case.

To examine correlations between force, deformation, and energy, the slopes of linear regressions between metrics were t-tested at the $p<0.05$ level. Total, vertical, rotational, and translational energy inputs were all evaluated independently as predictors of output peak force and peak deformation. Additionally, the internal energy and maximum vehicle CG vertical displacements were evaluated as predictors of the peak deformation metric.

Results

Kinematics

The timing, magnitude, and duration of events varied throughout the eight simulations, but they all demonstrated a similar kinematic response (**Figure 38**).

Figure 38: Example timeline of FE simulation vehicle response.

While the simulations ran for 500 ms, ground reaction forces reduced to almost zero by 250 ms in all simulations, so this period was examined in detail. Due to the imposed vertical velocity and gravity, the CG of the vehicle initially displaced downward (positive global Z) until a maximum was reached between 112 ms and 152 ms for the eight simulations (**Figure 39**) then the CG rose during unloading. The global Z velocity of the CG initially increases for around the first 9 ms before reversing direction and eventually going negative (vehicle CG moving away from the ground).

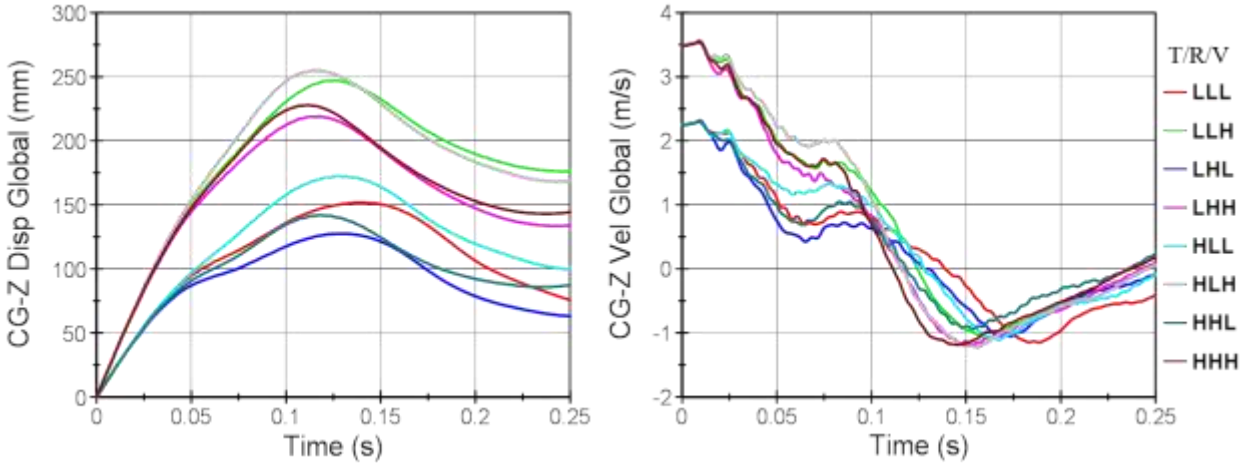

Figure 39: CG global kinematics. Vertical displacement (left). Vertical velocity (right).

The roll angle for all eight simulations increased throughout the impact with a range at 250 ms between 218° for case LLH and 258° for case HHL. The roll rate decreased dramatically upon impact, reached a minimum, and then began increasing for all simulations except case LLH (**Figure 40** left). Case HLL was unique in that it was the only case to have a higher roll rate at 250 ms than at 0 ms, gaining rotational kinetic energy through the impact.

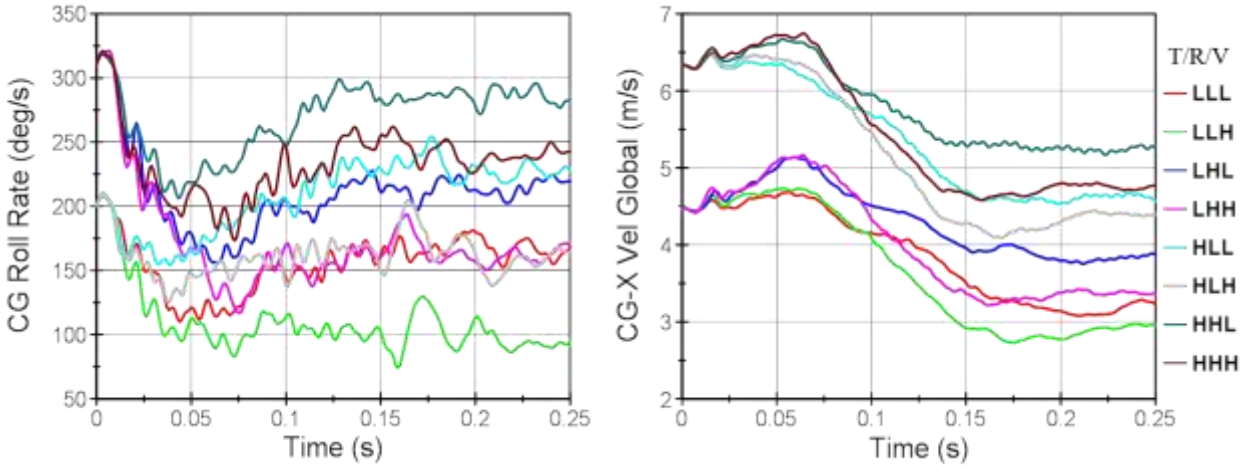

Figure 40: Roll rate about the local vehicle roll axis (left). Global translational velocity Vx (right).

The translational velocity of the vehicle in the eight simulations ended lower at 250 ms than at initial impact (**Figure 40** right). The four cases with high roll rate all gain translational energy over the first 70 ms, and then join the trend of losing translational velocity through 150 ms.

Force, Energy, Deformation

The vertical reaction force exhibited a bimodal response for the eight simulations (**Figure 41**). An initial peak was observed before 30 ms for all cases, with a local minimum following before 90 ms, and then a second maximum before 150 ms, with the force dropping to zero by 200 ms. The second force peak was larger than the first for all of the cases except for case LHL. The timing and magnitude of the two force peaks varied across the eight simulations, but four sets of test pairs exhibited phase and magnitude agreement (LLL and LHL, LLH and LHH, HLL and HHL, HLH and HHH). These pairs correspond to shared translational and vertical kinetic energy, with a change in rotational energy. Increasing the translational energy decreased the magnitude of the first peak, and increased the magnitude of the second peak across the four matched pairs. The first peak corresponded to the greenhouse loading, while the second peak resulted from hood and belt rail interaction with the ground.

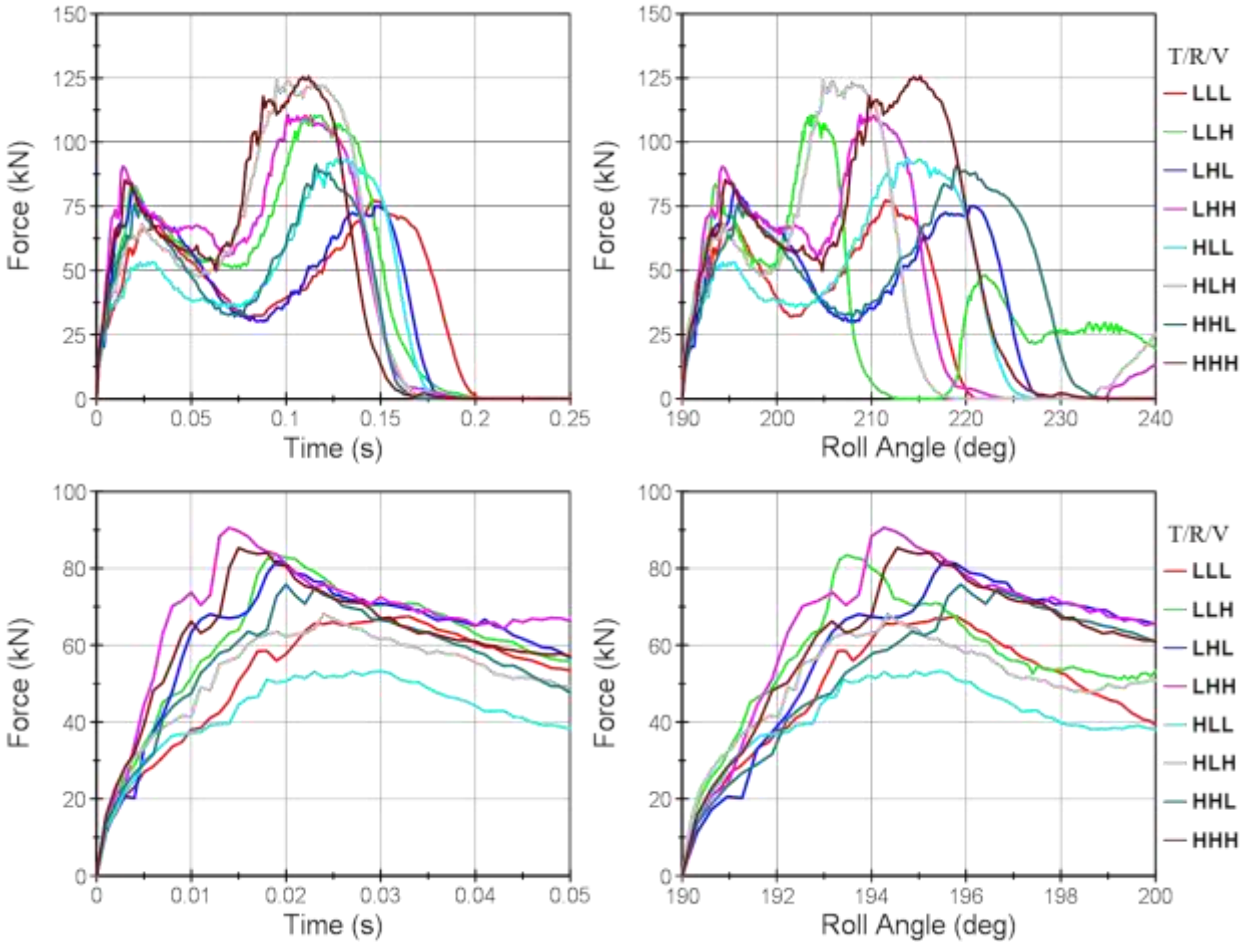

Figure 41: Ground vertical reaction force. Time scale (left), Roll angle scale (right). Peak in greenhouse structure force (bottom).

The distribution of the initial peak remained concentrated between 193° and 196° but the distribution of the second peak widened significantly with values ranging from 203° to 221°. Four different pairs exhibited similar responses (LLL and HLL, LLH and HLH, LHL and HHL, LHH and HHH), each pair of which shared rotational and vertical energy with different translational energy.

The internal energy, which is the strain energy accumulated to deform the elements, was tracked throughout the simulations (**Figure 42**). The peak response in internal energy was found to group the cases into a two sets. The cases that achieved higher internal energies (LLH, LHH, HLH, and HHH) had the high value of vertical energy, while the cases with the lowest internal energy (LLL, LHL, HLL, and HHL) had the lower value of vertical energy. Increasing the rotational energy slightly decreased the peak internal energy across the four matched pairs, while increasing the translational energy increased the peak internal energy. When plotted against roll angle, four pairs with exhibited similar response (LLL and HLL, LLH and HLH, LHL and HHL, LHH and HHH). These pairings had the same vertical and rotational energy, but had different translational energy.

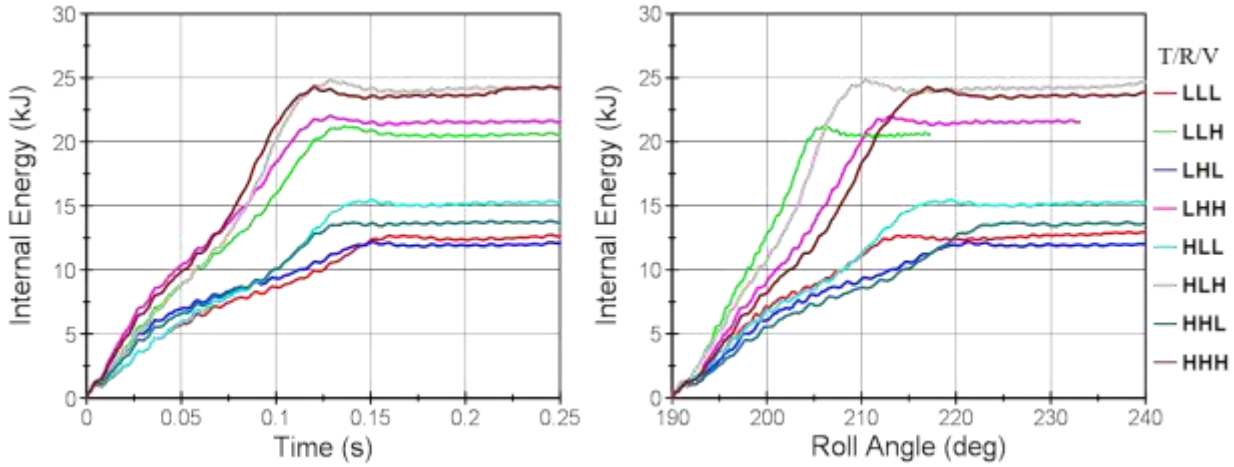

Figure 42: Sum internal energy of FE simulations. Time scale (left), Roll angle scale (right).

In all cases, the peak deformation was centered in the area of the driver side roof rail between the A- and B-pillars. The single value peak deformation for the eight cases produced a fairly evenly distributed range of peak values (176 mm to 340 mm), all of which occurred between 100 and 130 ms after contact (**Figure 43**). The four cases with the highest maximum deformation all had the higher vertical energy. An increase in rotational energy showed a reduction in peak deformation, while an increase in translational energy produced a slight increase in peak deformation. When plotted against roll angle, four pairs of similar responses are seen (LLL and HLL, LLH and HLH, LHL and HHL, LHH and HHH), with shared vertical and rotation and different translational energy. The higher translational energy cases produced a higher peak force that occurred at a greater roll angle.

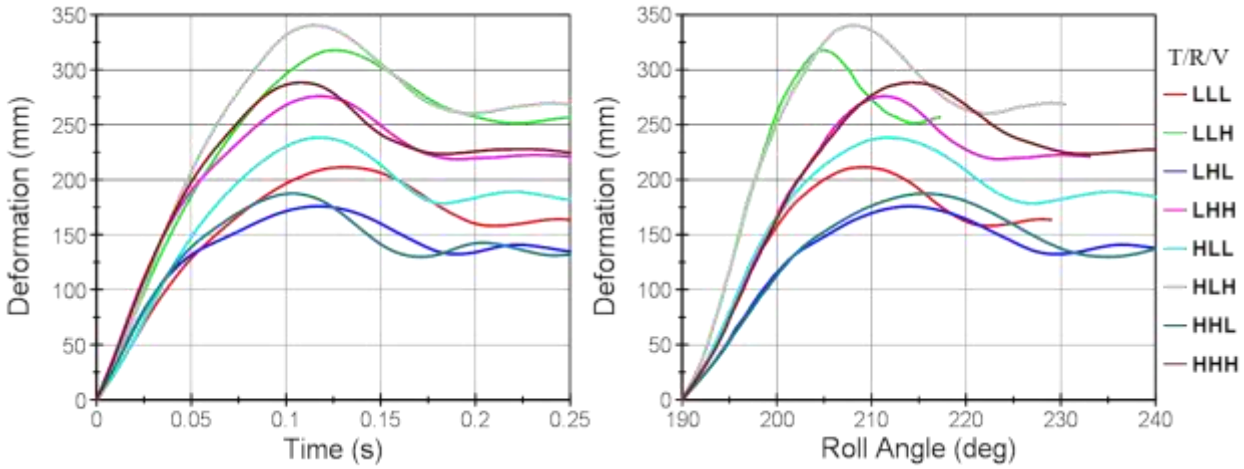

Figure 43: Maximum deformation curves. Time scale (left), Roll angle scale (right).

Correlation Analysis

Correlation analysis was performed using peak force recorded with less than 5 in of crush, and with internal energy, and peak deformation occurring before 250 ms. Statistically significant correlations were found between deformation and vertical kinetic energy, internal energy and CG displacement, and a marginally significant relationship was found between peak force and rotational kinetic energy (**Table 5**).

Table 5: Correlation coefficients and p-values for linear regression pairs.

	KE Trans.	KE Rot.	KE Vert.	KE Total	Internal Energy	CG-Z Disp.	Peak Force
Peak Force	-0.450 p=0.263	0.671** p=0.068	0.536 p=0.170	-0.023 p=0.957	0.344 p=0.404	0.246 p=0.557	N/A
Deformation	0.159 p=0.702	-0.396 p=0.330	0.904* p=0.002	0.295 p=0.464	0.930* p=0.001	0.992* p=0.000	0.141 p=0.749

*Denotes statistical significance of $p < 0.05$
**Denotes statistical significance of $p < 0.10$

Discussion

Experimental Design

Only two levels for each of the three velocities defining the kinetic energy distribution were selected due to the relatively low number of total cases required for a full factorial analysis. The high and low values for roll rate (200 and 311 deg/s), x velocity (4.48 and 6.34 m/s), and z velocity (2.24 and 3.48 ms/s) were chosen to be within the range of previous rollover experimental tests and simulations (Parent, 2011; Lockerby, 2014). The 190° roll angle and -5° pitch angle loaded similar structure to that of the IIHS platen test, with a similar loading vector at the time of peak deformation as the static roof crush test used

to validate the quasi-static response of the model. A yaw angle of -90° and a y velocity of zero were used to mimic the configuration of a vehicle in a DRoTS test while no constraint was applied. While the vertical, translational, and roll velocities were varied in this analysis, the effects of variations in the other six parameters defining the kinematic state at touchdown were not evaluated in this study, but should be considered in future research. Previous rollover FE studies have determined that roll angle and pitch angle have a significant effect on structural deformation in dynamic simulations (Tahan, 2010; Parent, 2011).

Deformation

An averaged deformation time history was calculated for each simulation to facilitate the selection of a single value to define the magnitude of vehicle deformation for use in the correlation analysis. The peak value identified in the center roofline was not included in the averaged calculation since the maximum deformation on this line was generally outward from the vehicle CG, and did not result in a loss of occupant compartment volume. Both the internal energy and maximum vehicle CG vertical displacement (two other surrogates for deformation) were significant predictors of the single deformation value for each test, which confirmed the accurate ranking of the simulations in order of deformation magnitude.

It was hypothesized that a vehicle subjected to an increase in kinetic energy at the initiation of a roof to ground impact would sustain more structural deformation. The results of the FE simulations of a far-side rollover impact on a mid-sized SUV in LS-DYNA conveyed that total kinetic energy was not a significant predictor of deformation, while the response of the FE model showed sensitivity to the distribution of kinetic energy. Vertical kinetic energy displayed a significant positive correlation with deformation, which agreed with previous investigations into rollover sensitivity (Parent, 2011). This result was expected as vertical velocity is normal to the reacting ground surface.

Rotational energy was not significantly correlated to deformation. However, after grouping by high and low vertical energy, the two simulations in each group with the lower deformation had the high value for rotational energy. It was observed that for a far-side only impact, a higher roll rate rotated the vehicle CG over the impact location faster, thus reducing the duration of loading on the structure. Since deformation required time (an average of 115ms to the peak for the eight simulations), a faster roll rate reduced the amount of deformation. The eight simulations run in this study did not provide enough statistical power to determine significance, but an inverse relationship between rotational energy and deformation was displayed.

The translational kinetic energy displayed no significant correlation to deformation, which due to its magnitude, had a substantial effect on the total energy. However, after examining the pairs of simulations, an increase in translational energy produced a slight increase in peak deformation. This result seemed counterintuitive as translational kinetic energy acted perpendicular to the reaction surface, and thus should have been dissipated mainly through frictional forces and not structural deformation. It was possible that more translational velocity increased the lateral shearing force at the interface and led to more lateral deformation and weakened the structure to vertical loading. It is hypothesized that while translational kinetic energy was shown to have only a minor effect on deformation for a single roof-to-ground impact, it would dictate whether additional roof inversions are completed by the vehicle during the rollover event. The number of roof inversions has been linked to a significant increase in occupant

injury probability (Funk, 2012), so a higher translational velocity could lead to a more sever rollover by enabling more quarter turns.

Force

The eight simulations all demonstrated a bimodal response in normal force to the rollover loading, as the first peak corresponded to the greenhouse loading, while the second peak resulted from hood and belt rail interaction with the ground. The initial peak within the first 5 inches of deformation was used as the output metric, as this was the dynamic analog to the FMVSS 216 roof strength criteria. The peak force was not significantly correlated to total, vertical, rotational, or translational kinetic energy. The maximum reaction force of the vehicle should have been dictated by the strength of the structure, and once sufficient energy was available to eclipse the gross yield point of the greenhouse, additional energy increased plastic deformation but did not have an effect on the peak force. Peak force was not a significant predictor of peak deformation, in contrast to the FMVSS 216 evaluation criteria that used only peak force (SWR) as the predictor for deformation magnitude.

Rotational kinetic energy showed a marginally significant positive correlation to force. It was hypothesized that either strain rate stiffening of the material (as increased rotational velocity increases the rate of loading), or the vehicle rotating onto a stiffer load path was responsible for this relationship. This result was in contrast to replicate experimental dynamic rollover tests where the vehicle with more rotational velocity had a lower peak force. It was unclear exactly how increased rotational energy caused an increase in peak reaction force from the eight simulations, and would require additional simulations to determine if this effect was significant.

It should be noted that these findings are only applicable to the specific vehicle FE model, in this specific rollover impact orientation. The FE vehicle model had not been validated for dynamic roof loading. From the outcomes of

Conclusions

Eight single roof-to-ground impact simulations were performed with an FE vehicle model of a late model mid-sized SUV in LS-DYNA. The study examined how variations in the distribution of initial kinetic energy between vertical, rotational, and translational velocities affected the force and deformation response of the vehicle roof structure in a rollover simulation. From the eight far-side roof impacts with the same roll, pitch, and yaw angle at touchdown:

- Vertical kinetic energy (drop height), not total kinetic energy, was found to be a significant predictor of deformation in rollover loading.
- Peak reaction force was not a significant predictor of peak roof deformation.

References

Batzer, S. A., & Hooker, R. M. (2005). Dynamic roof crush intrusion in inverted drop testing. In 19th international technical conference on the enhanced safety of vehicles (No. 05-0146).

Chou, C. C., McCoy, R. W., & Le, J. (2005). A literature review of rollover test methodologies. International Journal of Vehicle Safety, 1(1), 200-237.

DiMasi, F. (1995). TRANSFORMATION OF NINE-ACCELEROMETER-PACKAGE (NAP) DATA FOR REPLICATING HEADPART KINEMATICS AND DYNAMIC LOADING (No. DOT HS 808 282).

Friedman, D., Nash, C. E., & Caplinger, J. (2007). Results from two sided quasi-static (M216) and repeatable dynamic rollover tests (JRS) relative to FMVSS 216 tests. In 20th International Technical Conference on the Enhanced Safety of Vehicles (ESV), Paper (No. 07-0361).

Friedman, K., & Hutchinson, J. (2009). Review of existing repeatable vehicle rollover dynamic physical testing methods. In ASME International Mechanical Engineering Congress and Exposition (Vol. 16, pp. 51-59).

Funk, J. R., Cormier, J. M., & Manoogian, S. J. (2012). Comparison of risk factors for cervical spine, head, serious, and fatal injury in rollover crashes. Accident Analysis & Prevention, 45, 67-74.

Grzebieta, R. H., McIntosh, A. S., Bambach, M., & Young, D. P. (2010, August). Dynamic test protocol to assess rollover crashworthiness. In Proceedings of Australasian Road Safety Research, Policing and Education Conference, Canberra,, Australia.

Kerrigan, J. R., Jordan, A., Parent, D., Zhang, Q., Funk, J., Dennis, N. J., ... & Crandall, J. (2011). Design of a dynamic rollover test system. *SAE International Journal of Passenger Cars-Mechanical Systems*, *4*(1), 870-903.

Lockerby, J., Kerrigan, J., Seppi, J., & Crandall, J. Optical Measurement of High-Rate Dynamic Vehicle Roof Deformation during Rollover. Society of Automotive Engineers, 2013-01-0470.

Mao, M., Chirwa, E. C., Chen, T., Latchford, J., & Wang, W. (2005). Numerical analysis of a small European vehicle under rollover condition. Proceedings of the Institution of Mechanical Engineers, Part D: Journal of Automobile Engineering, 219(12), 1369-1379.

Moffatt, E. A., Cooper, E. R., Croteau, J. J., Orlowski, K. F., Marth, D. R., & Carter, J. W. (2003). Matched-pair rollover impacts of rollcaged and production roof cars using the controlled rollover impact system (CRIS). SAE transactions, 112(6), 145-152.

Mohan, P.; Kan, C.D.; Riley, J., “Evaluation of roof strength under multiple loading conditions.” Proceedings of the 2008 International Crashworthiness Conference, 22-25 July, Kyoto, Japan, 2008.

National Highway Traffic safety Administration. 2006. Laboratory test procedure for FMVSS 216 roof crush resistance. Report no. TP-216-05. Washington, DC: US Department of Transportation.

Office of the Federal Register, 2009. Federal Register, vol. 74, no. 90, pp. 22348-22393. National Highway Traffic Safety Administration – Final Rule. Docket no. NHTSA-2009-0093; 49 CFR Part 571 – Federal Motor Vehicle Safety Standards, Roof Crush Resistance. Washington, DC.

Parent, D.P.; Kerrigan, J.R.; Crandall, J.R., "Comprehensive computational rollover sensitivity study, Part 1: influence of vehicle pre-crash parameters on crash kinematics and roof crush." International Journal of Crashworthiness. Vol. 16, No. 6, December 2011, 633-644.

Tahan, F.; Digges, K.; Mohan, P., 2010. "Sensitivity Study of Vehicle Rollovers to Various initial Conditions – Finite Element Model Based Analysis." Paper 2010-083, Proceedings of the International Crashworthiness Conference, Washington, DC.

Thesis Addendum and General Discussion

Experiments vs Simulations

The results of the two experimental DRoTS tests were not in agreement with the FE simulation study about the effect of vertical energy on deformation. The first vehicle tested on the DRoTS had a higher vertical velocity and sustained similar deformation (or slightly less based on the single point maximum) than the second vehicle. The FE sensitivity study concluded that an increase in vertical velocity was a strong predictor of increased deformation. Although the FE vehicle model had not been validated for dynamic roof loading, it is hypothesized that the simulations predicted the correct relationship that greater vertical kinetic energy will result in more roof deformation, with all other touchdown parameters equal. The direct comparison of deformation and kinetic energy distribution between the two DRoTS tests in Study II was based on the assumption that the vehicle orientations at far-side touchdown were similar enough to remove geometric sensitivities. However, a relatively small difference in pitch angle (-1.86° compared to -0.71°) created a variation in the deformation pattern. A similar sensitivity to roll angle (185° vs 182°) could have accounted for the reduced deformation for the test with higher vertical velocity. Previous FE studies have found roll angle and pitch angle to be significant predictors of deformation along with vertical velocity (Tahan, 2010; Parent, 2011). Even slight changes in the roof-to-ground touchdown orientation of the vehicle can alter the load path and change the force-deformation response. Additionally, the results of the DRoTS experiment were based on two vehicle tests, a small sample size for generating general conclusions about the response a vehicle to rollover loading. A larger sample of DRoTS tests or a FE simulation study with variations to the touchdown conditions instead of the energy inputs could provide additional insight into the conflicting results of Study II and Study III.

Energy Criterion for Rollover Crashworthiness

Vehicle crashworthiness for rollover loading is currently only evaluated by the FMVSS 216 quasi-static platen test, which requires each vehicle to produce a reaction force of 3.0 times its weight (strength-to-weight ratio SWR≥3.0). NHTSA has supported the choice of peak SWR as the metric to evaluate roof strength based on a retrospective analysis of rollover crashes, roof deformations, and vehicle SWRs that displayed a relationship between increased SWR and decreased vertical roof intrusion in real-world rollovers (Austin, 2010). Researchers have argued that solely attaining a level of peak force (or SWR) is not a useful indicator of roof crush resistance performance because the peak forces often drop significantly due to breaking glass and other structural failures, and instead have recommended an energy absorption requirement in order to prevent roof collapse after initial peak forces are attained (Office of the Federal Register Comments, 2009). The results from Studies II and III in this thesis are in agreement with this recommendation. In the replicate vehicle dynamic rollover tests, the two vehicles sustained similar deformation even though one produced a higher reaction force. In the FE simulation study, peak force was not found to be a significant predictor of deformation.

It is assumed that the logic behind the use of the peak SWR metric to evaluate roof strength is that for a given energy level, a greater force will reduce the amount of deformation. However, the total

deformation not only depends on the peak value of force (a single point) but on the entire force-deformation curve. An additional metric that captures the full force-deformation response is required to predict deformation. Rollover crashes are finite energy events, with all of the energy available at the time of initial vehicle to ground touchdown, and the deformation depending on the strength of the vehicle structure. On the contrary, the FMVSS 216 and IIHS roof strength evaluations are finite deformation tests (with an imposed 10 inches of platen displacement) capable of inputting infinite amounts of energy based on the strength of the vehicle structure.

The IIHS roof strength SWR-deformation curves for six mid-sized SUV's with a model year between 2010 and 2013 show a range of peak SWR values between 3.05 to 6.68, with all of the vehicles satisfying the required level of 3.0 (**Figure 44** left). The stiffness of the structures up to the peak SWR and the shape of the curve after the peak SWR vary between the six vehicles. The area under the force-deformation curve equates to the energy absorbed by the structure through deformation. Once the force has been normalized by vehicle weight, integrating the SWR-deformation curve produces a normalized energy absorption measure known as Equivalent Drop Height (EDH) with units of distance (**Figure 44** right).

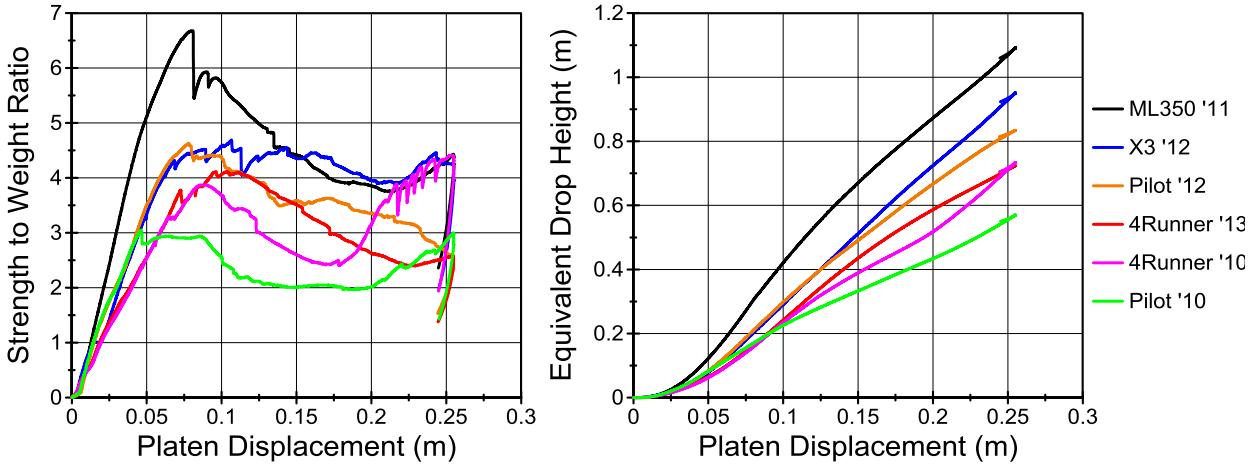

Figure 44: Sample IIHS roof strength evaluation results for six mid-sized SUV's with a model year between 2010 and 2013 (left). Equivalent drop height normalized energy metric (right).

The 2011 ML350 has the highest peak SWR and also the largest EDH at 125 and 250 mm of platen displacement, and conversely the 2010 Pilot has the lowest SWR and EDH metrics. However, the 2012 X3 and the 2012 Pilot have very similar peak SWR (4.63 vs 4.69 for a 1.3% difference), the same EDH at 125 mm of crush (0.41 and 0.41 m), but different EDH at 250 mm of crush (0.83 vs 0.95 m for a 14.4% difference). This is the result of the drastic reduction in force of the 2012 Pilot beyond the peak value, while the 2012 X3 produces a fairly consistent curve after the peak. Additionally, the 2010 4Runner has a lower SWR than the 2013 4Runner (3.88 vs 4.12), but has a slightly higher EDH at 250 mm of crush (0.73 vs 0.72 m). These comparisons communicate that SWR and EDH are related, but that the two measures would not necessarily rank the vehicles in the same order or provide the same relative difference.

Modified FE Simulations, SWR and EDH

Two vehicles with the same quasi-static peak SWR could have very different levels of energy absorption over 5" or 10" of roof crush. Therefore, it is hypothesized that if two vehicles with the same peak SWR but different EDH are subjected to the same rollover impact, the vehicle with the higher EDH will sustain less deformation.

To test out this theory, two additional simulations were performed with a reinforced version of the FE model of the mid-sized SUV from Study III. Three structural members, high strength steel reinforcements in the B-pillars (**Figure 45**), were duplicated and overlaid in the model to double the stiffness and bending resistance of the structure in these locations. The reinforcements added an additional 0.9% to the total mass, and 1.7% to the moment of inertia about the roll axis. The input parameters at impact matched Case 2 (LLH low translational, low rotational, high vertical kinetic energies) from Study III.

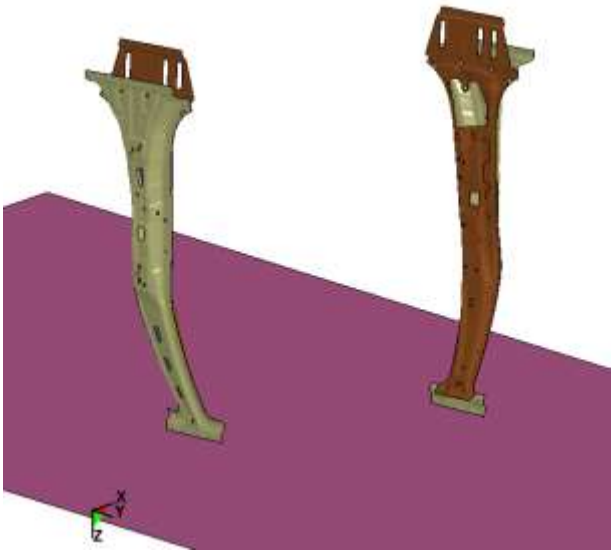

Figure 45: Reinforcement of the FE model structure. B-pillar structural members duplicated to increase the stiffness to roof loading.

The reinforced vehicle simulation was run for the full 250 ms after impact, and the time of the peak greenhouse reaction force was identified. The second reinforced vehicle simulation was run with the reinforcements included until the peak force was reached then the reinforcements were removed for the remainder of the simulation. This produced two vehicles with the same peak SWR rating, but different EDH (**Figure 46**). The B-Pillar reinforcements raised the dynamic SWR of the vehicle in this loading condition from 4.18 to 5.03 accounting for a 20% increase. Once the reinforcements were removed in the second simulation, the force dropped dramatically back in line with the original structural response.

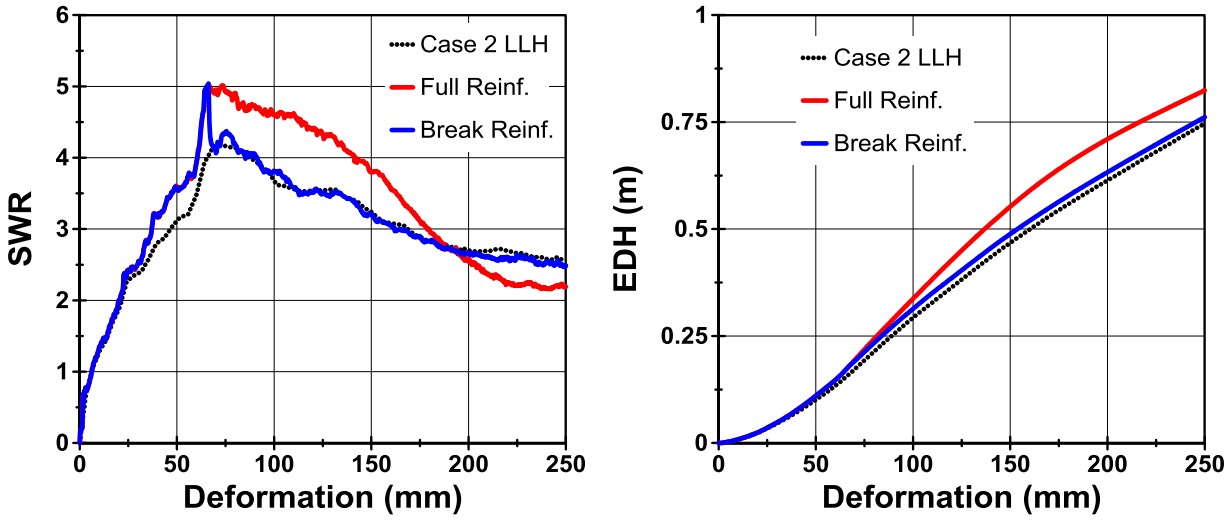

Figure 46: Strength to weight ratio (Left) and Equivalent drop height (Right) vs deformation for Case 2 normal, reinforced, and reinforcements removed at peak force.

The full reinforced model had an EDH that was 10.9% higher at 250 mm of deformation than when the reinforcements were removed. The average maximum deformation was derived from the Driver, A-Pillar, and B-pillar rooflines (same method as in Study III) for the three simulations (**Figure 47**). Reinforcing the model for the full simulation reduced the peak deformation by 15 mm compared to when the reinforcement was removed at the peak SWR, while reinforcing the vehicle only up to the peak SWR showed little effect on deformation compared to the original unreinforced model.

While the sharp drop in the force-deflection response of the second simulation was artificially created by removing parts from the model, similar response has been observed from vehicles during the IIHS evaluation when the windshield glazing abruptly buckles and separates from the frame. For the fully reinforced vehicle, the SWR-deformation curve actually dips below the unreinforced response after 180 mm of deformation. This is thought to be the result of the stronger B-pillar transmitting more load to support structure that was not also modified to handle increased loading, causing localized buckling and failure. The unintended consequences of this simple reinforcement demonstrate the complex nature of vehicle greenhouse structural design.

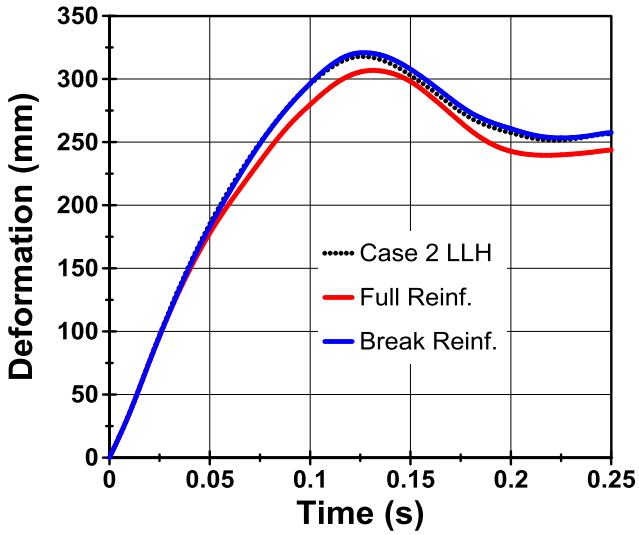

Figure 47: Maximum deformation average of the Driver, A-Pillar, and B-Pillar roof lines.

Acceleration

If a vehicle is subjected to a roof-to-ground impact, an increase in roof stiffness (peak SWR) will arrest the vehicle's vertical velocity more rapidly, resulting in higher accelerations sustained by the occupant. This will place more load and energy carrying requirements on the restraint system to prevent occupant excursion, with the potential for head contact with a minimally deformed roof. Previous studies have found that severe occupant injuries, especially those to the cervical spine, frequently occur without significant roof intrusion (Funk, 2012). This suggests that a higher peak SWR does not always reduce occupant injury probability, and that vehicle roof structure and interior occupant restraints should be complimentary designs.

Rollover Crash Database Studies

Previous studies by the IIHS have investigated the correlation between roof strength and occupant injury outcome in real world rollover crashes for mid-sized SUV's and small passenger cars (Brumbelow, 2009). The studies presented four possible roof strength metrics (peak strength, SWR, energy absorbed, and EDH) at three levels of platen displacement (2, 5, and 10 inches) to predict a reduction in the risk of fatal or incapacitating occupant injury (**Figure 48**). Of the two normalized measures, EDH provides a similar odds ratio reduction to SWR for three of the six combinations (2 and 5 inches for SUV's, and 10 inches for passenger cars). EDH shows a larger reduction in odds ratio for two of the six (10 inches for SUV's, and 5 inches for passenger cars), and less of a reduction at one of the six combinations (2 inches for passenger cars). Overall, the regression data from these studies suggests that EDH provides an equivalent or improved roof strength metric compared to SWR for reducing the risk of occupant injury during rollover.

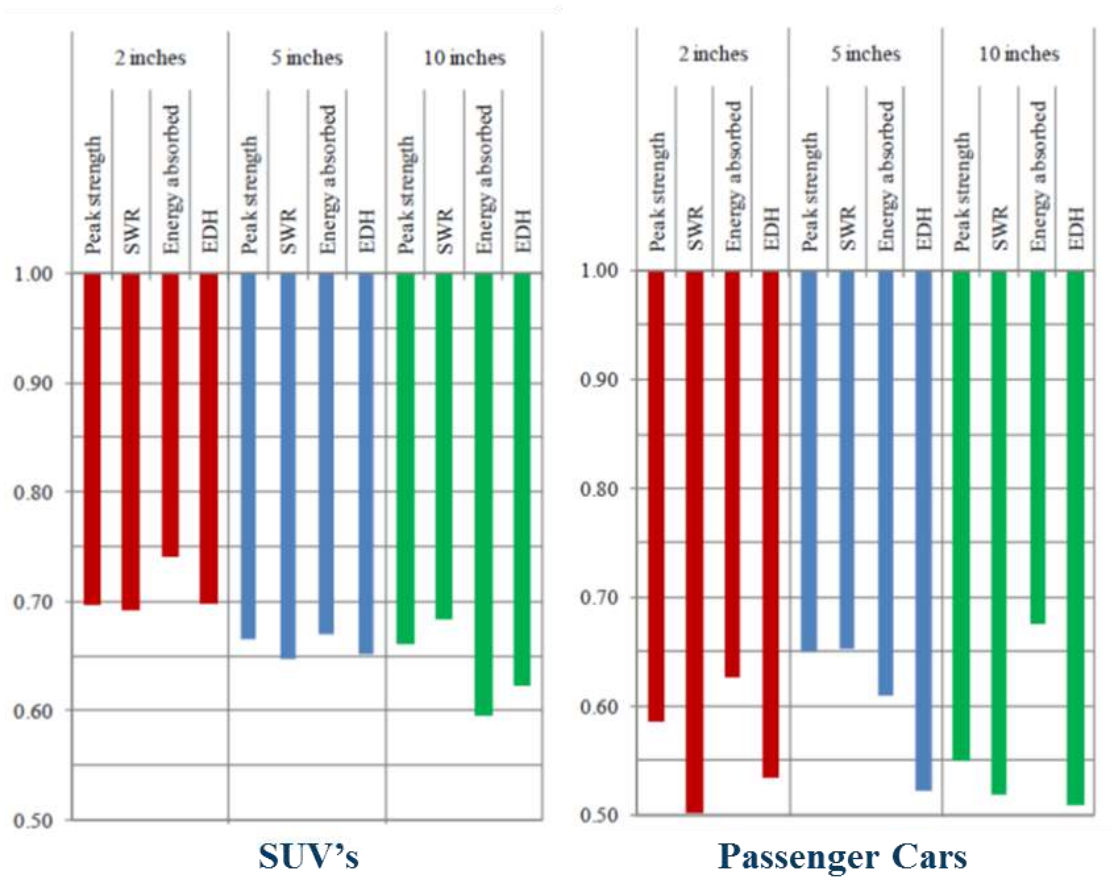

Figure 48: Odds ratios for risk of fatal or incapacitation driver injury with increasing roof strength for SUV's (Left) and Small Passenger Cars (Right) reproduced from Brumbelow, 2009.

Thesis Summary and Conclusions

This collection of three studies evaluated the relationship between force, energy, and deformation in rollover crashes. Study I examined the dynamic force-deformation and kinematic response of a late model van subjected to an inverted drop test and evaluated the accuracy of three-dimensional multi-point roof deformation measurements made by an on-board optical system. The force-deformation response between the drop test and the IIHS roof crush test on the same make and model vehicle showed comparable stiffness, with limited rate dependence. The optical system was validated against independent deformation measurements from string potentiometers, and was shown to be a useful tool for measuring dynamic roof deformations, in three dimensions, at high rates, across a large area of the vehicle structure, from inside a vehicle subjected to rollover crash test. Use of optical measurements shows promise as a data collection method for researchers studying the complex relationship between roof deformation timing, vehicle to occupant interactions, and injury mechanisms.

Study II quantified the effect of variations in touchdown conditions on vehicle kinematic and deformation response through two full-scale dynamic rollover tests using replicate mid-sized SUV's on the dynamic rollover test system (DRoTS). The test with less total kinetic energy sustained similar peak roof deformation (149 mm to 153 mm) but generated a larger peak reaction force (135 kN to 120 kN) than the test with greater kinetic energy. The total kinetic energy dissipated during the roof-to-ground impact of each test was similar (-20.7 kJ and -21.1 kJ) and the two vehicles absorbed similar amounts of energy to structural crush (10.7 kJ). Contrary to the results of previous FE simulation studies, the vehicle with the larger drop height did not sustain more deformation.

Study III characterized how variations in the distribution of initial kinetic energy (vertical, rotational, translational) effect the force and deformation response of the vehicle roof structure in a rollover through FE simulation. Eight single roof-to-ground impact simulations were performed with a FE vehicle model of a mid-sized SUV in LS-DYNA, with the three kinetic energies varied between a high and low value. Only vertical kinetic energy was found to be a significant predictor of peak roof deformation ($p=0.002$), while none of the kinetic energies were a significant predictor of peak reaction force. Peak reaction force was not a significant predictor of peak roof deformation.

From the results of the three studies, it was hypothesized that ranking vehicles based only on peak SWR (FMVSS 216) is not an optimized assessment of roof strength compared to including an energy absorption criterion. Two additional simulations were performed on a reinforced version of the FE vehicle model which demonstrated how an increase in the normalized energy absorption (EDH) of the structure reduced deformation in a rollover crash simulation, whereas an increase to peak SWR did not. This leads to the chief conclusion of this thesis**: *that an increase in the peak SWR of a vehicle will not reduce deformation if it is not accompanied by a similar increase in energy absorption (EDH).***
Therefore, it is recommended that an energy absorption criterion be added to the vehicle rollover crashworthiness evaluations (FMVSS 216 and IIHS roof crush).

Improving FMVSS 216

The FMVSS 216 and IIHS roof strength evaluation tests record data for a full force-deformation curve up to 10 inches of platen displacement, but currently only evaluate the vehicles based on a single maximum point. Therefore, it is proposed that to achieve the stated goal of FMVSS 216, to reduce roof intrusion

during rollover, a criteria based on the normalized energy metric equivalent drop height (EDH) should be added. EDH is a normalized measure of energy absorption that incorporates the full force-deformation response, and not just a single point. More robust vehicle greenhouse designs would result from a combined criterion of two requirements:

1. A minimum peak SWR before 5 inches of platen displacement to dictate the initial stiffness response of the roof structure (already included in the rule at SWR>3.0 for FMVSS 216 and SWR>4.0 for "good" rating with IIHS).
2. A minimum EDH at 10 inches of platen displacement to ensure that all vehicle roof structures will absorb a satisfactory amount of energy beyond the point of maximum force.

Incorporating EDH into the rollover safety ratings would not require any changes to the testing procedures, as the full curve of data already exists as an output from these tests. Previous studies have recommended procedural changes to the safety standard that could also be incorporated to encourage stronger roof design. These include testing at multiple roll and pitch angles (Mao, 2005; Peng 2010), and testing without the windshield glazing (IIHS, 2005). FE simulations have predicted a 30% drop in peak force when the windshield is removed (Mohan, 2008), a condition that is possible for rollover crashes with multiple roof inversions.

A repeatable, full-scale, dynamic test would provide the most accurate assessment of vehicle structural response to the complex loading produced by rollover impacts. Until such a system is validated and adopted by NHTSA, vehicle roof designs would be improved by including an energy absorption criterion in the quasi-static test evaluation.

References

Aga, M., & Okada, A. (2003, May). Analysis of vehicle stability control (VSC)'s effectiveness from accident data. In Proceedings of the 18 th ESV Conference, paper (No. 541).

Austin, R., M. Hicks, and S. Summers. 2005. "The Role of Post-Crash Headroom in Predicting Roof Contact Injuries to the Head, Neck, or Face During FMVSS No. 216 Rollovers." Office of Vehicle Safety, National Highway Traffic Safety Administration.

Austin, R. (2010). "Roof strength testing and real-world roof intrusion in rollovers." NHTSA, (No. HS-811 365). August, 2010.

Atkinson, T., Cooper, J., Patel, B., & Atkinson, P. (2004). Considerations for rollover simulation. Society of Automotive Engineers, Paper, (2004-01), 0328.

Bahling, G. S., Bundorf, R. T., Moffatt, E. A., & Orlowski, K. F. (1995). The influence of increased roof strength on belted and unbelted dummies in rollover and drop tests. The Journal of Trauma and Acute Care Surgery, 38(4), 557-563.

Batzer, S. A., & Hooker, R. M. (2005). Dynamic roof crush intrusion in inverted drop testing. In 19th international technical conference on the enhanced safety of vehicles (No. 05-0146).

Beard, D. A., & Schlick, T. (2003). Unbiased Rotational Moves for Rigid-Body Dynamics. Biophysical Journal, 85, 2973-2976.

Boyd, P. L. (2005). NHTSA's NCAP Rollover Resistance Rating System. In *Proc. 19th International Technical Conference on the Enhanced Safety of Vehicles*.

Brumbelow, M.L.; Teoh, E.R.; Zuby, D.S.; and McCartt, A.T., "Roof Strength and injury risk in rollover crashes." Traffic Injury Prevention. Vol. 10, Issue 3, 2009, 252-265.

Brumbelow, M.L.; Teoh, "Roof Strength and injury risk in rollover crashes of passenger cars." Traffic Injury Prevention. Vol. 10, Issue 6, 2009, 584-592.

Chirwa, E. C., Stephenson, R. R., Batzer, S. A., & Grzebieta, R. H. (2010). Review of the Jordan Rollover System (JRS) vis-a-vis other dynamic crash test devices. International Journal of Crashworthiness, 15(5), 553-569.

Chou, C. C., McCoy, R. W., & Le, J. (2005). A literature review of rollover test methodologies. International Journal of Vehicle Safety, 1(1), 200-237.

Conroy, C., Hoyt, D. B., Eastman, A. B., Erwin, S., Pacyna, S., Holbrook, T. L., Velky, T. (2006). Rollover crashes: predicting serious injury based on occupant, vehicle, and crash characteristics. Accident Analysis & Prevention, 38(5), 835-842.

Croteau, J. et al., "Dynamic Response of Vehicle Roof Structure and ATD Neck Loading During Dolly Rollover Tests," SAE Technical Paper 2010-01-0515, 2010, doi: 10.4271/2010-01-0515

Digges, K.H., and A.M. Eigens. 2003. “Crash Attributes That Influence the Severity of Rollover Crashes.” Proceedings of the 18th ESV Conference, No. 231, Nagoya.

Funk, J., Wirth, J., Bonugli, E., & Watson, R. An Integrated Model of Rolling and Sliding in Rollover Crashes. Society of Automotive Engineers, 2012-01-0605, doi: 10.4271/2012-01-0605.

Funk, J. R., Cormier, J. M., & Manoogian, S. J. (2012). Comparison of risk factors for cervical spine, head, serious, and fatal injury in rollover crashes. Accident Analysis & Prevention, 45, 67-74.

Friedman, D., & Nash, C. E. (2001). Advanced roof design for rollover protection. In 17th International Technical Conference on the Enhanced Safety of Vehicles. Amsterdam, The Netherlands.

Friedman, D., & Nash, C. E. (2003). Measuring rollover roof strength for occupant protection. International Journal of Crashworthiness, 8(1), 97-105.

Friedman, D., Nash, C. E., & Caplinger, J. (2007). Results from two sided quasi-static (M216) and repeatable dynamic rollover tests (JRS) relative to FMVSS 216 tests. In 20th International Technical Conference on the Enhanced Safety of Vehicles (ESV), Paper (No. 07-0361).

Friedman, K., & Hutchinson, J. (2009). Review of existing repeatable vehicle rollover dynamic physical testing methods. In ASME International Mechanical Engineering Congress and Exposition (Vol. 16, pp. 51-59).

Gloeckner, D. C., Moore, T. L., Steffey, D., Bare, C., & Corrigan, C. F. (2006). Implications of vehicle roll direction on occupant ejection and injury risk. In Annual Proceedings/Association for the Advancement of Automotive Medicine (Vol. 50, p. 155). Association for the Advancement of Automotive Medicine.

Grzebieta, R. H., McIntosh, A. S., Bambach, M., & Young, D. P. (2010, August). Dynamic test protocol to assess rollover crashworthiness. In Proceedings of Australasian Road Safety Research, Policing and Education Conference, Canberra,, Australia.

Hanson, R. J., & Norris, M. J. (1981). Analysis of Measurements Based on the Singular Value Decomposition. Siam J. Sci. Stat. Comput., 2(3), 363-373.

Heinz, S. R., & Wiggins, J. S. (2010). Uniaxial compression analysis of glassy polymer networks using digital image correlation. Polymer Testing, 29(8), 925-932.

Hu, J., Chou, C. C., Yang, K. H., & King, A. I. (2007). A weighted logistic regression analysis for predicting the odds of head/face and neck injuries during rollover crashes. In Annual Proceedings/Association for the Advancement of Automotive Medicine (Vol. 51, p. 363). Association for the Advancement of Automotive Medicine.

IIHS Comment to the National Highway Traffic Safety Administration concerning proposed changes to Federal Motor Vehicle Standard 216, Roof Crush Resistence (Docket No. NHTSDA-2005-22143), November 18. 2005.

Insurance Institute for Highway Safety status report, Vol. 42, No. 2, March 15, 2008.

Insurance Institute for Highway Safety, 2012. Crashworthiness Evaluation Roof Strength Test Protocol (Version II).

Insurance Institue for Highwar Safety status report, Vol. 48, No. 7. September 27, 2013. "ESC, strong roofs reduce but don't eliminate all rollover injuries."

Jordan, A.; Bish, J., 2005. "Repeatability Testing of a Dynamic Rollover Test Fixture." 19th International Conference on the Enhanced Safety of Vehicles, Paper Number 05-0362, Washington, DC.

Kerrigan, J. R., Jordan, A., Parent, D., Zhang, Q., Funk, J., Dennis, N. J., ... & Crandall, J. (2011). Design of a dynamic rollover test system. *SAE International Journal of Passenger Cars-Mechanical Systems*, *4*(1), 870-903.

Kerrigan, J. R., Dennis, N. J., Parent, D. P., Purtsezov, S., Ash, J. H., Crandall, J. R., & Stein, D. (2011). Test system, vehicle and occupant response repeatability evaluation in rollover crash tests: the deceleration rollover sled test. *International Journal of Crashworthiness*, *16*(6), 583-605.

Lockerby, J., Kerrigan, J., Seppi, J., & Crandall, J. Optical Measurement of High-Rate Dynamic Vehicle Roof Deformation during Rollover. Society of Automotive Engineers, 2013-01-0470.

Mandell, S. P., Kaufman, R., Mack, C. D., & Bulger, E. M. (2010). Mortality and injury patterns associated with roof crush in rollover crashes. Accident Analysis & Prevention, 42(4), 1326-1331.

Mattos, G. A., Grzebieta, R. H., Bambach, M. R., & McIntosh, A. S. (2013). Validation of a dynamic rollover test device. International Journal of Crashworthiness, 18(3), 207-214.

Mattos, G. A., Grzebieta, R. H., Bambach, M. R., & McIntosh, A. S. (2013). Passenger vehicle structural response in a dynamic rollover test. In *23rd International Technical Conference on the Enhanced Safety of Vehicles, Seoul, Korea*.

Mao, M., Chirwa, E. C., Chen, T., Latchford, J., & Wang, W. (2005). Numerical analysis of a small European vehicle under rollover condition. Proceedings of the Institution of Mechanical Engineers, Part D: Journal of Automobile Engineering, 219(12), 1369-1379.

Mao, M., Chirwa, E. C., & Wang, W. (2006). Assessment of vehicle roof crush test protocols using FE models: inverted drop tests versus updated FMVSS No. 216. International Journal of Crashworthiness, 11(1), 49-63.

Moffatt, E. A., & Padmanaban, J. (1995). The relationship between vehicle roof strength and occupant injury in rollover crash data. Publication of: ASSOCIATION FOR THE ADVANCEMENT OF AUTOMOTIVE MEDICINE.

Moffatt, E. A., Cooper, E. R., Croteau, J. J., Orlowski, K. F., Marth, D. R., & Carter, J. W. (2003). Matched-pair rollover impacts of rollcaged and production roof cars using the controlled rollover impact system (CRIS). SAE transactions, 112(6), 145-152.

Mohan, P.; Kan, C.D.; Riley, J., "Evaluation of roof strength under multiple loading conditions." Proceedings of the 2008 International Crashworthiness Conference, 22-25 July, Kyoto, Japan, 2008.

Moore, T. L., Vijayakumar, V., Steffey, D. L., Ramachandran, K., & Corrigan, C. F. (2005). Biomechanical factors and injury risk in high-severity rollovers. In Annual Proceedings/Association for the Advancement of Automotive Medicine (Vol. 49, p. 133). Association for the Advancement of Automotive Medicine.

National Highway Traffic safety Administration. 2006. Laboratory test procedure for FMVSS 216 roof crush resistance. Report no. TP-216-05. Washington, DC: US Department of Transportation.

Office of the Federal Register. 1971. Federal Register, vol. 36, no. 236, pp. 23299-23300. National Highway Traffic Safety Administration – Final Rule. Docket no. 2-6, Notice 5; 49 CFR Part 571 – Motor Vehicle Safety Standards. Washington, DC.

Office of the Federal Register, 2008. Federal Register, vol. 73, no. 20, pp. 5484-5493. National Highway Traffic Safety Administration – Supplemental notice of proposed rulemaking. Docket no. NHTSA-2008-0015; 49 CFR Part 571 – Federal Motor Vehicle Safety Standards, Roof Crush Resistance. Washington, DC.

Office of the Federal Register, 2009. Federal Register, vol. 74, no. 90, pp. 22348-22393. National Highway Traffic Safety Administration – Final Rule. Docket no. NHTSA-2009-0093; 49 CFR Part 571 – Federal Motor Vehicle Safety Standards, Roof Crush Resistance. Washington, DC.

Orlowski, K. F., Bundorf, R. T., & Moffatt, E. A. (1985). Rollover crash tests—the influence of roof strength on injury mechanics. SAE paper, 851743.

Padmanaban, J., Moffatt, E. A., & Marth, D. R. (2005). Factors influencing the likelihood of fatality and serious/fatal injury in single-vehicle rollover crashes. SAE transactions, 114(6), 1072-1085.

Parent, D.P.; Kerrigan, J.R.; Crandall, J.R., "Comprehensive computational rollover sensitivity study, Part 1: influence of vehicle pre-crash parameters on crash kinematics and roof crush." International Journal of Crashworthiness. Vol. 16, No. 6, December 2011, 633-644.

Parenteau, C.S.; Shah, M., 2000. Driver injuries in US single-event rollovers. Society of Automotive Engineers, Paper 2000-01-0633.

Parker, D.D.; Ray, R.M.; Moore, T.; Keefer, R. E., 2007. Rollover severity and occupant protection – a review of NASS/CDS data. Society of Automotive Engineers, Paper 2007-01-0676.

Peng, Q., Chirwa, E. C., & Yang, J. (2012). The newly updated FMVSS 216 roof crush modelling and analysis. International Journal of Crashworthiness, 17(2), 195-207.

Society of Automotive Engineers (SAE), Inc., Instrumentation for Impact Tests. SAE J211/1 JUL2007, July 2007.

Shi, M. and Meuleman, D., "Strain Rate Sensitivity of Automotive Steels," SAE Technical Paper 920245, 1992, doi:10.4271/920245.

Strashny, A. 2007. "The Role of Vertical Roof Intrusion and Post-Crash Headroom in Predicting Roof contact Injuries to the Head, Neck, or Face During FMVSS No. 216 Rollovers; An Updated Analysis."

Tahan, F.; Digges, K.; Mohan, P., 2010. “Sensitivity Study of Vehicle Rollovers to Various initial Conditions – Finite Element Model Based Analysis.” Paper 2010-083, Proceedings of the International Crashworthiness Conference, Washington, DC.

Viano, D.C.; Parenteau, C.S; Edwards, M.L., 2007. Rollover injury: effects of near- and far-seating position, belt use, and number of quarter rolls. Traffic Injury Prevention 8, 382-392.

Yan, B., & Urban, D. (2003). Characterization of fatigue and crash performance of new generation high strength steels for automotive applications. American Iron and Steel Institute, Final Report, East Chicago, IN, USA.